

Dissertation zur Erlangung des Doktorgrades  
der Medizinischen Fakultät  
der Ludwig-Maximilians-Universität München

**Molecular Imaging for Characterization of  
Lymphoma Biology and Monitoring Response  
to Cancer Drug Therapy**

vorgelegt von

Zhoulei Li aus Shandong, China

2013

Aus der Medizinischen Klinik und Poliklinik II der Ludwig Maximilian  
Universität München

Direktor: Prof. Dr. med. Burkhard Göke

**Molecular Imaging for Characterization of Lymphoma Biology and  
Monitoring Response to Cancer Drug Therapy**

Dissertation zur Erlangung des Doktorgrades der Humanbiologie  
an der Medizinischen Fakultät  
der Ludwig-Maximilians-Universität München

vorgelegt von

Zhoulei Li

aus Shandong, China

2013

Mit Genehmigung der Medizinischen Fakultät  
der Universität München

Berichterstatter: Prof. Dr. med. Christine Spitzweg

Mitberichterstatter: PD. Dr. rer. nat. Klaus Dornmair  
Prof. Dr. med. Martin Dreyling  
Univ. Prof. Dr. Reinhold Tiling

Mitbetreuung durch den  
promovierten Mitarbeiter: **Prof. Dr. Andreas Buck**

**Dekan:** Prof. Dr. med. Dr.h.c. Maximilian Reiser,  
**FACR, FRCR**

Tag der mündlichen Prüfung: 19. Dez. 2013

## List of recent international publications:

1. FLT-PET is superior to FDG-PET for very early response prediction in NPM-ALK-positive lymphoma treated with targeted therapy. **Zhoulei Li**, Nicolas Graf, Ken Herrmann, Alexandra Junger, Michaela Aichler, Annette Feuchtinger, Anja Baumgart, Axel Walch, Christian Peschel, Markus Schwaiger, Andreas Buck, Ulrich Keller, and Tobias Dechow. et.al Cancer Reserach 2012
2. Enhanced efficacy of combined <sup>213</sup>Bi-DTPA-F3 and paclitaxel therapy of peritoneal carcinomatosis is mediated by enhanced induction of apoptosis and G2/M phase arrest. Vallon M, Seidl C, Blechert B, **Li Z**, Gilbertz KP, Baumgart A, Aichler M, Feuchtinger A, Gaertner FC, Bruchertseifer F, Morgenstern A, Walch AK, Senekowitsch-Schmidtke R, Essler M. et. al Eur J Nucl Med Mol Imaging 2012
3. Early Prediction of Response to Therapy in Malignant Lymphoma and Ewing Sarcoma using in-vivo Proliferation Marker <sup>18</sup>F-FLT. **Zhoulei Li**, Kathrin Abbrederis, Andreas Buck, Sabine Pirsig, Christian Peschel, Markus Schwaiger, Klemens Scheidhauer, Tobias Dechow, and Ulrich Keller. et. al Abstract AACR 2012 (manuscript in preparing)
4. [<sup>18</sup>F]FLT-PET: a Superior Non-Invasive Imaging for very Early Prediction of Response to Therapy in Malignant Lymphoma. **Zhoulei Li**, Ken Herrmann, Nicolas Graf, Alexandra Junger, Daniel Weh, Markus Schwaiger, Tobias Dechow, and Andreas Buck. et. al SNM 2011 (talk)

# Index

<b>Zusammenfassung</b> .....	8
<b>Summary</b> .....	10
<b>1 Abbreviations</b> .....	12
<b>2 Introduction</b> .....	14
2.1 Hodgkin´s and Non Hodgkin´s lymphoma .....	14
2.1.1 Classification of lymphoma .....	14
2.1.2 ALK-positive anaplastic large cell lymphoma .....	15
2.2 New therapeutic approaches for lymphoma and monitoring of the therapeutic response .....	18
2.3 Lymphoma diagnosis and Imaging – CT and PET .....	21
2.4 Purpose .....	24
<b>3 Methods</b> .....	26
3.1 Kinase inhibitors .....	26
3.2 Cell culture .....	26
3.3 Cell counting .....	26
3.4 Cell proliferation and viability assay .....	27
3.5 Cell cycle distribution and apoptosis analysis (fluorescence activated cell sorting – FACS) .....	27
3.6 Radiosynthesis of FLT and FDG .....	29
3.7 Cellular uptake of FLT and FDG .....	29
3.8 Western blot analysis .....	30
3.8.1 Stock solution .....	30
3.8.2 Gel electrophoresis .....	31
3.8.3 Protein detection .....	33
3.8.4 Developing solution .....	34
3.8.5 Membrane stripping .....	35
3.8.6 Bio-Rad protein assay .....	35
3.9 Animal models and induction of lymphoma xenotransplants .....	35
3.10 Therapeutic regimens .....	36
3.11 Tumor immunohistochemistry .....	36
3.12 Paraffin section method and technique .....	36
3.13 Statistical methods .....	37
<b>4 Results</b> .....	38
4.1 Dual inhibition of AKT and mTOR blocks the proliferation of multiple NPM-ALK lymphoma cell lines .....	38
4.1.1 Dual blockage of AKT and mTOR affects the viability of ALK+ lymphoma cells .....	38

4.1.2 Dual inhibition of AKT and mTOR activity induces the cell cycle arrest of ALK+ lymphoma cells .....	40
4.1.3 Down-regulation of several oncogenic proteins during exposure of human lymphoma cells to PI3K/mTOR inhibitor .....	42
4.2 Functional <i>in vivo</i> imaging of response to PI3K/mTOR (BGT226) inhibition in SUDHL-1 lymphoma by FLT-PET is superior to FDG-PET .....	44
4.2.1 Blockage of PI3K/mTOR activity decrease the tumor growth of NPM-ALK lymphoma <i>in vivo</i> .....	44
4.2.2 FDG-PET imaging analysis shows inhibitory effect of PI3K/mTOR on the NPM-ALK lymphoma metabolism .....	45
4.2.3 FLT-PET imaging analysis shows inhibitory effect of PI3K/mTOR on the cellular proliferation of NPM-ALK lymphoma.....	47
4.2.4 Histological analysis shows decreased proliferation and increased apoptosis induced by the treatment with PI3K/mTOR inhibitor in NPM-ALK lymphoma.....	51
4.3 Inhibition of Hsp90 blocks the proliferation of multiple ALK+ lymphoma cell lines .....	54
4.3.1 The blockage of Hsp90 activity affects the viability of ALK+ lymphoma cells .....	54
4.3.2 Inhibition of Hsp90 activity triggers the cell cycle arrest and apoptosis of ALK+ lymphoma cells .....	58
4.3.3 Down-regulation of several oncogenic proteins during exposure of human lymphoma cells to Hsp90 inhibitor .....	64
4.3.4 A sensitive measure for Hsp90 inhibition of NPM-ALK+ ALCL using FLT-uptake in vitro .....	67
4.4 Functional <i>in vivo</i> imaging of response to Hsp90 inhibition in SUDHL-1 lymphoma by FLT-PET is superior to FDG-PET .....	69
4.4.1 <i>In vivo</i> Hsp90 inhibition blocks the growth of the NPM-ALK lymphoma.....	69
4.4.2 FDG-PET imaging analysis shows inhibitory effect of Hsp90 inhibitor on the NPM-ALK lymphoma metabolism .....	71
4.4.3 FLT-PET imaging analysis shows the inhibitory effect of Hsp90 inhibitor on the proliferation of NPM-ALK lymphoma.....	76
4.4.4 Histological analysis shows decreased proliferation and increased apoptosis induced by treatment with Hsp90 inhibitor in NPM-ALK lymphoma .....	77
4.5 Inhibition of mTOR blocks the proliferation of multiple ALK+ lymphoma cell lines .....	80
4.5.1 Inhibition of mTOR activity affects the viability of ALK+ lymphoma cells .....	80
4.5.2 Inhibition of mTOR activity triggers the cell cycle arrest but not apoptosis in ALK+ lymphoma cells <i>in vitro</i> .....	81
4.5.3 Down-regulation of several oncogenic proteins during exposure of human lymphoma cells to mTOR inhibitor .....	86
4.5.4 A sensitive measure for mTOR inhibition of NPM-ALK+ ALCL using FLT-uptake in vitro .....	87
4.6 Functional imaging of mTOR inhibition in ALCL xenografts by FLT-PET is superior to FDG-PET .....	89

4.6.1 <i>In vivo</i> mTOR inhibition blocks the growth of the NPM-ALK lymphoma .....	89
4.6.2 FDG-PET imaging analysis shows inhibitory effect of mTOR inhibitor on the NPM-ALK lymphoma metabolism .....	90
4.6.3 FLT-PET imaging analysis shows inhibitory effect of mTOR inhibitor on the proliferation of NPM-ALK lymphoma.....	91
4.6.4 Histological analysis shows decreased proliferation and increased apoptosis induced by treatment with mTOR inhibitor in NMP-ALK lymphoma .....	94
4.7 Validating the predictive value of FLT-PET imaging for therapy monitoring <i>in vivo</i> and <i>in vitro</i> .....	97
<b>5 Discussion .....</b>	<b>101</b>
<b>6 Literature .....</b>	<b>111</b>
<b>Acknowledgements .....</b>	<b>122</b>

## Zusammenfassung

Das anaplastisch-großzellige Lymphom (ALCL) ist ein malignes T-Zell-Lymphom, das nach der WHO-Klassifikation zu den Non-Hodgkin-Lymphomen (NHL) gezählt wird. Es wurde erstmals 1985 als eigenständige Tumorentität beschrieben. ALCL tritt vor allem bei Kindern und Jugendlichen auf, aber auch ältere Erwachsene können betroffen sein. Etwa 15 % der kindlichen NHL gehen auf ALCL zurück. Bei 50-60% der ALCL Patienten ist eine chromosomale Translokation beobachtbar, die das Gen für die anaplastische Lymphomkinase (ALK) einschließt. Das dadurch entstehende onkogene Fusionprotein, Nucleophosmin anaplastische Lymphomkinase (NPM-ALK), bewirkt eine konstitutive Aktivierung der Rezeptor-Tyrosinkinasefunktion und nachgeschalteter Signalkaskaden wie z.B. von STAT3, PI-3K/Akt und mTOR.

Bei der Therapie maligner Lymphome spielt die Chemotherapie, teilweise ergänzt durch die Strahlentherapie, eine entscheidende Rolle. Viele Zytostatika verursachen jedoch schwerwiegende Nebenwirkungen und sind selbst karzinogen. Daher erscheint eine zielgerichtete Therapie, die selektiv Signaltransduktionswege von Tumorzellen inhibiert, als viel versprechende Alternative für die Therapie von malignen hämatologischen Erkrankungen sowie auch von soliden Tumoren.

Die Diagnose maligner Lymphome wird mittels histopathologischer Untersuchung nach Biopsie eines betroffenen Lymphknotens gestellt. Die Untersuchung des Ausbreitungsgrades eines malignen Tumors (Staging) vor Therapiebeginn sowie die Kontrolle der Effizienz einer angewandten Therapie werden nicht invasiv mittels bildgebender Verfahren durchgeführt. Dabei ist die Computertomographie (CT) das derzeit am häufigsten angewandte Verfahren bei malignen Lymphomen. Allerdings lassen sich mit CT nur vergleichsweise große Tumore nachweisen. Daneben liefert die CT keine Einblicke in den Stoffwechsel der Tumorzellen und Läsionen, die nur schwachen Kontrast zum umgebenden, gesunden Gewebe aufweisen, werden nicht erkannt. Mittels der [18F]-FDG Positronen-Emissions-Tomographie (PET) lässt sich die Effizienz einer Therapie beim malignen Lymphom verfolgen. Zusätzlich können mit [18F]-FDG-PET metabolische Veränderungen in malignen Lymphomen erkannt werden. Da jedoch auch Entzündungszellen mit erhöhtem Glukosebedarf [18F]-FDG anreichern, kommt es in der Tumordiagnose auch zu falsch positiven Befunden. Dagegen akkumuliert das Thymidin-Analogon [18F]-FLT (3'-Desoxy-3'-[18F] fluorothymidine) in Tumorgewebe aufgrund der stark erhöhten Proliferationsaktivität von Tumorzellen. [18F]-FLT-PET ermöglicht daher, im Gegensatz zur [18F]-FDG-PET, eine selektive Bildgebung der Tumorphosphorylation.

Das Ziel dieser Studie war es, die Anreicherung von [18F]-FLT als Surrogat-Marker zur Kontrolle des Therapieerfolgs, in einer frühen Phase nach Applikation einer zielgerichteten Therapie zu etablieren. Dazu wurden neun verschiedene ALK-positive ALCL-Zelllinien in vitro und zwei davon auch im Tiermodell untersucht. An den ALCL-Zelllinien wurde die zytotoxische Wirkung des HSP90-Inhibitors NVP-AUY922, des mTOR-Inhibitors RAD001 (Everolimus), und des PI3K/Akt Inhibitors BGT226 analysiert. Diese Inhibitoren hemmen nachweislich ALK-abhängige Signaltransduktionswege. Ihre zytotoxische Wirkung wurde in vitro mittels MTT-Assay, Analyse des Zellzyklus-Arrests, [18F]-FDG und [18F]-FLT Aufnahme, sowie mittels Western-Blot Analyse von Proteinen der ALK-Signalwege untersucht. Weiterhin wurde die therapeutische Effizienz der Inhibitoren an immundefizienten SCID Mäusen mit ALK-positiven s.c. Xenotransplantaten (SUDHL-1, Karpas299) untersucht. Die Effizienz der Inhibitor-Therapie wurde mittels [18F]-FDG- und [18F]-FLT-PET überwacht.

SUDHL-1-Zellen zeigten in vitro zytotoxische Reaktionen unterschiedlicher Stärke im Hinblick auf die drei eingesetzten Inhibitoren. Außerdem wurde eine signifikante Reduktion der [18F]-FLT Aufnahme in SCID Mäusen mit SUDHL-1 Xenotransplantaten bereits 5 Tage nach Beginn der zielgerichteten Therapie bei allen Inhibitoren beobachtet. Mittels Immunhistochemie konnte an Tumorschnitten eine Abnahme der Ki-67 Färbung und eine Zunahme der Färbung von cleaved Caspase-3 gezeigt werden, entsprechend einer Abnahme der Zellproliferations-Rate und einer Zunahme der Apoptose-Rate. Im Gegensatz dazu zeigte sich nur eine unwesentliche Verringerung in der Aufnahme von [18F]-FDG. In Karpas299 Xenotransplantaten, die sich als resistent gegen Behandlung mit NVP-AUY922, jedoch als empfindlich gegenüber RAD001 Behandlung erwiesen, waren eine Zunahme der [18F]-FLT Aufnahme am Tag 2 nach der Verabreichung von NVP-AUY922 sowie eine signifikante Reduktion der [18F]-FLT Aufnahme nach Applikation von RAD001 beobachtbar. Zusammenfassend belegen die Ergebnisse, dass mittels [18F]-FLT-PET, nicht aber mittels [18F]-FDG-PET, eine frühe Prognose hinsichtlich der Wirksamkeit der angewandten Inhibitor-Therapie getroffen werden kann.

## Summary

Anaplastic large-cell lymphoma (ALCL) is a type of non-Hodgkin lymphoma involving aberrant T-cells. It features in the World Health Organisation (WHO) classification of lymphomas. The anaplastic large-cell lymphoma occurs mainly in children and young people, However, older adults can also be affected. It makes up about 15% of the child's non-Hodgkin lymphomas. 50-60% of anaplastic large cell lymphoma (ALCL) are associated with the t(2;5)(p23;q53) chromosomal translocation involving the anaplastic lymphoma kinase (ALK) gene. ). A number of studies have shown that the constitutively active tyrosine kinase function of NPM-ALK is a key oncogenic event in the pathogenesis of t(2;5)-positive ALCLs, which leads to the constitutive activation of several signalling pathways including the STAT3, PI-3K/Akt and mTOR pathways .

In the treatment of malignant lymphomas, chemotherapy , complemented by radiation therapy, plays a crucial role. But many cytotoxic drugs cause serious side effects and are even carcinogenic. Meanwhile, targeted therapy or molecularly targeted therapy is a type of medication that blocks the growth of cancer cells by interfering with specific targeted molecules needed for carcinogenesis and tumor growth, rather than by simply interfering with all rapidly dividing cells (e.g. with traditional chemotherapy). Furthermore, targeted therapy has produced promising results for various haematological malignancies and solid tumors. Therefore, targeted cancer therapies are expected to be more effective than current treatments and less harmful to normal cells.

The diagnosis of malignant lymphomas requires a combination of morphological, molecular, genetic, immunohistochemical, and clinical data. Once the diagnosis HD or NHL has been established by biopsy of a particular site, determination of disease extent (staging) is important for therapeutic management and determining prognosis. Computed tomography (CT) is currently the most commonly used means for staging patients with malignant lymphoma. However, an important drawback of CT is its failure to detect pathologic changes in normal-sized structures and to detect lesions that have poor contrast with surrounding tissue. The increased glycolytic rate of malignant cells is the rationale behind the common use of 18F-fluoro-2-deoxyglucose (FDG) as a radiotracer in oncological PET studies. But because of the dependent on glucose metabolism is FDG not tumor specific, there is false-positive result in inflammation and false-negative uptake in hyperglycaemic patients. The thymidine analog [18F]-FLT (3'-deoxy-3'-[18F]fluorothymidine) accumulates in tumor tissue

according to the proliferative activity, and [18F]-FLT PET therefore allows more specific imaging of tumor progresses.

The purpose of this study is to establish FLT as superior surrogate marker for very early prediction of response to targeted drugs therapy in malignant lymphoma. We used various ALK-positive anaplastic large cell lymphoma (ALCL) cell lines to evaluate two inhibitors, the HSP90 inhibitor NVP-AUY922, and the mTOR inhibitor everolimus, both of which have shown to interfere with ALK-dependent oncogenic signal transduction. Their therapeutic effect was determined in vitro by MTT assay, [18F]fluorodeoxyglucose- (FDG) and [18F]fluorothymidine- (FLT) uptake, and by biochemical analysis of ALK-induced signalling. Micro FDG- and FLT-PET imaging studies in immunodeficient mice bearing ALCL xenotransplants were performed with the cell lines SUDHL-1 and Karpas299 to assess early treatment response to NVP-AUY922 or everolimus in vivo. SUDHL-1 cells showed sensitivity to both inhibitors in vitro. Importantly, we detected a significant reduction of FLT-uptake in SUDHL-1 bearing animals using both inhibitors compared to baseline as early as 5 days after initiation of targeted therapy. Immunostaining showed a decrease in Ki67 and an increase in cleaved caspase-3 staining. In contrast, FDG-uptake did not significantly decrease at early time points. Karpas299 xenotransplants, which are resistant to NVP-AUY922 and sensitive to everolimus treatment, showed an increase of mean FLT-uptake on day 2 after administration of NVP-AUY299, but a significant reduction in FLT-uptake upon everolimus treatment. In conclusion, we show that FLT- but not FDG-PET is able to predict response to treatment with specific inhibitors very early in the course of treatment and thus enables early prediction of treatment efficacy.

# 1 Abbreviations

7AAD: 7-Amino-Actinomycin

ALCL: anaplastic large cell lymphoma

ALK: anaplastic lymphoma kinase

APS: Ammoniumpersulfat

BFI: blood flow index

BFU: 1-(2'-deoxy-2'-fluoro-beta-D-arabino-furanosyl)-5-[76Br]-bromouracil

BSA: bovine serum albumin

BVD: in blood vessel density

CT: Computed tomography

DNA: Deoxyribonucleic acid

DTT: dithiothreitol

EDTA: ethylenediaminetetraacetic acid

ELISA: Enzyme-linked immunosorbent assay

ENT: equilibrative nucleoside transporters

FACS: Fluorescence activated cell sorting

FDG: 18F-fluoro-2-deoxyglucose

FLT: 3'-deoxy-3'-[18F]fluorothymidine

FMAU: 2'-[18F]-fluoro-beta-D-arabinofuranosyl-uracil

FOXO: Forkhead box o class

5-FU: 5-fluorouracil

GI50: the concentration of the anti-cancer drug that inhibits the growth of cancer

Hsp90: Heat shock protein 90

HUVEC : human umbilical endothelial cell

IC<sub>50</sub>: the concentration of a drug that inhibits a biological activity by 50%

IHC: immunohistochemistry

MCL: mantle cell lymphoma

MK: midikine

mTOR: mammalian target of rapamycin

mTORC1: mTOR Complex 1

MTT: 3-(4,5-Dimethylthiazol-2-yl)-2,5-diphenyltetrazolium bromide

NHL: non-Hodgkin lymphoma

NPM-ALK: nucleophosmin-anaplastic lymphoma kinase

P70 S6K: Ribosomal protein S6 kinase

PBS: phosphate-buffered saline

PCNA: proliferating cell antigen

PD: pharmacodynamic

PET: Positron emission tomography

PI3K: phosphatidylinositol 3-kinase

PI: Propidium iodide

PIP<sub>3</sub>: Phosphatidylinositol (3,4,5)-triphosphate (PtdIns(3,4,5)P<sub>3</sub>)

PMSF: phenylmethylsulfonyl fluoride

PTN: pleiotrophin

PS: phosphatidylserine

PVDF: polyvinylidene difluoride

REAL: Revised European-American Lymphoma classification

RNA: Ribonucleic acid

ROI: regions of interest

SCID: severe combined immunodeficient

SDS: sodium dodecyl sulfate

STAT3: Signal transducer and activator of transcription 3

TBF: tumor blood flow

TBR: Tumor-to-background ratios

Temed: Tetramethylethylenediamine

TK1: thymidine kinase-1

TSC: tuberous sclerosis

VEGF: vascular endothelial growth factor

## **2 Introduction**

### **2.1 Hodgkin´s and Non Hodgkin´s lymphoma**

#### **2.1.1 Classification of lymphoma**

Lymphoma is a cancer of the lymphocytes, a type of cell that forms part of the immune system. Typically, lymphoma is present as a solid tumor of lymphoid cells. Treatment might involve chemotherapy and in some cases radiotherapy and/or bone marrow transplantation, and can be curable depending on the histology, type, and stage of the disease (1). These malignant cells often originate in lymph nodes, presenting as an enlargement of the node (a tumor). It can also affect other organs in which case it is referred to as extra-nodal lymphoma. Extra-nodal sites include the skin, brain, bowels and bone. Lymphomas are closely related to lymphoid leukemias, which also originate in lymphocytes but typically involve only circulating blood and the bone marrow (where blood cells are generated in a process termed haematopoiesis) and do not usually form static tumors (1). There are many types of lymphomas, and in turn, lymphomas are a part of the broad group of diseases called hematological neoplasms.

Thomas Hodgkin published the first description of lymphoma in 1832, specifically of the form named after him, Hodgkin's lymphoma (2). Since then, many other forms of lymphoma have been described, grouped under several proposed classifications. The 1982 working formulation classification became very popular. It introduced the category non-Hodgkin lymphoma (NHL), divided into 16 different diseases. However, because these different lymphomas have little in common with each other, the NHL label is of limited usefulness for doctors or patients and is slowly being abandoned.

The WHO Classification, published in 2001 and updated in 2008 (3), is the latest classification of lymphoma and is based upon the foundations laid within the "Revised European-American Lymphoma classification" (REAL). This system attempts to group lymphomas by cell type (i.e. the normal cell type that most resembles the tumor) and defining phenotypic, molecular or cytogenetic characteristics. There are three large groups: the B cell, T cell, and natural killer cell tumors. Other less common groups, are also recognized. Hodgkin lymphoma, although considered separately within the World Health Organization (and preceding) classifications, is now recognized as being a tumor of, albeit markedly abnormal, lymphocytes of mature B cell lineage.

As reported from German Cancer Registry in 2008, the non-Hodgkin´s lymphoma in male adults stood 10th (a total of 7270) in most frequently occurring type of cancer and 9th (a total

of 6430) in female adults. Hodgkin's lymphomas in adults are much rarer. In 2012, the Cancer Registry counts with 7800 new cases from male and 6500 new cases from female on NHL diagnosed. Additionally, it is reported from Cancer Registry of 1100 estimated new male cases and of 900 new female cases who developed Hodgkin's lymphoma.

### **2.1.2 ALK-positive anaplastic large cell lymphoma**

ALK-positive anaplastic large cell lymphoma (ALCL) was recognized as a distinct entity in the 2008 World Health Organization (WHO) classification of malignant lymphomas (4). Anaplastic large-cell lymphoma (ALCL) is a type of non-Hodgkin lymphoma involving aberrant T-cells. The hallmark cells (and variants) show immunopositivity for CD30 (5)(also known as Ki-1). True positivity requires localisation of signal to the cell membrane and/or paranuclear region (cytoplasmic positivity is considered non-specific and non-informative). Another useful marker which helps to differentiate this lesion from Hodgkin lymphoma is Clusterin. The neoplastic cells have a golgi staining pattern (hence paranuclear staining), which is characteristic of this lymphoma. The cells are also typically positive for a subset of markers of T-cell lineage. However, as with other T-cell lymphomas, they are usually negative for the pan T-cell marker CD3. Occasional examples are of null (neither T nor B) cell type. These lymphomas show immunopositivity for ALK protein in 70% of cases. They are also typically positive for EMA. In contrast to many B-cell anaplastic CD30 positive lymphomas, they are negative for markers of Epstein-Barr Virus (EBV).

50-60% of anaplastic large cell lymphoma (ALCL) are associated with the t(2;5)(p23;q53) chromosomal translocation involving the anaplastic lymphoma kinase (ALK) gene (6, 7). The t(2;5) results in the expression of the oncogenic fusion protein nucleophosmin-anaplastic lymphoma kinase (NPM-ALK). A number of studies have shown that the constitutively active tyrosine kinase function of NPM-ALK is a key oncogenic event in the pathogenesis of t(2;5)-positive ALCLs, which leads to the constitutive activation of several signalling pathways including the STAT3, PI-3K/Akt and mTOR pathways (8, 9).

Other karyotype aberrations including oncogenic fusion of *ALK* to other fusion partners have been identified in inflammatory myofibroblastic tumors, non-small-cell lung cancers and other solid tumors (10, 11). Fusion proteins resulted from oncogenic translocations carry constitutive tyrosine kinase activity because of dimerization and kinase domain autoactivation induced by fusion partner. Although the exact function of full-length ALK is not fully understood, it is believed that it is involved in neuronal cell differentiation, regeneration, synapse formation and muscle cell migration (12).

In its native, full-length single chain receptor form, ALK consists of 1620 amino acids. Within these 1620 amino acids, there is a 1030 residue extracellular region. It contains multiple subdomains such as an LDL-A domain, a MAM domain (meprin, A5, mu), and a glycine-rich region (Fig. 1)(13, 14)and a cytoplasmic portion. It contains 563 residues coding for the kinase catalytic domain. This full-length form is implicated in malignancies where ALK promotes tumorigenesis via the activation by pleiotrophin (PTN) and midikine (MK) (15, 16). Upon the ligand binding, it leads to receptor dimerization and activation via *trans*-autophosphorylation of tyrosine residues within kinase domain activation loop (A-loop) segments. Phosphorylation of sites outside the A-loop serve as docking sites for downstream SH2 and PTB domain-containing effector and adapter proteins involved in the signal transduction cascade. Genetic abnormalities or disease states leading to ALK hyperactivation manifest in oncogenic transformation from overstimulation of downstream STAT, Ras/Raf/MEK, PI3K/AKT, and PI3K/PLC-  $\gamma$  pathways involved in cell survival, differentiation and apoptosis (11). One of STAT signalling pathway is the STAT3 pathway (17-19).STAT3 has been proved to be oncogenic in a variety of human cancer (20-24). Many studies suggest that STAT3 activation is crucial for the pathogenesis of ALK-ALCL as well as NPM-ALK (17, 19, 25). Recently, the *ALK* locus was found to be a site of genetic alteration in the form of comatic and germline mutations that play a major role in advances neuroblastoma (26-28).

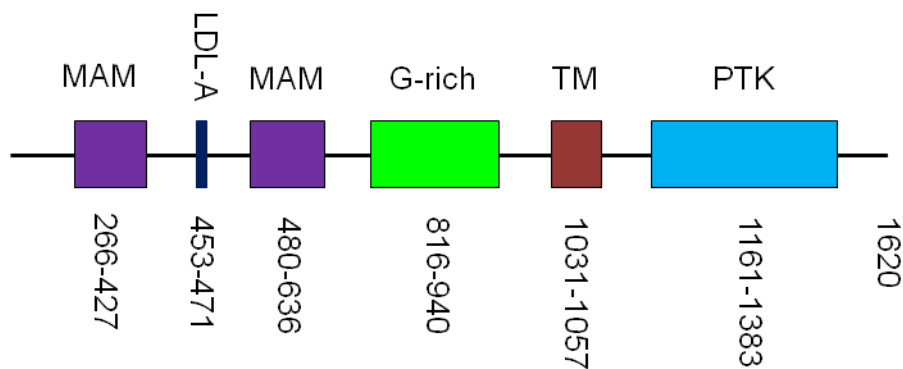


**Fig. 1:** Full-length single chain receptor form of ALK ( according to Christian C. Lee et al. BJ 2010)

Moreover, recent studies suggest that ALK exhibits a unique peptide substrate specificity and autoactivation mechanism (29). In contrast to other RTKs, a narrower substrate peptide specificity profile is reported for ALK. Phosphorylating peptide substrates of ALK has greater

efficiency in corresponding to its own A-loop sequence than generic and conventional peptide substrates, frequently used in tyrosine kinase activity measurements (29).

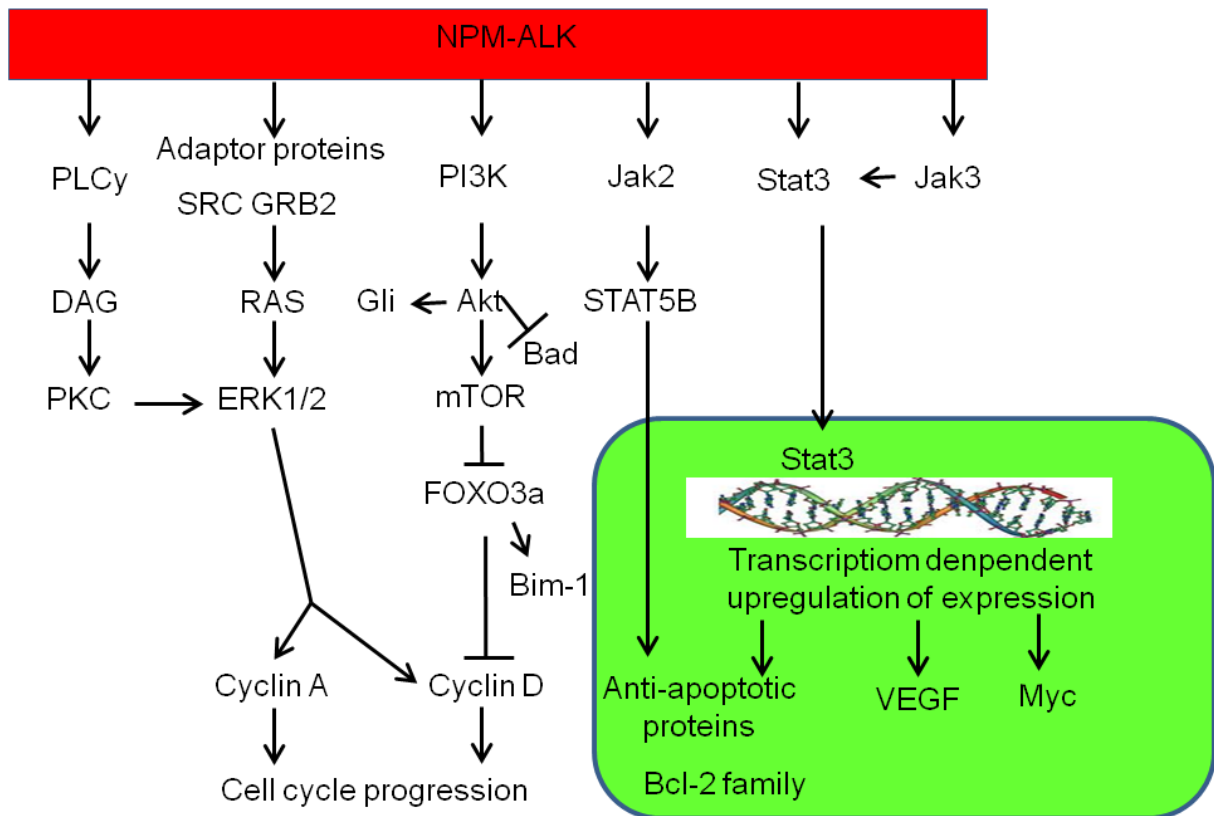


**Fig. 2:** The Anaplastic lymphoma kinase (ALK) signaling cascade (according to Yael P. et al. Clin Cancer Res 2009)

Additionally, variant translocations involving ALK and other partner genes on chromosomes 1, 2, 3, 17, 19 and 22 have been reported (12). These translocation result in abnormal expression of ALK chimeric proteins with tyrosine kinase activity and oncogenic properties (12). ALK fusion proteins can be detected using anti-ALK antibodies, which has crucial diagnostic value. (30, 31).The NPM-ALK kinase exhibits phosphotransferase activity (Fig. 2). Meanwhile, through its interaction with various ALK-adapter proteins, it induces cell transformation and increase cell proliferation *in vitro*. The chaperones heat shock proteins 90 (Hsp90) and 70(Hsp70) play a critical role in the folding and maturation of several oncogenic protein kinases. This is because of perturbation of Hsp90 structure affects the stability and degradation of Hsp90- and Hsp70-bound substrates. This process is triggered by benzoquinone ansamycin antibiotics, a Hsp90-binding small molecule.

## **2.2 New therapeutic approaches for lymphoma and monitoring of the therapeutic response**

Targeted therapy against an oncogenic molecule or pathway has produced promising results for various haematological malignancies and solid tumors such as chronic myelogenous leukemia (imatinib) (32) and lung cancer (gefitinib). Hsp90 is essential for eukaryotic cell survival. In many tumors, Hsp90 is either overexpressed and/or exclusively in an activated state with a high chaperoning efficiency (33). Hsp90 is an attractive cancer target, due to its frequent dysregulation in client proteins among solid and haematological malignancies. These client proteins include transcription factors (i.e. hormone receptors), signalling kinases (for example BCR-ABL, NPM-ALK) and chromatin remodelling factors.

Hsp90 inhibitors affect multiple targets in signal transduction pathways by inactivating a large number of oncoproteins. This theory is supported by pre-clinical studies, where HSP90 inhibitors induced cell cycle arrest and apoptosis in a variety of haematological and solid malignancies including lymphomas and sarcomas.

Hsp90 inhibitors act synergistically with a range of standard therapeutic agents. This means Hsp90 inhibitors could be particularly effective in combination therapies.

Hence, Hsp90 has attracted considerable interest in recent years as a potential therapeutic target for lymphoma and other malignancies (34).

The phosphatidylinositol 3-kinase (PI3K/AKT) pathway is the pathway that is altered in many tumors as well as lymphomas (35). This multifunctional pathway has been recognized as a particularly attractive target for patients with lymphoma. "The PI3K pathway appears continuously deregulated among lymphoma malignancies," reported Sonali M. Smith, MD, director of the Lymphoma Program at the University of Chicago Medical Center, Illinois. Molecular ties linked to abnormal PI3K pathway signaling have been demonstrated in mantle cell lymphoma (MCL) (36), non-Hodgkin lymphoma (37), as well as in Hodgkin lymphoma (38). Specifically, mTOR, a serine/threonine kinase that is a key downstream target of the PI3K pathway, as well as an important regulator of normal development, has been associated with lymphoma genesis.

The PI3K/AKT pathway affects various aspects of malignant behaviors such as cell growth proliferation and survival signals (39, 40). Hsp90 inhibitors affect AKT activity indirectly

through depletion of upstream signalling molecules (for example, ERBB family members) and directly through preventing Hsp90-dependent conformational stability of AKT (41-43). Hsp90 is a ubiquitously expressed molecular chaperone playing an important role in the post-translational conformational maturation and in the activation of a large number of client proteins that have been implicated in oncogenesis (44). Hsp90 functions as a dimer and operates in a highly regulated ATP-cycle together with a group of co-chaperones (45). Inhibition of the ATPase activity at the N-terminus of Hsp90 is used by clinical inhibitors. Currently, the most advanced HSP90 inhibitor in clinical trials are the benzoquinone ansamycin class. They have shown promising results in human tumor xenograft models (44, 46) and are tested in phase II/III clinical trials for solid tumors and haematological malignancies. The most studied compound of this class, tanespimycin or benzoquinone ansamycin antibiotics (17-AAG). It has relatively poor physicochemical properties, poses a delivery challenge in clinical use (47). This issue is partially resolved from the development of the water-soluble analog alvespimycin (17-DMAG) (46). The 17-AGG hydroquinone IPI-504 has also been developed as less toxic and/or more soluble drugs (48, 49). The development of Hsp90 inhibitors with more favourable pharmaceutical properties is being intensely investigated. NVP-AUY922 is a potential synthetic small-molecule Hsp90 inhibitor (50). NVP-AUY922 is an isoxazole-base compound which competitively inhibits the ATPase activity of Hsp90. Heat shock proteins act as molecular chaperones. They are involved in the folding of cellular proteins. Many of heat shock proteins are also involved in the regulation of cell proliferation, survival, and apoptosis. Inhibition of Hsp90 by NVP-AUY922 shows degradation of client proteins. This translates into an anti-tumor effect of NVP-AUY922, which is shown in non-clinical *in vitro* and *in vivo* studies. Binding of NVP-AUY922 also induces a stress response that is manifested by changes to the Hsp90-p23 complex and increased levels of Hsp70. NVP-AUY922 is an ATP-competitive inhibitor of Hsp90. It prevents the binding of ATP to Hsp90 and impairs the formation of a complex of Hsp90 with the co-chaperone p23, an essential for the function of Hsp90. NVP-AUY922 reduced the cellular levels of important client proteins in tumor cells, such as, ErbB2 (Her2) and p-AKT, indicating that inhibition of Hsp90 by NVP-AUY922 leads to destabilization and degradation of these proteins. In addition, NVP-AUY922 induces degradation of client proteins and inhibition of downstream signalling. At the cellular level, NVP-AUY922 leads to cell cycle arrest and apoptosis. This mediates inhibition of cell proliferation of a panel of tumor and non-tumor cell lines at low nanomolar concentrations. *In vivo* anti-tumor effect has been observed in a number of mouse xenograft models with corresponding effects on pharmacodynamic markers.

BGT266 is a potent pan-class I PI3K and mTOR inhibitor, belongs to the class of imidazoquinoline derivatives. The inhibitory effect of BGT226 is mediated through binding to Valine-882 and Serine-805 in the hinge region of the ATP-binding pocket of the p110 subunit of PI3K, displaying a flight preference for the  $\alpha$ -isoform. Based on preclinical research from Novartis BGT266 effectively inhibits proliferation and colony formation of a variety of tumor cell lines. It also inhibits growth of tumors in a variety of mouse xenograft models, such as breast cancer, prostate cancer, glioblastoma multiforme, lung cancer and colorectal cancer models. BGT266 has no relevant inhibitory activity against either receptor tyrosine kinases involved in proliferation and survival (e.g. EGFR/HER-1, IGF-1R, cMet) or the angiogenic switch (e.g. Kdr, Tek, EpB4). However, it has inhibitory activity against AGC family kinase members known to be activated by the PI3K pathway (e.g. PDK1) and AKT/PKB itself. BGT226 dramatically reduces the phosphorylation of PKB, a direct downstream effector of PI3K. This biological activity correlates with strong inhibition of other effectors of PI3K signalling, such as p70 S6K protein and inhibition of proliferation and colony formation of a variety of tumor cell lines, regardless of their genetic background. Therefore, BGT226 was chosen as a PI3K inhibitor in our study to treat the ALCL ALK+ lymphoma.

As a widely used small molecular inhibitor, RAD001 (everolimus) was also chosen to build up this research. RAD001 is a derivative of rapamycin. It acts as a signal transduction inhibitor. Its target is mTOR, a key serine-threonine kinase regulation protein synthesis and ultimately cell growth, cell proliferation, angiogenesis and survival. Downstream of PI3/AKT, mTOR can be considered as a component in the PI3K/AKT/mTOR pathway which is known to be dysregulated in numerous human cancers. Molecular epidemiological studies show that in addition to a high frequency in specific cancers, activation of the PI3K/AKT/mTOR pathway is often a characteristic of worsening prognosis (through increased aggressiveness), resistance to treatment, extension and progression.

A variety of preclinical studies have confirmed the role of this pathway in tumor development. Moreover, function models have demonstrated that constitutive activation of kinases such as AKT, can lead to the inexorable development of cancers resembling those are characterized by frequent activation of the same kinase. This is complemented by demonstration of the antitumor activity of kinase inhibitors acting in vitro and in vivo. Many experiments (51-53) showed that RAD001 is capable of inhibiting the proliferation and growth of a wide spectrum of tumor cell lines and tumors. The antiproliferative effects of RAD001 are achieved in nanomolar concentrations that already show positive results in clinical trials. An important aspect of the antitumor effect of RAD001 is its potential to act on both tumor cells directly (to inhibit growth) and indirectly (by inhibiting angiogenesis). During observation of in vivo

sensitivity of xenograft, however, in vitro cells are detected to be resistance to RAD001. This means the drug has the potential to act on the vascular component of the supporting peritumoral stroma. The antiangiogenic property of RAD001 has been confirmed through experiments which demonstrate the effect of RAD001 in countering VEGF-induced proliferation of human umbilical endothelial cells (HUVECs) (54) in vitro. RAD001 has been in clinical development since 1996 to prevent rejection in patients undergoing solid organ transplants. It is developed by an immunosuppressant, associated with cyclosporine and glucocorticoids. In this context mTOR inhibition oppose interleukin-stimulated proliferation of activated T-lymphocytes. An antiproliferative effect on immuno-competent cells is another reason for investigation on the drug's activity in autoimmune diseases. The use of RAD001 in the inhibition of intimal proliferation has been investigated after coronary angioplasty through its incorporation into drug-eluding stents.

### **2.3 Lymphoma diagnosis and Imaging – CT and PET**

The diagnosis of malignant lymphomas requires a combination of morphological, molecular, genetic, immunohistochemical, and clinical data. Once the diagnosis HD or NHL has been established by biopsy of a particular site, determination of disease extent (staging) is important for therapeutic management and determining prognosis. Moreover, knowing the sites of involvement at time of diagnosis makes it possible to accurately restage at the end of therapy and document a complete remission (55, 56). Staging of HD and NHL is based on the Ann Arbor classification with the addition of a definition of bulky disease often referred to as the Cotswold modification (Table 1) (57). This staging system encompasses the number of sites of disease involved, the type of involvement (nodal or extra-nodal), and the distribution of disease (58). Computed tomography (CT) is currently the most commonly used means for staging patients with malignant lymphoma (55, 56). The introduction of CT in the early 1970s was a tremendous breakthrough in non-invasive imaging, and its potential for staging malignant lymphoma was soon recognized and investigated (59). Lymph nodes of 5 mm or less in diameter can be detected throughout the whole body. In combination with powered injectors for rapid bolus administration of intravenous contrast medium, focal extra-nodal lesions on the order of a few millimetres can be identified (60, 61).

**Table 1.** Cotswold and Ann-Arbor classification (Thomas C. Kwee et al. Blood 2008)

Stage	Involvement
I	Single lymph node region (I) or one extralymphatic site (IE)
II	Two or more lymph node regions, same side of the diaphragm (II) or local extralymphatic extension plus one or more lymph node regions same side of the diaphragm (IIE)
III	Lymph node regions on both sides of the diaphragm (III), which may be accompanied by local extralymphatic extension (IIIE)
IV	Diffuse involvement of one or more extralymphatic organs or sites

Suffix	
A	no systemic symptoms
B	presence of at least one of these symptoms: unexplained weight loss of 10% or more of body weight in the 6 months preceding staging; recurrent unexplained fever > 38°C; recurrent night sweats.

Bulky tumor	either a single mass exceeding 10 cm in the largest diameter or a mediastinal mass exceeding one third of the maximum transverse trans-thoracic diameter measured on a standard posterior-anterior chest X-ray at the level of the T5-T6 intervertebral disk
-------------	--

Determination of nodal involvement is based on size criteria. Lymph nodes with a short-axis diameter greater than 10 mm are generally considered positive. Furthermore, clustering of normal sized but prominent lymph nodes in the anterior mediastinum and the mesentery is suspicious for disease. The use of intravenous contrast medium is not helpful in differentiating normal from malignant lymph nodes. General criteria for extra-nodal involvement are organomegaly, abnormal mass or structural changes in a normal-sized organ, and abnormal contrast enhancement (61).

However, as Kwee et al. have described in 2008, an important drawback of CT is its failure to detect pathologic changes in normal-sized structures and to detect lesions that have poor contrast with surrounding tissue. Another weakness of CT is that it is not reliable in the detection of bone marrow disease, which, if present, by definition indicates stage IV disease (61). Furthermore, CT may not be able to differentiate residual viable tumor tissue from therapy-induced fibrosis. Additionally, two other CT studies reported a low-to-mode rate specificity in restaging malignant lymphoma (62, 63).

Positron emission tomography (PET) was developed in the early 1970s soon after CT (64). PET is based on the use of positron-emitting radiopharmaceuticals and the detection in coincidence of the 2 nearly collinear 511-keV photons emitted following positron annihilation with an electron. The increased glycolytic rate of malignant cells is the rationale behind the common use of <sup>18</sup>F-fluoro-2-deoxyglucose (FDG) as a radiotracer in oncological PET studies (65). Imaging of malignant lymphoma with FDG was first described in 1987 (66), and the first reports on FDG-PET as a whole-body staging method in malignant lymphoma appeared in the 1990s (67-70). PET technology has improved dramatically since its development. Initial patient imaging units had a system resolution greater than 15 mm, whereas current units have a 4 to 5 mm resolution (65). FDG-PET examinations for staging malignant lymphoma should be performed on dedicated (full ring) PET scanners, because dual-head gamma cameras in coincidence mode are unreliable in detecting lesions less than 15 to 20mm in diameter (71-73).

Functional imaging with positron emission tomography (PET) and the glucose analog [<sup>18</sup>F]-FDG has been recently suggested to identify responding lymphomas and determine ongoing treatment in patients with malignant lymphoma (74, 75). This strategy is based on the assumption that viable cancer cells have a significantly higher glucose use compared to surrounding normal tissues.

Therefore, the main advantage of FDG-PET over anatomical imaging techniques, such as CT, is its ability to detect metabolic changes in areas involved with malignant lymphoma before structural changes become visible. It also is likely that FDG-PET surpasses CT in differentiating residual viable tumor tissue from therapy-induced fibrosis (57). Indeed, accuracy of FDG-PET in restaging of malignant lymphoma seems to be higher than that of CT (57). Routinely, FDG avid malignant lymphomas (HD, diffuse large B-cell lymphoma, follicular lymphoma, and mantle cell lymphoma) are well visualized, both in initial staging and restaging (76-78). However, some subtypes of NHL, predominantly low-grade lymphomas, may have low or even no uptake of FDG. Nodal and extra-nodal marginal zone lymphomas (77-84), small lymphocytic lymphomas (85), primary duodenal follicular lymphoma (86), cutaneous T-cell lymphomas (87), and peripheral T-cell lymphomas (77) all have been

reported to be possibly FDG negative. Most recent advances in cancer treatment have derived from the development of disease-specific molecular-targeted agents. Deregulated cell cycle progression is a hallmark of various human cancers including malignant lymphomas. Notably, with respect to in vivo imaging, proliferative activity has been shown to be more specific for malignant tumors than that of glucose metabolism (88). The thymidine analog [18F]-FLT (3'-deoxy-3'-[18F]fluorothymidine) accumulates in tumor tissue according to the proliferative activity and that FLT-PET enables non-invasive imaging of tumor proliferation. FLT is accumulated after its phosphorylation by cellular thymidine kinase-1 (TK1). TK1 is a key enzyme of the pyrimidine salvage pathway of DNA synthesis whose activity is higher in malignant than in benign cells (89, 90). Since this enzyme is only functional during the S-phase, uptake of FLT is tied to the cell proliferation (91). This has been substantiated by the correlations between FLT-uptake and TK enzyme activity and cell proliferation which is measured by Ki-67 and proliferating cell antigen (PCNA) expression (92-97). The reason to use [<sup>18</sup>F]-FLT as a surrogate marker for cellular proliferation is based on its substrate specificity for the cell cycle regulated protein TK1. Barthel et al. recently reported that in vivo uptake of [<sup>18</sup>F]-FLT is closely related to TK1 activity and cellular concentration of ATP (98). Since, [18F]-FLT acts as chain terminator and only a small amount of intracellular [18F]-FLT is incorporated into DNA. [18F]-FLT is therefore not a direct marker of proliferation. However, several studies in humans show still a significant correlation of tumor proliferation and [18F]-FLT-uptake in lymphoma and other solid tumors (93, 99, 100). As a preclinical model for monitoring therapeutic response, a significant decrease of FLT-uptake was observed in tumor-bearing mice as early as 24 hours after chemotherapy (101-103). Importantly, in a clinical study, we were able to demonstrate that the reduction of FLT-uptake in aggressive lymphomas after the first course of therapy correlates with response at the end of the treatment (104).

Therefore, the [18F]-FLT as a proliferation marker as well as the golden standard [18F]-FDG are chosen to predict the therapeutic response in our study using anaplastic lymphoma kinase (ALK) -positive anaplastic large cell lymphoma (ALCL).

## **2.4 Purpose**

The aim of this study is to establish FLT as an adequate and robust surrogate marker for response to treatment which can be used very early in the course a targeted drug therapy. Additionally, thymidine uptake in SCID mice bearing SUDHL-1 or Karpas299 lymphoma xenotransplants was assessed prior to and early in the course of therapy with Hsp90 inhibitor

NVP-AUY922, mTOR inhibitor RAD001 or PI3K inhibitor BGT266 using a modern micro PET-CT scanner. Tumor-to-background ratios (TBR) of the FLT-uptake were compared to those of corresponding FDG-PET scans. PET findings were correlated with histopathology and in-vitro data including cellular tracer uptake, cell cycle related protein expression, cell cycle distribution and viability assessment.

## **3 Methods**

### **3.1 Kinase inhibitors**

NVP-AUY922 (HSP 90 inhibitor), BGT226 (PI3K inhibitor) and RAD001 (mTOR inhibitor) were produced from Novartis (Consumer health GmbH, Germany). NVP-AUY922 and RAD001 were solubilised in 5% glucose solution to 200 $\mu$ M and 1 $\mu$ M, BGT266 was diluted with 0.01% HCl to 1 $\mu$ M as primer solution for cell treatment It was stored at -20°C and protected from light. The primer solution was then diluted in the concentration rang 0-1000 nM for AUY922, 0-100 nM for BGT226 and 0-100 nM for RAD001 with DMEM for in vitro research.

### **3.2 Cell culture**

The murine pro-B-lymphoid cell line Ba/F3 ((ALK)-positive ALCL cell, pro-B-cell, murine, COPE), was maintained in DMEM (Dulbecco's Modified Eagle Medium) (Invitrogen GmbH, Darmstadt Germany) and was recombinant with 10% fetal bovine serum, 1mM L-glutamine, 1% penicilline/streptomycine (Invitrogen, Darmstadt Germany) and 1ng/ml murine recombinant interlerkin-3 (IL-3, R&D Systems, DPC Bierman GmbH, Wiesbaden, Germany). Ba/F3-NPM-ALK transformed cells and ALK+ALCL (JB-6: (ALK)-positive ALCL cell, human histiocytic lymphoma cell, ATCC; Karpas299: (ALK)-positive ALCL cell, humen T cell lymphoma, ATCC; SUDHL-1: (ALK)-positive ALCL cell, human histiocytic lymphoma cell, ATCC; SUP-M2: (ALK)-positive ALCL cell, human histiocytic lymphoma cell,ATCC; SR-789: (ALK)-positive ALCL cell, human histiocytic lymphoma cell, ATCC) were cultured in DMEM medium supplemented with 10% fetal bovine serum, 1mM L-glutamine, and 1% penicilline/streptomycine. All cell lines were cultured in an incubator (UniTec GmbH, Regensburg, Germany) at 37°C with 5% CO<sub>2</sub>.

### **3.3 Cell counting**

For cell counting, 20 $\mu$ l cells with cell culture was mixed with trypan blue to 80 $\mu$ l Eppendorf Tubes Pipette (1:5 dilution), 20 $\mu$ l from the mixture was placed in Neubauer counting chamber, Under microscope, cells were counted in 4x16 large squares and thus the number of vital and dead (blue stained) cells determined.

### **3.4 Cell proliferation and viability assay**

Cells were seeded in 96-well flat-bottom plates and incubated with the indicated cytostatic drugs for 24h, 48h or 72h to determine of IC<sub>50</sub>. NVP-AUY922 stock solution was diluted in cell culture medium and tested in concentration ranging from 0 to 1000 nM. RAD001 and BGT266 were diluted from 0 to 100 nM. Cell density was adjusted to  $5 \times 10^5$  or  $2 \times 10^5$  cell/well for cell lines in final volume of 100  $\mu$ l per well Cell viability and growth retardation was determined by the 3-(4, 5-Dimethylthiazol-2-yl)-2, 5-diphenyltetrazolium bromide, which is a yellow tetrazolium (MTT) cell proliferation assay (Aqueous Celltiter96®, Promega, Mannheim, Germany). All experiments with cell lines were performed in threefold approach. Mean and standard deviation were determined to analyse the effect.

### **3.5 Cell cycle distribution and apoptosis analysis (fluorescence activated cell sorting – FACS)**

Cell cycle distribution was detected using PI-staining. Propidium iodide (PI) binds to DNA by intercalating between the bases with little or no sequence preference and with a stoichiometry of one dye per 4.5 base pairs of DNA. PI also binds to RNA which treatment with nucleases to distinguish between RNA and DNA staining. When bind to nucleic acids, the absorption maximum for PI is 535 nm and the fluorescence emission maximum is 617 nm. PI can be excited with a xenon or mercury-arc lamp or with the 488 line of an argon-ion laser. It is membrane impermeable and generally excluded from viable cells. PI is commonly used for identifying dead cells in a population and as a counterstain in multicolor fluorescent techniques.

The  $2 \times 10^6$  cells were collected after 24, 48 and 72 hours (For co-incubations with sequential exposure, treatment was started with 24 hours incubation for the first feed and the second feed was added to the first feed last 24hours of incubation, resulting in a total incubation time of 72hours.) of treatment and washed twice in phosphate-buffered saline, then fixed overnight using 70% ethanol. Following centrifugation the supernatant was discarded and the cell pellet was resuspended in 0.2% propidium iodide (Fluka, Heidelberg, Germany) dilution buffer and then supplemented with 80  $\mu$ g/ml RNase (RNase, DNase free; Roche Diagnostics GmbH, Mannheim, Germany). Samples were kept at 37°C for 30 min and then were analysed by flow cytometry (FACS Calibur System; BD Biosciences, Heidelberg, Germany).

Fragments of damaged or apoptotic cells were determined as pre-G1 fraction using Flow Cytometry Analysis software (FlowJo). All experiments were performed in triplicate.

Apoptosis is a process, occurs during embryonic development as well as in maintenance of tissue homeostasis. The apoptotic program is characterized by several morphologic features, such as loss of plasma membrane asymmetry and attachment, condensation of the cytoplasm or nucleus, as well as internucleosomal cleavage of DNA. Loss of plasma membrane is one of the earliest features. In apoptotic cells, the membrane phospholipid phosphatidylserine (PS) is translocated from the inner to the outer leaflet of the plasma membrane, thereby exposing PS to the external cellular environment. Annexin V is a 35-36 kDa  $\text{Ca}^{2+}$  dependent phospholipid-binding protein which has a high affinity for PS, and binds to cells with exposed PS. Annexin V could be conjugated to fluorochromes including FITC. This format retains its high affinity for PS and thus serves as a sensitive probe for flow cytometric analysis of cells that are undergoing apoptosis. Since externalization of PS occurs in the earlier stages of apoptosis, FITC Annexin V staining can identify apoptosis at an earlier stage than assays based on nuclear changes such as DNA fragmentation. FITC Annexin V staining precedes the loss of membrane integrity which accompanies the latest stages of cell death resulting from either apoptotic or necrotic processes. Therefore, staining with FITC Annexin V is typically used in conjunction with a vital dye such as propidium iodide (PI) or 7-Amino-Actinomycin (7-AAD) to allow the investigator to identify early apoptotic cells (PI negative, FITC Annexin V positive). Viable cells with intact membranes exclude PI, whereas the membranes of dead and damaged cells are permeable to PI. For example, cells that are considered viable are FITC Annexin V and PI negative; cells that are in early apoptosis are FITC Annexin V positive and PI negative; and cells that are in late apoptosis or already dead are both FITC Annexin V and PI positive. This assay does not distinguish between cells that have undergone apoptotic death versus those that have died as a result of a necrotic pathway because in either case, the dead cells will stain with both Annexin-FITC and PI.

The  $2 \times 10^6$  cells were collected after 48 hours of treatment and washed twice in phosphate-buffered saline, then suspended in Annexin V binding-Buffer (0.1 M HEPES/NaOH (pH 7.4), 1.4 M NaCl, 25 mM  $\text{CaCl}_2$ . For a 1X working solution, dilute 1 part of the 10X Annexin V Binding Buffer to 9 parts of distilled water.), then supplemented with 2.5  $\mu\text{g}$  Annexin V-FITC (FITC Annexin V, BD Pharmingen™, Heidelberg, Germany) and 5  $\mu\text{g}$  PI (50  $\mu\text{g}/\text{ml}$ , Fluka, Heidelberg, Germany). Samples were kept at  $0^\circ\text{C}$  for 15 min and then were analysed by flow cytometry (FACS Calibur System; BD Biosciences, Heidelberg, Germany). Fragments of damaged or apoptotic cells were determined as PI+ and Annexin V+ fraction using Flow Cytometry Analysis software (FlowJo). All experiments were performed in triplicate.

### 3.6 Radiosynthesis of FLT and FDG

FLT was provided by Prof. H.-J. Wester according to a simplified labelling approach reported by Machulla et al (105). Before administration of the radiotracer, all mice were anesthetized with 4% isoflurane (Abbott GmbH, Wiesbaden, Germany) using a veterinary anesthesia System (Vetland Medical Sales and Services, Louisville, KY, USA). During PET imaging, the dose was reduced to 1.5% isoflurane. Imaging with FLT- or FDG-PET was performed using a dedicated small animal PET system (MicroPET, Focus 120, SIEMENS Preclinical Solutions, Knoxville, TN, USA). FLT or FDG/mouse (3.7–7.4 MBq) was injected intravenously, and data acquisition was started 45 min after the tracer administration. Data were acquired for 15 min. All acquisitions were done in listmode format and histogrammed into a frame sinogram. The sinogram was reconstructed into a 128×128×95 voxel image with filtered back projection method with a cut-off at the Nyquist frequency. The voxel size equals 0.433×0.433× 0.796 mm<sup>3</sup>. Data were normalized and corrected for randoms, deadtime, and decay. Tumor-to-background ratios (TBR) were calculated to semi-quantitatively assess the tracer accumulation in the tumor. For this purpose, region of interest (3D-ROI) were manually placed over the tumor and corresponding regions of interest (ROIs) were drawn on the contralateral side of transaxial sections. The tracer uptake in latter region or mean tracer uptake in the two spinal muscles is defined as background.

### 3.7 Cellular uptake of FLT and FDG

5× 10<sup>5</sup> cells were cultured after 24hrs as above in 1ml DMEM with above described supplements in 9-well flat-bottom plates for inhibitor treatment. After treatment, cell cultures were moved to 1.5ml Eppendorf-cups (Eppendorf AG, Hamburg, Germany) and 370KBq [<sup>18</sup>F]-FLT or [<sup>18</sup>F]-FDG in 100 µl was added into the samples. After incubation at 37°C for 45 minutes, the samples were washed with PBS for 3 times. The PBS must be completely removed in the end. The cells were then analyzed for radioactivity using an automated gamma-counter (Cobra II, Packard Instruments). Data were decay corrected and expressed as percentage of uptake / total activity administered. All experiments were performed in triplicate.

### 3.8 Western blot analysis

$2 \times 10^6$  cells were cultured as above in 3 ml DMEM with above described supplements for inhibitor treatment. After treatment, cells were washed twice in ice-cold PBS and were lysed in 150 $\mu$ l ice-cold lysis buffer containing one protease-inhibitor-tablet, 20% prime lysis buffer (5 times), 4% phosphate-buffer (pH 7.0), 20% Na-pyrophosphate (pH 7.0 – 7.5), 10% NaF-buffer, 1% phenylmethylsulfonyl fluoride (PMSF) buffer and 1% orthovanadate (100mmolar) buffer. Whole cell lysates (130-150 $\mu$ l) were mixed with an equal volume of 2x loading buffer. The lysates and pre-stained molecular weight markers were heated for 15 min at 95°C and separated by 7.5% SDS-polyacrylamide gel electrophoresis (SDS-PAGE) at 160V per gel for 4 hours or at 30 V for overnight. Then proteins were transferred to a PVDF membrane at 800 mA for 60-90 min, depending on the protein weight. The membrane was blocked in Tris-buffered saline containing 5% BSA or milk and 1%PBS-Tween-20 for 45 min. Concentrations of proteins were determined via the Bio-Rad Protein assay strictly following the manufacturer's instructions. Proteins (30-40  $\mu$ g/lane) were separated on a denaturing 7.5% SDS polyacrylamide gel and transferred to a nitrocellulose membrane. Membranes were blocked in 5% BSA in phosphate-buffered saline (PBS) and subsequently incubated overnight at 4°C or 2 hours at room temperature with primary antibody. After three times washes, the membranes were incubated with secondary antibody against rabbit IgG or mouse IgG diluted 1: 10,000 in % PBS- Tween for 30min. to 45min. at room temperature. For detection of  $\beta$ -actin, the same membranes were incubated with mice polyclonal anti-beta actin antibody overnight at 4°C or 1h at room temperature and processed as described.

#### 3.8.1 Stock solution

5x prime lysis buffer: 50 mM Tris-HCl, pH 7.4; 650 mM NaCl; 25 mM EDTA (ethylenediaminetetraacetic acid), pH 8.0; 5%Triton X-100

5x Na-Pyrophosphat buffer (50 mM): pH 7.0-7.5: 2.66 g solubilised in 200 ml dist. water

10x NaF (0.5 M): 4.2 g solubilised in 200 ml

100x benzamidine (5 mM): 7.85 g equated in 50 ml isopropanol, and stored in -20°C

100x PMSF (0.1 mM): 0.174 g equated in 10 ml isopropanol, and stored in -20°C

100x orthovanadate (100 mM): about 5 mg solubilised in dist. Water

Volume of dist. Water in ml =  $m_{(\text{weight})}$  in mg / 183 (mg/mmol)

2x loading buffer: 10 ml DTT (dithiothreitol); 5ml Tris-HCl; 20 ml 10% SDS, 2.5 ml 1% bromphenolblue and 10 ml 100% glycerol

DTT (1M): 15.4 g dithiothreitol solubilised in 100 ml dist. Water

Tris-HCl (1M): 12.1 g Tris solubilised in 100 ml dist. Water, pH set with HCl to 6.8

10% SDS: 10 g SDS solubilised in 100 ml dist. Water

1% bromphenolblue: 0.1 g bromphenolblue solubilised in 100 ml dist. water

### 3.8.2 Gel electrophoresis

- Stacking-gel buffer:
  - Acrylamide/Bis-acrylamide
  - Staking-gel buffer 0.5 M TRIS HCl pH 6.8  
6.05 g TRIS, 0.40 g SDS in 100 ml dist. water, pH- value setting with HCl
  - Dist. water
  - Temed ( Tetramethylethylenediamine)
  - 10% APS ( Ammoniumpersulfate)  
100 mg dissolved in 1 ml dist. water
- Running-gel buffer:
  - Acrylamide/Bis-acrylamide
  - Running-gel buffer 1.5 M TRIS HCl pH 8,8  
91 g TRIS, 2 g SDS dissolved in 500 ml dist. water pH- value setting with HCl
  - Dist. water
  - Temed ( Tetramethylethylenediamine)
  - 10% APS ( Ammonium persulfate)  
100 mg dissolved in 1 ml dist. water

For different applications, we need to change the desired percentage of acrylamide, make up 30 ml of running gel by selecting one of the following percentages and mixing the ingredients shown below. Gel will polymerize fairly quickly after adding TEMED and APS, so they will not be added until the gel is been ready to pour.

- Running-gel Solution

	7%	10%	12%	15%
H <sub>2</sub> O	15.3 ml	12.3 ml	10.2 ml	7.2 ml
1.5 M Tris-HCl, pH 8.8	7.5 ml	7.5 ml	7.5 ml	7.5 ml
20% (w/v) SDS	0.15 ml	0.15 ml	0.15 ml	0.15 ml
Acrylamide/Bis-acrylamide (30%/0.8% w/v)	6.9 ml	9.9 ml	12.0 ml	15.0 ml
10% (w/v) ammonium persulfate (APS)	0.15 ml	0.15 ml	0.15 ml	0.15 ml
TEMED	0.02 ml	0.02 ml	0.02 ml	0.02 ml

- Stacking-gel Solution (4% Acrylamide):

H <sub>2</sub> O	3.075 ml
0.5 M Tris-HCl, pH 6.8	1.25 ml
20% (w/v) SDS	0.025 ml
Acrylamide/Bis-acrylamide (30%/0.8% w/v)	0.67 ml
10% (w/v) ammonium persulfate (APS)	0.025 ml
TEMED	0.005 ml

- 1x Running Buffer  
100 ml 10x Running- Buffer with dist. water QS to 1 l
- 10x Running- Buffer
  - 288 g Glycin
  - 60 g TRIS
  - 20 g SDS
 QS to 2l with dist. water
- Precision Plus Protein™ Standards Dual Color

Transferring proteins to nitrocellulose membrane: “wet” or “semidry” apparatus

- Wet transfer:
  - Disassemble gel casting plates so the gel is flat on one side or the other.
  - Using a clean razor, remove the stacking gel and clip the top right corner of the blot (according to the loading).
  - Using gloved hands and tweezers, quickly cut a piece of 0,45 mM Immobilon-P- PVDF- Membrane to the same size of the gel.
  - Pre-wet the membrane in Methanol
  - Cut four pieces of Whatman paper to the size of the membrane.
  - Assemble the ‘sandwich’ as below make sure the cassette is open with the black side down before assembly
    - Wet and place a Dacron pad nearest the hinge
    - Wet two pieces of Whatman paper, place on the Dacron pad
    - Put gel right-side-up and back-to-front on the filter paper
    - Place pre-wet membrane on top of gel, matching the clipped edge of gel with the clipped edge of the membrane
    - Place two more pieces of wet Whatman paper onto the filter
    - Wet and place the other Dacron pad on the top.

- Close and lock the cassette, place it into the electrode cassette and cover with trans-blotting buffer.
  - Add a stir bar and ice pack, and start transfer
  - Time and voltage of transfer will vary depending on the properties of the protein and the trans-blotting buffer used.
- Continuous semidry transfer:
  - Disassemble gel-casting plates so the gel is flat on one side or the other.
  - Using a clean razor, remove the stacking gel and clip the top right corner of the blot (according to the loading).
  - Using gloved hands and tweezers, quickly cut a piece of 0,45 mM Immobilon-P- PVDF- Membrane to the same size of the gel. (measure the gel area in centimeters)
  - Pre-wet both the membrane in methanol
  - Cut 16 pieces of Munktell Grade 1 filter paper to the size of the membrane.
  - Assemble the apparatus as follows:
    - Soak 8 pieces of filter paper in trans-blotting buffer and make sure they are air bubble free on the anode plate.
    - Place the pre-wet nitrocellulose filter onto the stack
    - Place the pre-soaked gel onto the membrane
    - Place 8 more soaked pieces of filter paper on the gel.
    - Purge the stack of any air bubbles with a glass pipette.
    - Assemble the cathode plate and start the transfer
  - The equation to calculate the amperage for a 1 hour transfer is:
    - $0.8 \text{ mA} / \text{cm}^2 \text{ gel}$ .
  - After 1 hour, disassemble apparatus and western blot the membrane.
- Trans-blotting buffer
  - 3.5 l dist. water
  - 1 l methanol
  - 0.5 l 10x Running Buffer

### 3.8.3 Protein detection

- Protein-solution:
  - Nonfat dried milk 5%, 1 g dissolving in 20 ml PBS/ TWEEN
    - 1x PBS, 10 g dissolved in 1 l H<sub>2</sub>O

- 0,1% TWEEN, 1 ml in 1000 ml PBS solution
  - BSA 5%
    - 1 g dissolved in 20 ml PBS/TWEEN
  - 200x Na-azide
    - 4% NaN<sub>3</sub> 2 g dissolved in 50 ml dist. water
- Antibodies:
  - ALK
  - p-Tyrosine
  - Akt
  - p-Akt
  - STAT3
  - p-STAT3
  - P70
  - p-P70 S6K
  - anti-Log Rabbit
  - anti-log mouse

#### Developing the blot using PIERCE chemiluminescence substrates (Supersignal)

- Mix equal parts of “stable peroxide solution” (white bottle) and “luminol solution” (brown bottle). For a minigel filter, 1 ml of each is ample in a square petri dish.
- Mix by swirling and allow the solution to come to room temp (~ 5 minutes)
- Incubate washed membrane with developing solution for 1 minute, swirling constantly and keeping membrane covered with solution.
- Place the membrane face down on a piece of saran wrap, and fold edges under to seal the membrane
- Place the wrapped membrane into an X-ray film cassette and tape edges to hold in place.
- In the dark room, expose film to the filter and develop using the automatic film processor.
- In ambient light, mark the position of the mw markers on the autorad using a marker. The tape marks on the autorad can be used to align the membrane with the autorad.

#### 3.8.4 Developing solution

- PICO- developing solution
- Dura- developing solution
- Femto- developing solution

### 3.8.5 Membrane stripping

- Amido black destain
  - 100 ml methanol 100%
  - 100 ml acetic acid 100%
  - 800 ml dist. water

### 3.8.6 Bio-Rad protein assay

Prepare 6 dilutions of a BSA (bovine serum albumin) protein standard (Nr. 500-0007, Bio-Rad Laboratories GmbH, Munich, Germany), which representative of protein solution to be test (the prime concentration of BSA protein standard is 3 mg/ml, it was diluted with distilled, deionized water to the concentration of 1.5, 0.75, 0.375, 0.188 and 0.094 mg/ml). 5 µl of distilled water, each BSA protein standard and protein lysis was pipetted into a clean and dry 96-well flat-bottom plates, each sample was two times pipetted for double research. 200µl (Nr.500-0114) and 25 µl reagent mixture containing reagent A (Nr.500-0113, Bio-Rad Laboratories, Munich Germany) and reagent S (Nr.500-0115, Bio-Rad Laboratories, Munich Germany) was added to the sample-well. The mixture was incubated at room temperature for at least 5 minutes and measured absorbance at 595 nm using ELISA reader. The incubation of samples at room temperature should not more than 1 hour.

## 3.9 Animal models and induction of lymphoma xenotransplants

Six - to eight – week – old female immunodeficient mice (CB-17 SCID) were obtained from Charles River (Wilmington, MA, USA). Ten million ( $10 \times 10^6$ ) lymphoma cells (SUDHL-1 or Karpas299) suspended in sterile PBS (100µl) were injected subcutaneously into the right shoulder region. All animal experiments were authorized by a regional government agency (Regierung von Oberbayern, licence number 55.2 – 1 – 54 2531 – 52-07). Tumor diameters were measured daily with a shifting calliper, and tumor volume was calculated as  $(\text{length} \times \text{width} \times \text{width})/2$ . Treatment was performed when xenotransplants reached a tumor volume rang during 0.1 and 0.8 cm<sup>3</sup>.

Additionally to xenotransplant models, transgenic models of lymphoma were used for monitoring of early and very-early response to treatment. Previously we have established a transgenic (Eµ-myc) lymphoma model representing an aggressive histology.

### **3.10 Therapeutic regimens**

Groups of 20 mice each undergo with targeted drugs treatment. Response to therapy is valuated in respective groups starting 24hrs after initiation of treatment. Imaging and in vivo measurement of FLT- and FDG-uptake were performed at additional time points at d-1 and d0; d+1 and d+2; d+5 and d+6; d+13 and d+14. With targeted drugs treatment was performed including HSP90 inhibitors (NVP-AUY922), PI3K inhibitors (BGT266) and mTOR inhibitors (RAD001). The NVP-AUY922 was diluted with 5% glucose to the concentration of 50 µg/ml and stored in -80 °C for daily intraperitoneal (i.p.) injection using. Accordingly, the RAD001 was diluted with 5% glucose to the concentration of 10µg/ml, and the BGT266 was diluted with 0.01 M HCl to 1.5 mg/ml. The treatment of RAD001 and BGT266 used the oral administration (p.o.) in daily and 4on/3off weekly administration. The control group received glucose solution (0.5%) only.

### **3.11 Tumor immunohistochemistry**

The apoptosis and proliferation markers were used for the immunohistochemistry. Sample of the tumor xenografts were routinely fixed in 4% buffered formalin and embedded in paraffin, and then cut in 5 µm sections. The Immunostainer (Ventana medical Systems, Inc., Tucson, AZ, USA) was used according to the company's protocols, with slight modification. After deparaffinization and rehydration, the slide were placed in a microwave pressure cooker in 0.01 mol/l citrate buffer, pH 6.0, containing 0.1% Tween 20, and heated in a microwave oven at maximum power for 30 min for 8 min. (hot start). Thereafter, sections were washed in Tris-buffered saline (pH 7.6) containing 5% fetal calf serum (Life Technologies, Grand Island, NY, USA) for 20 min. The primary antibodies were incubated overnight at room temperature. The anti-cleaved caspase 3 antibody was obtained from Cell Signaling (New England Biolabs, Frankfurt, Germany) and the monoclonal rabbit anti-Ki67 antibody (clone SP6) from Lab Vision Corp (Fremont, CA, USA). The rest of the procedure was performed on the automated immunostainer, using diaminobenzidine as chromogen.

### **3.12 Paraffin section method and technique**

1. Fix tissues with 10% formalin or other fixatives for 24-48 hours at room temperature. Make sure you have enough fixative to cover tissues. Fixative volume should be 5-10 times of tissue volume.
2. Trim fixed tissues into appropriate size and shape and place in embedding cassettes.

3. Process for paraffin embedding schedule as follow (total 16 hours):
  - 70% Ethanol, two changes, 1 hour each
  - 80% Ethanol, one change, 1 hour
  - 95% Ethanol, one change, 1 hour
  - 100% Ethanol, three changes, 1.5 hour each
  - Xylene or xylene substitute (i.e. Clear Rite 3), three changes, 1.5 hour each
  - Paraffin wax (58-60 °C), two changes, 2 hours each
  - Embedding tissues into paraffin blocks.
4. Trim paraffin blocks as necessary and cut at 3-10  $\mu\text{m}$  (5  $\mu\text{m}$  is commonly used).
5. Place paraffin ribbon in water bath at about 40-45 °C.
6. Mount sections onto slides.
7. Allow sections to air dry for 30 min and then bake in 45-50 °C oven overnight. NEVER allow baking temperature go higher than 50 °C for sections thicker than 25 $\mu\text{m}$ . Otherwise sections may crack, especially 25-50  $\mu\text{m}$  thick sections, and result in sections falling off slides during staining.
8. The deparaffinize sections in 2-3 changes of xylene, 10 min each. Use three changes of xylene for sections thicker than 25  $\mu\text{m}$ .
9. Hydrate in 2 changes of 100% ethanol for 3 min each, 95% and 80% ethanol for 1 minute each. Then rinse in distilled water.

### 3.13 Statistical methods

GraphPad Prism 5 (GraphPad Software, Inc, La Jolla, CA, USA) software Excel 2007 (Microsoft) was used for statistical analysis. Mean values, median, and standard deviation of tumor size and TBR in controls and treated mice were calculated. Tumor sizes were log-transformed to estimate the slope of log-linear tumor growth. The paired T test was used to test for signification changes between two related measurements. Unpaired T test was used to test for differences of tumor size and tumor growth rates between two independent mice groups. Furthermore, linear mixed regression models were calculated to confirm the results of univariate analysis, regarding for dependency of repeated measurements within the same individual. A  $p$  value, lower than 0.05, was considered as statistically significant.

## **4 Results**

### **4.1 Dual inhibition of AKT and mTOR blocks the proliferation of multiple NPM-ALK lymphoma cell lines**

#### **4.1.1 Dual blockage of AKT and mTOR affects the viability of ALK+ lymphoma cells**

Based on preclinical research from Novartis, BGT226 inhibits proliferation and colony formation in tumor cell lines / tumor stem cells of glioblastoma multiforme (GI50=4.5-12 nM), breast cancer (GI50= 1.1-4.9 nM), prostate cancer (GI50= 6.1-8 nM), NSCLC (GI50= 4.1 nM), colorectal cancer (GI50= 12 nM) and ovarian cancer (GI50= 7.8 nM). To assess the biological effect of BGT266 on lymphoma cell survival, we performed MTT assays on SUDHL-1, BaF3-NPMAL and Karpas299 cells incubated with increasing concentrations of drug for 24 hours and 48 hours (Figs. 3A-3F). SUDHL-1 and BaF3-NPM-ALK cells showed a dose-dependent decrease in the cell viability, while Karpas299 cells showed partially resistance to BGT266 treatment. Although the lower concentration (0.1 nM) of BGT266 had no effect on cell proliferations, it remarkably inhibited proliferation of SUDHL-1 cells in a dose dependent manner. The SUDHL-1 cell viability was reduced from 96.1% (0.1 nM) to 14.1% (100 nM) with BGT226 treatment for 24 hours (Fig. 3B). Additionally, after treatment SUDHL-1 cells were dramatically inhibited. No surprisingly, BGT226 also reduced the cell viability in time-dependent manner. Taking SUDHL-1 cell line as an example, a 50% inhibition of the cell viability was first detected with a dose of 10nM after 24 hours incubation (Fig. 3B), but decreased to 1 nM after the 48 hours treatment with BGT226 (Fig. 3E). Similar results were also found in BGT266 treated BaF3-NPMALK cells, and a 50% inhibition rate was detected with a dose between 1 and 10 nM as early as 24 hours after treatment. Moreover, the inhibition rate rose to 75% after treatment with a dose of 100nM (Fig. 3C). However, an effective inhibition of the karpas299 cells viability was only found with a concentration of 100 nM after treatment with BGT226 (Fig. 3A and 3D).

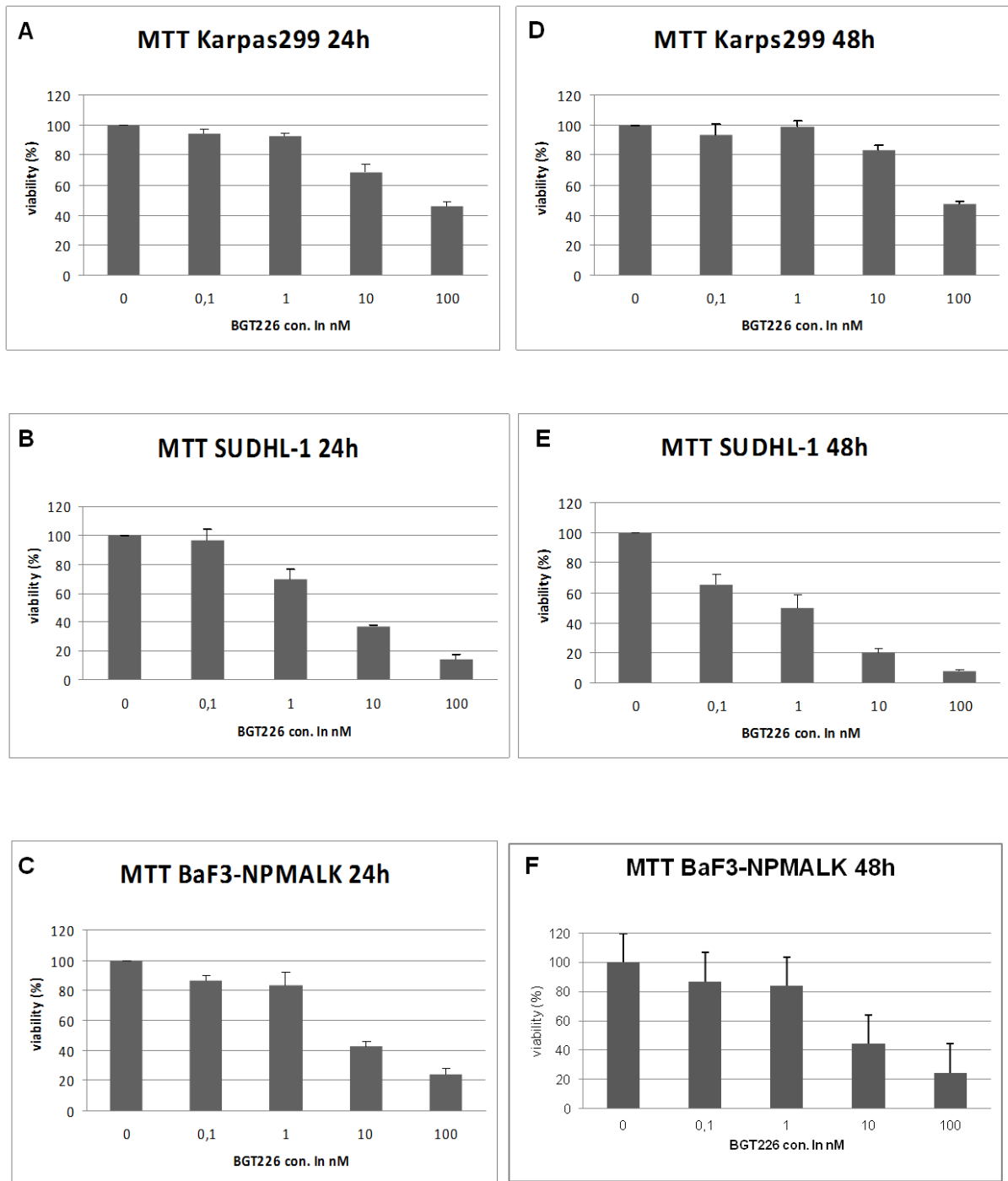


**Fig. 3:** PI3K/mTOR inhibitor BGT226 inhibits the cell viability in the time and dose dependent Manner. Cells were treated with the indicated concentration of BGT226 for 24 hours and 48 hours. The bars represent the mean  $\pm$  SD of the mean from n=3 experiments.

#### **4.1.2 Dual inhibition of AKT and mTOR activity induces the cell cycle arrest of ALK+ lymphoma cells**

We examined the effects of BGT266 on cell cycle progression. BGT266 led to an increase in the percentage of cells in the SubG1/G1 phase compared to control conditions in SUDHL-1 cells (Fig. 4B and E). The results showed that BGT226 arrested SUDHL-1 lymphoma cells in the original G1 phase (from 41.1% in control to 71.3% at 100 nM), while reduced cells in the S phase (from 25.8% in control to 4.6% at 100nM). The percentage of dead cells rose from 7.8% to 22.4% flowing dose of 100 nM as early as 24 hours (Fig. 4B). At 48 hours, cell percentage was reduced about 30% (from 30.7% to 1.9% at 100 nM) from S phase and the cells traversed to the G1 phase (from 44% in control to 60% at 100 nM) and the SubG1 (from 3.9% to 23.7% at 100 nM) (Fig 4E). There was no change in the SubG1 phase indicating apoptosis during treatment with BGT226 in Karpas299 cells (Fig. 4A and D), and only a slight increase in the G1 Phase was detected from 32% to 49% with a dose of BGT226 at 100 nM after 48 hours incubation (Fig. 4D). Compared with SUDHL-1 cells experienced a S Phase reduction of 30%, Karpas299 cells only decreased from 32% to 16% (48 hours, 100 nM) in the S phase, while the Karpas299 cells in S phase decreased minimal from 22% in control reaching a value of 16% at 100 nM dosage after 24 hours of the treatment period (Fig. 4A). After 24 hours incubation with 100 nM BGT266 in BaF3-NPMALK cells, BGT226 caused a G1 phase arrest (from 50% to 77%), a reduction of the S phase (11%) and the G2 phase (14%) and a slight increase of cell death. However, we found no reduction of the S phase during treatment with 10 nM BGT226 (Fig. 4C). At 48 hours, the cell percentage was reduced from 19% to 12% at 100 nM in the S phase and the cells traversed to the G1 phase with 10% at 10 nM. There was no marked increase in the Sub G1 phase (Fig. 4F).

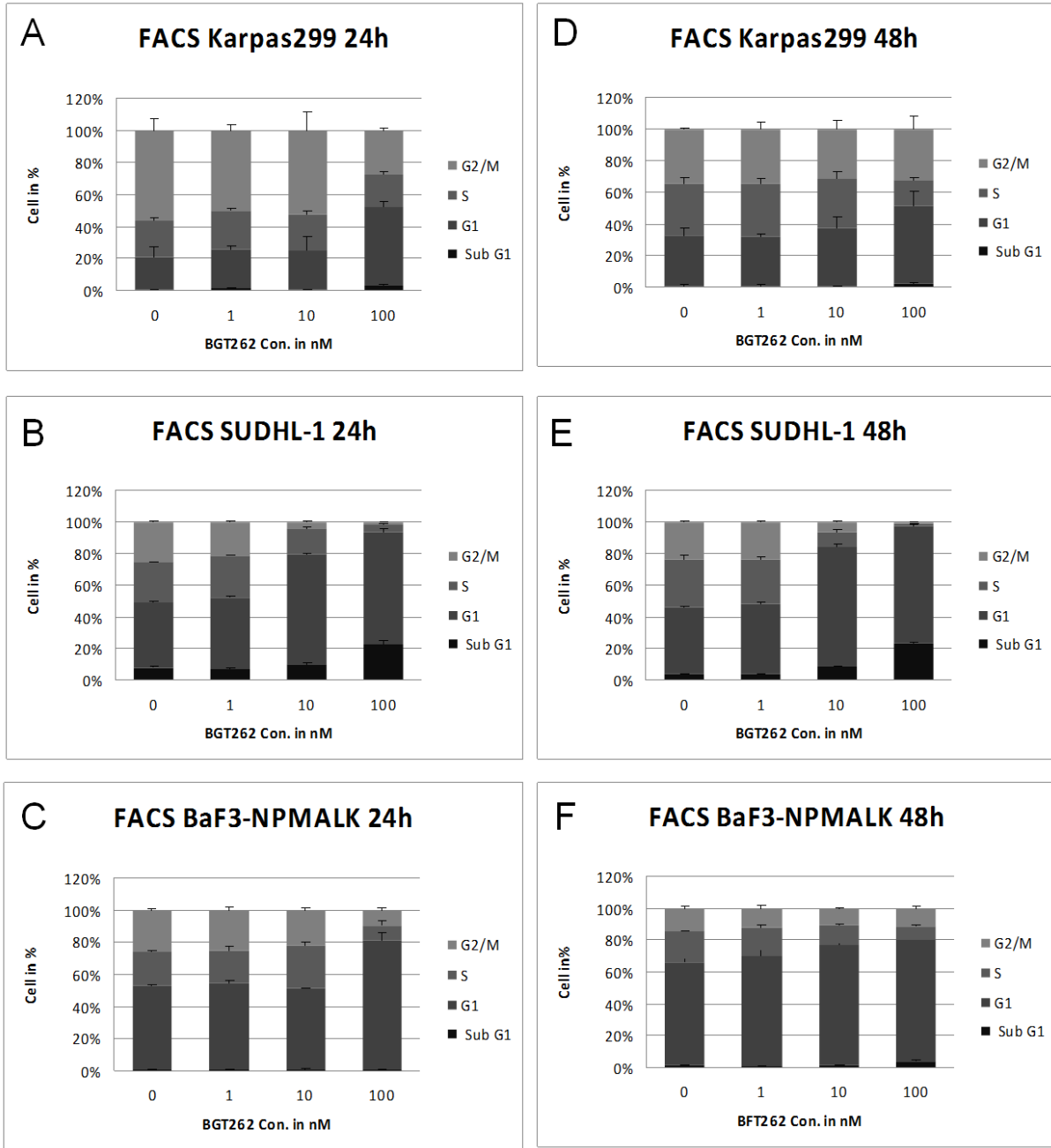
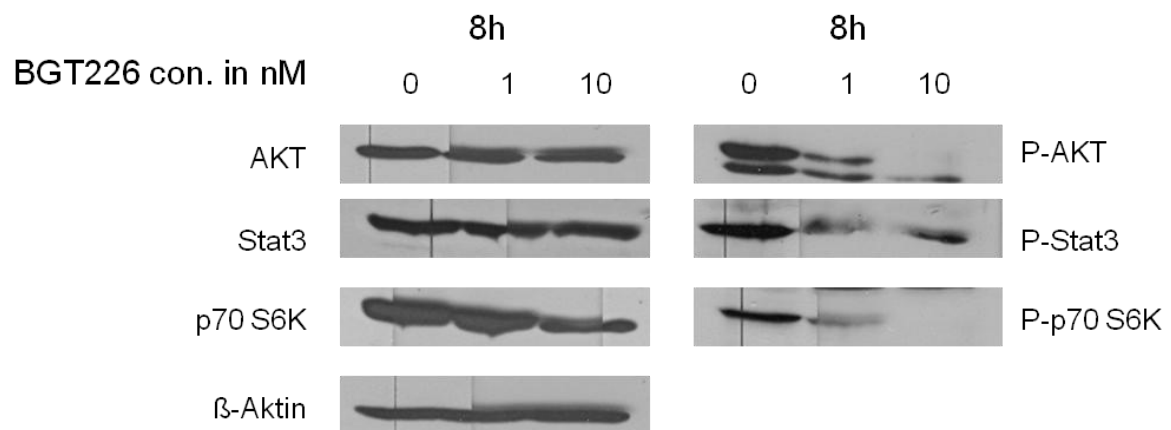


**Fig. 4:** PI3K/mTOR inhibitor BGT226 induces the cell cycle arrest (G1-phase) and apoptosis in ALCL lymphoma cells. Cells were treated with the indicated concentration of BGT226 for 24 hours and 48 hours. The bars represent the mean  $\pm$  SD of the mean from n=3 experiments.

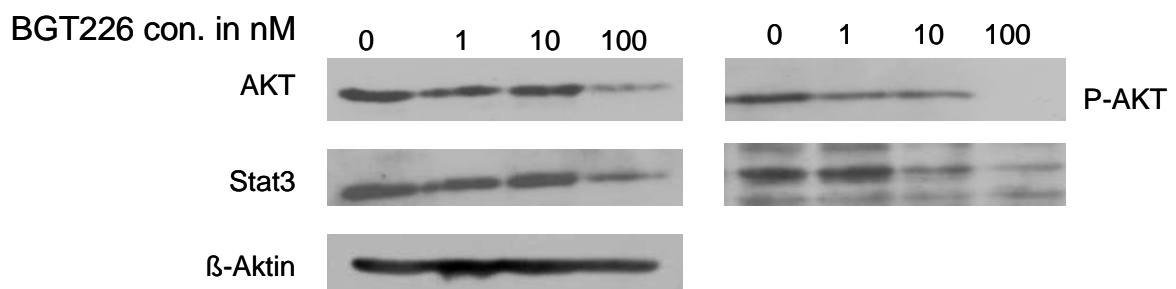
#### **4.1.3 Down-regulation of several oncogenic proteins during exposure of human lymphoma cells to PI3K/mTOR inhibitor**

BGT226 is a pan-class I PI3K and mTOR inhibitor. To further investigate the effect of BGT226 on the PI3K/AKT and mTOR signalling pathways, all cell lines were treated with BGT226 in 0, 1, 10 and 100 nM for 16 hours and / or 8 hours. As shown in Fig. 5A to Fig. 5C, BaF3-NPMALK, SUDHL-1 and Karpas299 cells were selected to investigate concentrations and time effect of BGT226 on PI3K/mTOR signalling pathways. The expression levels of p-AKT and p-STAT3 were decreased in BaF3-NPMALK and SUDHL-1 cells as early as 8 hours after treatment with BGT226 following a dose of 10 nM (Figs. 5A and B). In contrast, no change of oncoprotein expression was found up to 16 hours incubation with BGT226 in Karpas229 cells (Fig. 5C). The mammalian target of rapamycin (mTOR) is a serine/threonine protein kinase belongs to the PI3K protein family regulating cell growth, cell proliferation, cell motility, cell survival, protein synthesis and transcription. And mTOR Complex 1 (mTORC1) is composed of mTOR, regulatory associated protein of mTOR (Raptor) and p70-S6 Kinase (p70-S6k). The p70-S6k is one of the best characterized targets of mTORC1. Thus, the change of p-p70-S6k during the treatment in BaF3-NPMAL cells was observed 8 hours after incubation with inhibitor. As shown in Fig. 5A, compared to control, p-p70-S6k was strongly inhibited with a 1 nM BGT226 treatment as early as 8 hours.

A



B



C

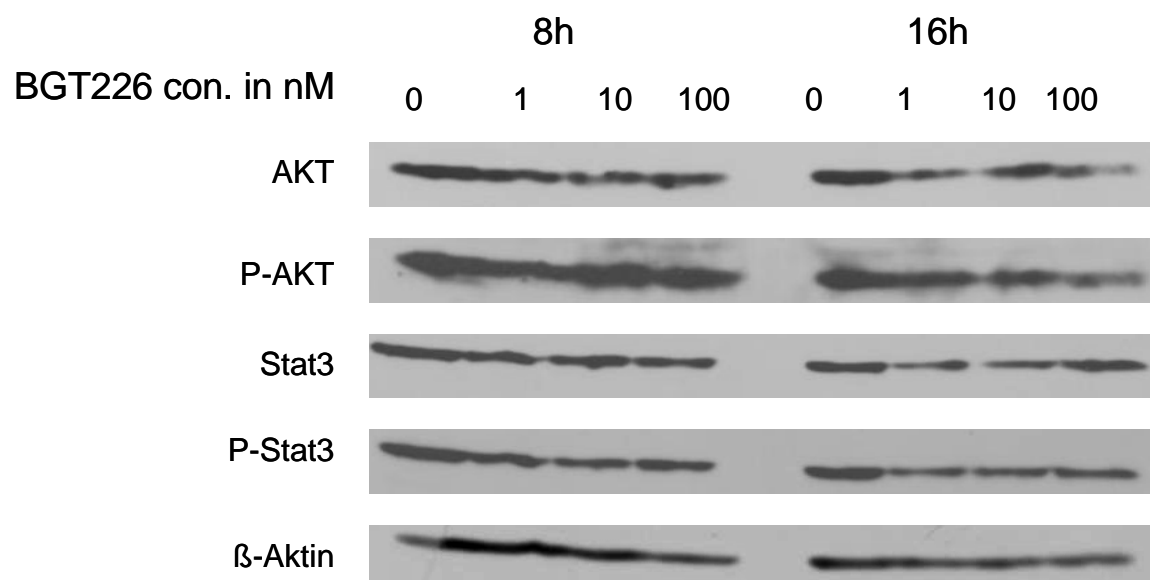


**Fig. 5:** PI3K/mTOR inhibitor BGT226 inhibits expression of several oncoproteins in ALCL lymphoma cells (A: BaF3-NPMAL cells, B: SUDHL-1 cells, C: Karpas299 cells). Cells were treated with the indicated concentration of BGT226 for 8 hours and/or 16 hours.

## 4.2 Functional *in vivo* imaging of response to PI3K/mTOR (BGT226) inhibition in SUDHL-1 lymphoma by FLT-PET is superior to FDG-PET

### 4.2.1 Blockage of PI3K/mTOR activity decrease the tumor growth of NPM-ALK lymphoma *in vivo*

To evaluate FDG- and FLT-PET imaging for early response monitoring *in vivo*, we generated xenograft SUDHL-1 and Karpas299 tumors. To mimic the clinical situation, the treatment was initiated once the tumor volume reached approximately 500mm<sup>3</sup>. In SUDHL-1 bearing mice, the control group showed a 6.3-fold (n=3, SD=0.6, range 5.7-6.9-fold) increase of tumor volume (Fig. 6A). The tumors of BGT226-treated mice had a 2.1-fold increase at d+7 (n=6, SD=0.66, range 1.3-2.8-fold). Until d+14, tumors of the therapeutic group remained nearly constant during the observation period (n=6, mean 2.2-fold increase, SD=0.65, range 1.2-2.9-fold). In contrast, the tumor volume of the controls increased to 12.2-fold (n=3, SD=2.2, range 9.9-14.2-fold) at d+14. During the tumor growth of SUDHL-1 bearing mice treated with BGT226, there was no remarkable Inhibition effect on Karpas299 tumor growth (Fig. 6b). The therapeutic group showed a 3.3-fold (n=9, SD=1.1, range 1.8-4.6-fold) increase in tumor volume and the tumors of the control mice had a 3.5-fold increase at d+7 (n=7, SD=1.1, range 2.7-5.8-fold). The tumor volume of the control group continuously increased to 5.7-fold (n=3, SD=1.3, range 5.7-7.8) and to 6.1-fold in the therapeutic group (n=4, SD=0.6, range 5.2-6.6-fold) at d+14.

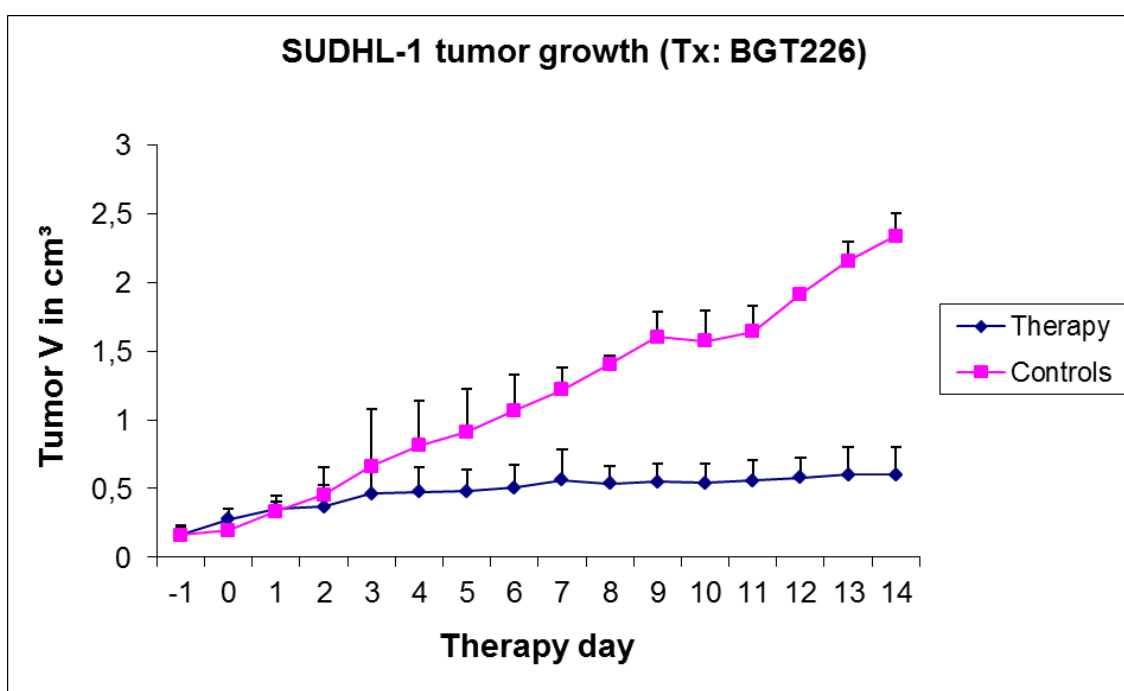


**Fig. 6A:** BGT226 blocks the SUDHL-1 tumor growth. The SUDHL-1 lymphoma bearing mice were treated oral with 7.5 mg/kg BGT226 (Therapy) or only placebo (Control) three times pro week. The bars represent the mean  $\pm$  SD.

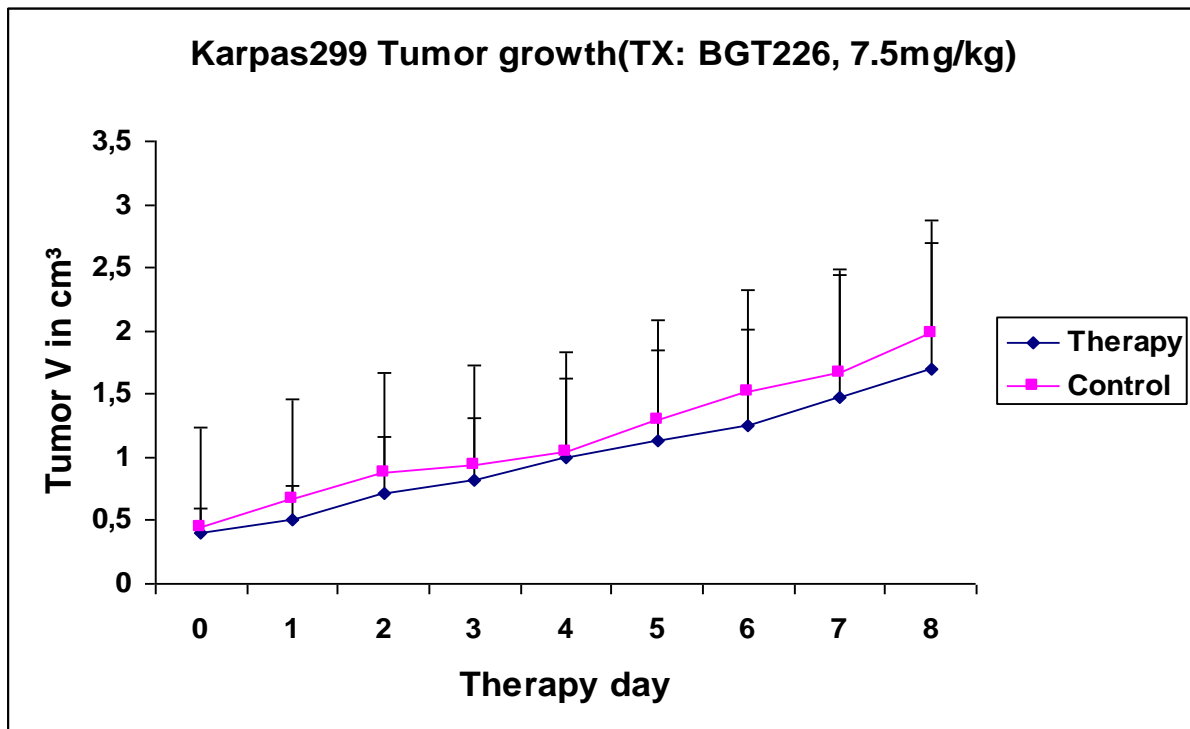


**Fig. 6B:** Karpas299 lymphoma shows resistant to BGT226 therapy. The karpas299 lymphoma bearing mice were treated oral with 7.5 mg/kg BGT226 (Therapy) or only placebo (Control) three times pro week. The bars represent the mean  $\pm$  SD.

#### 4.2.2 FDG-PET imaging analysis shows inhibitory effect of PI3K/mTOR on the NPM-ALK lymphoma metabolism

To investigate SUDHL-1 and Karpas299 lymphoma in response to BGT226 treatment, FDG-PET was performed both before and after therapy at d-1, d+8 and d+13 (Fig. 7A and 7B). In SUDHL-1 lymphoma bearing group, the mean TBR of treated mice with dose of 7.5 mg/kg reduced from 8.1 (at d-1: n=7, range 4.0-11.4, SD= 5.7) to 7.0 (at d+8: n=7, range 4.0-7.7, SD= 1.7) and then to 5.2 (at d+12: n=6, range 4.5-6.3, SD=0.7). The mean TBR of untreated mice was increased from 5.7 (at d-1: n= 4, range 4.0-7.7, SD= 1.2) to 7.0 (at d+8: n=4, range 5.2-8.4, SD= 1.6). The mean TBR ended at 6.5 (n=3, range 5.6-7.1, SD= 0.8) until d+14.

In karpas299 lymphoma bearing group, the mean TBR of treated mice increased from 4.7 at d-1 (n=4, range 3.1-6.2, SD=1.3) to 6.1 (n=4, range 4.4-9.9, SD=2.6) at d+8, and remained no reduction with 6.2 (n=3, range 5.0-7.0, SD=1.1) until d+13. The mean TBR of the controls increased from 6.5 (at d-1: n=4, range 4.3-8.7, SD=1.8) to 7.2 (n=4, range 6.3-8.0, SD=0.9) at d+8, but then went down to 5.2 (n=4, range 4.5-6.3, SD=0.7) at d+13 (Fig. 7B).

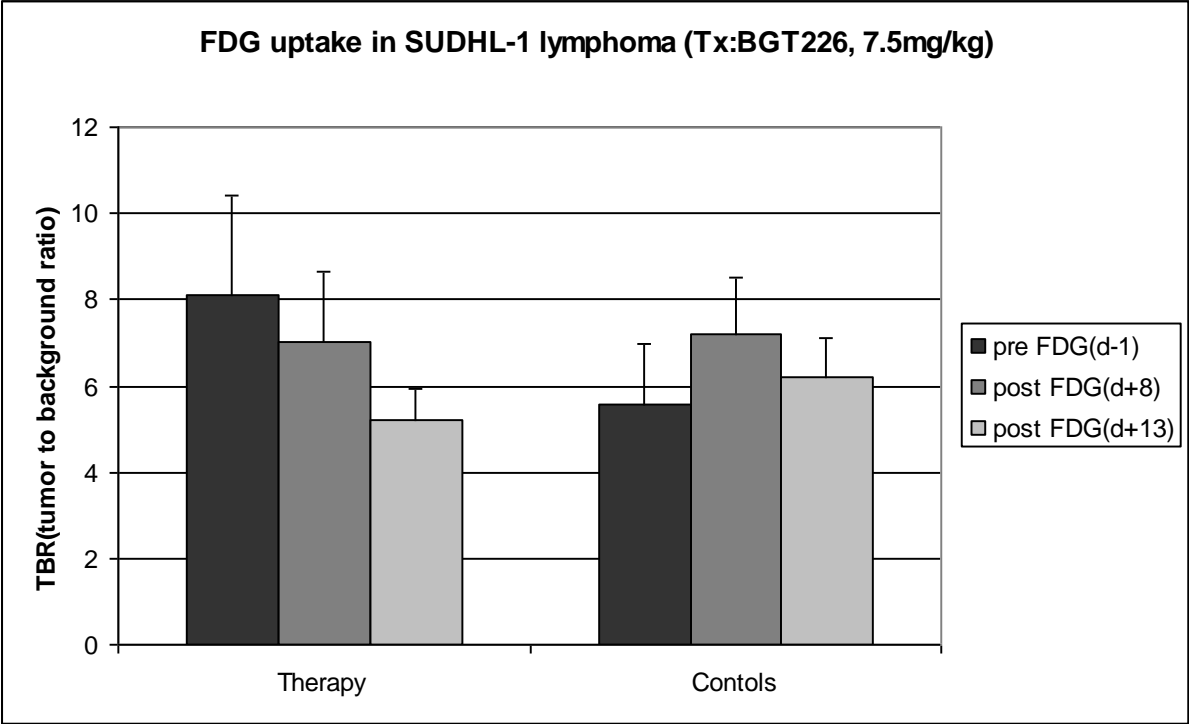


**Fig. 7A:** BGT226 treatment reduces the FDG-tracer-uptake in SUDHL-1 lymphoma. The SUDHL-1 lymphoma bearing mice were treated oral with 7.5 mg/kg BGT226 (Therapy) or only placebo (Control) three times pro week. The bars represent the mean  $\pm$  SD.

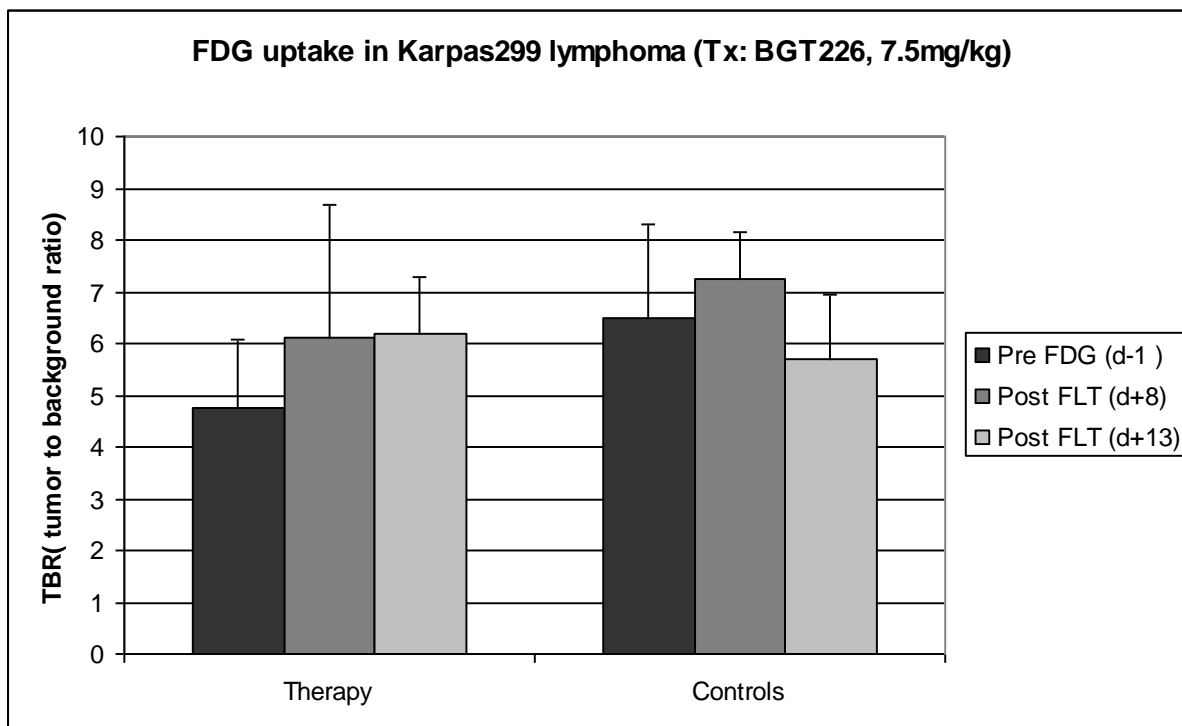


**Fig. 7B:** No remarkable reduction of FDG-tracer-uptake was found in Karpas299 lymphoma under treatment with BGT226. The karpas299 lymphoma bearing mice were treated oral with 7.5 mg/kg BGT226 (Therapy) or only placebo (Control) three times pro week. The bars represent the mean  $\pm$  SD.

#### 4.2.3 FLT-PET imaging analysis shows inhibitory effect of PI3K/mTOR on the cellular proliferation of NPM-ALK lymphoma

As a more tumor specific tracer, FLT was also applied to detect the therapeutic response in lymphomas during BGT226 treatment. SUDHL-1 and Karpas299 bearing mice were scanned with FLT-PET both before and after therapy at d-1, d+2, d+7, and d+14, respectively. Figs. 8a and 8b showed representative TBRs of different therapeutic groups. A remarkable decrease of the FLT-uptake in SUDHL-1 bearing mice can be detected two weeks after therapy with 7.5 mg/kg BGT226 (n=6, pre-therapeutic uptake: mean TBR= 2.9, range 2.3-4.7, SD=0.7; post-therapeutic uptake: mean TBR=1.3, range 1.0-1.7, SD=0.2) (Fig. 8A). In contrast, the FLT-uptake remained no change in the control mice (n=3, pre-therapeutic uptake: mean TBR= 2.6, range 1.9-2.7, SD=0.5; post-therapeutic uptake: mean TBR=2.6, rang 2.7-3.6, SD=0.7). The FLT-uptake decreased only slightly until d+7. The mean TBR of the therapeutic mice was 2.4 (n=6, range 1.9-2.8, SD=0.6), and the mean TBR in control mice increased slightly to 2.9 (n=3, range 2.1-3.4 SD=0.1) at d+7. The FLT-PET

was also performed on AUY922 resistant Karpas299 lymphoma bearing mice with a dose of 25 mg/kg. The mean TBR of the therapeutic group increased from 3.5 (n=8, range 2.6-4.1, SD=0.6) to 5.8 (n=4, range 4.2-6.8, SD=1.1) at d+2, and remained with 5.0 (n=4, range 3.6-6.0, SD=1.0) at d+7 (Fig. 8B). The mean TBR of FLT-uptake in therapeutic karpas299 lymphoma was reduced to 3.7 (n=4, range 3.3-4.1, SD=0.4) at d+14. In controls, the mean TBR was also increased from 4.3 (n=7, range 2.3-6.3, SD=1.4) to 5.4 (n=3, range 4.9-6.1, SD=0.6) at d+2, remained no change until d+7 (n=3, mean=5.2, range 4.8-5.8, SD=0.5) and then reduced to 4.1 (n=4, range 3.1-4.7, SD=0.7) at d+14.

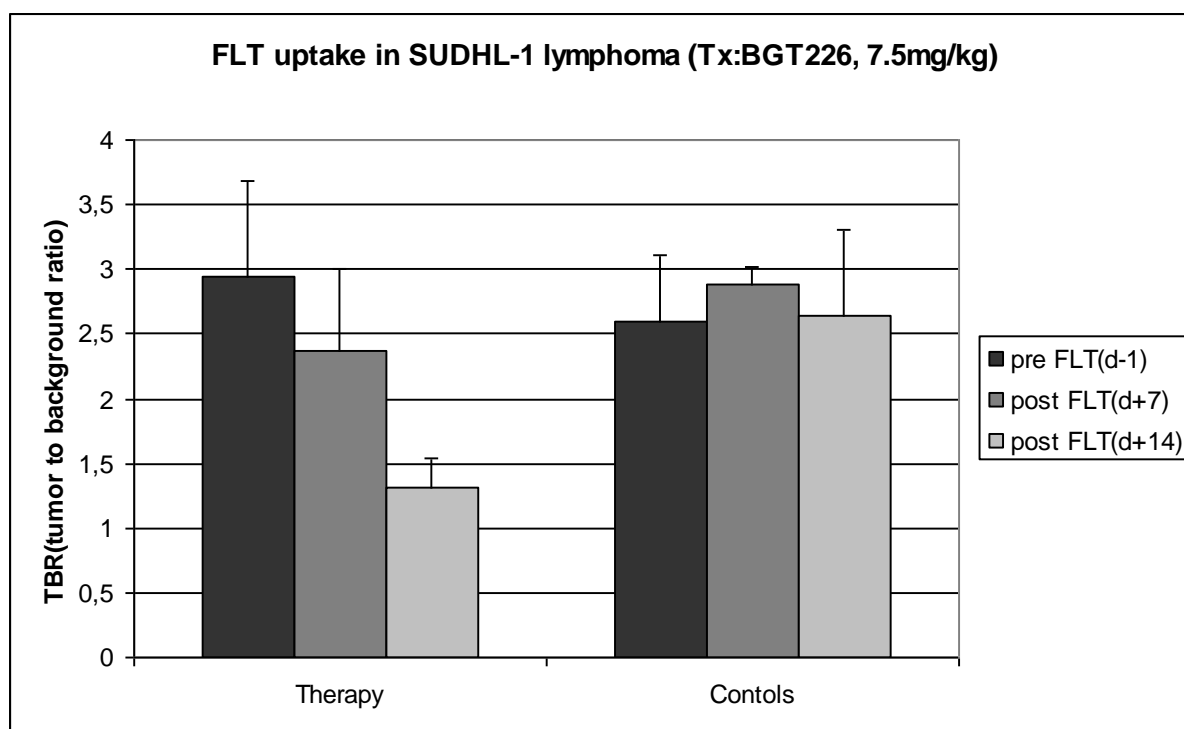


**Fig. 8A:** BGT226 treatment reduces the FLT-tracer-uptake in SUDHL-1 lymphoma. The SUDHL-1 lymphoma bearing mice were treated oral with 7.5 mg/kg BGT226 (Therapy) or only placebo (Controls) three times pro week. The bars represent the mean  $\pm$  SD.

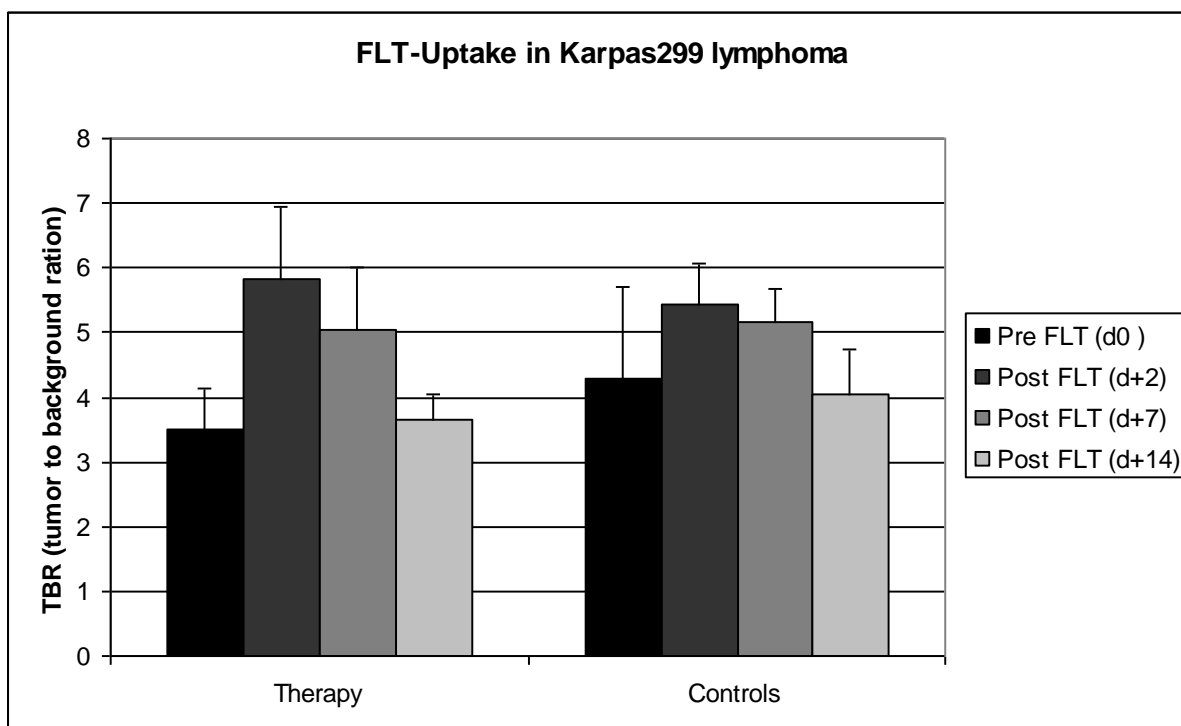


**Fig. 8B:** No remarkable reduction of FLT-tracer-uptake was found in Karpas299 lymphoma under treatment with BGT226. The karpas299 lymphoma bearing mice were treated oral with 7.5 mg/kg BGT226 (Therapy) or only placebo (Controls) three times pro week. The bars represent the mean  $\pm$  SD.

To analyse the predictive value of early functional imaging for response assessment, the statistical analyses were also done in this work. We performed FDG- and FLT-PET scans using a micro PET/CT system before, one and two weeks after initiation of BGT226 treatment (Fig. 9A). To do so, the change of TBR after therapy was compared to pre-treatment TBR, which was defined as 100%, was calculated (relative TBR). FDG-PET analysis of control animals revealed a significant increase in FDG-uptake on day 8 ( $n=3$ , mean TBR 138.3%, range 118.4%-133.4%, SD=13.2%,  $p=0.01$ , Fig. 11B right) and day 13 ( $n=3$ , mean TBR 120.8%, range 106.1%-143.4%, SD=19.9%,  $p=0.01$ , Fig. 9B). In BGT226 treated animals, relative TBR of early FDG-PET showed a significant reduction compared to the pre-treatment control ( $n=6$ , mean TBR 91.1%, SD=23.1%, range 63-129.5%;  $p=0.3$ ). Interestingly, the mean TBR of FDG-uptake at later time points (day 14) decreased to 74% ( $n=3$ , SD=23.1%, range 49.9-96.4%;  $p=0.04$ ). At the same time, the relative mean TBR of FLT-uptake decreased also not significantly to 92.5% compared to baseline ( $n=6$ , SD=37.5%, range 54.8-119.3%,  $p=0.3$ ) at d+6 after initiation of therapy (Fig. 9C). The relative TBR of untreated controls increased to 122% during the same time period ( $n=3$ , range 99.9%-151%, SD=26%,  $p=0.02$ ). Later time points within the treatment group (day 8 to 14) showed a

further significantly reduction in FLT-uptake with p value of 0.002 (n=6, mean=50.6%, range 38.7%-69.9%, SD=19.7%).

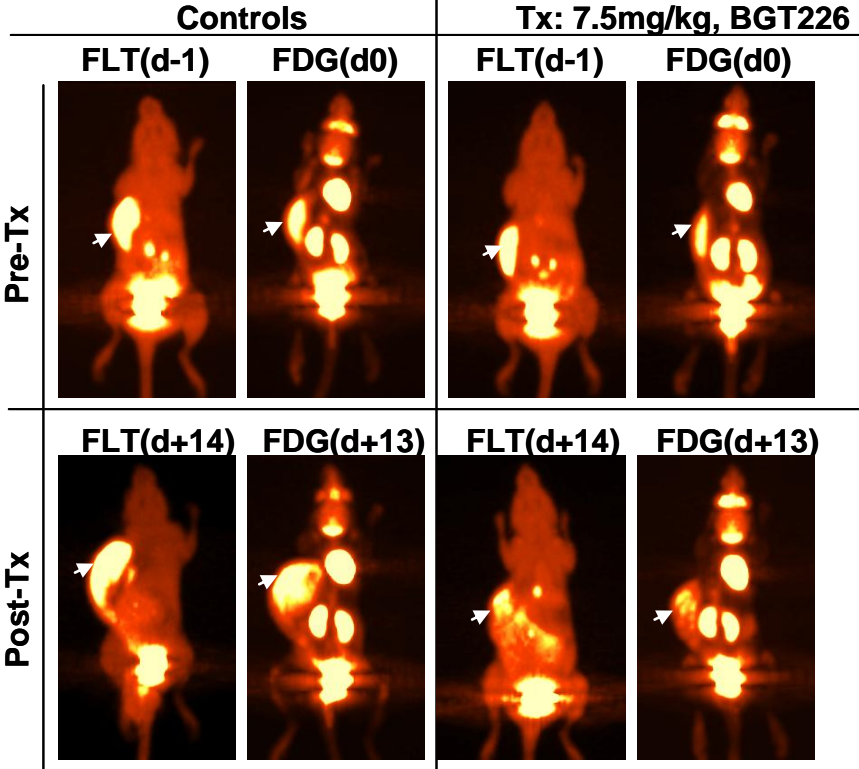


**Fig. 9A:** Functional *in vivo* imaging of response to BGT226 inhibition in SUDHL-1 lymphoma using FLT- and FDG-PET

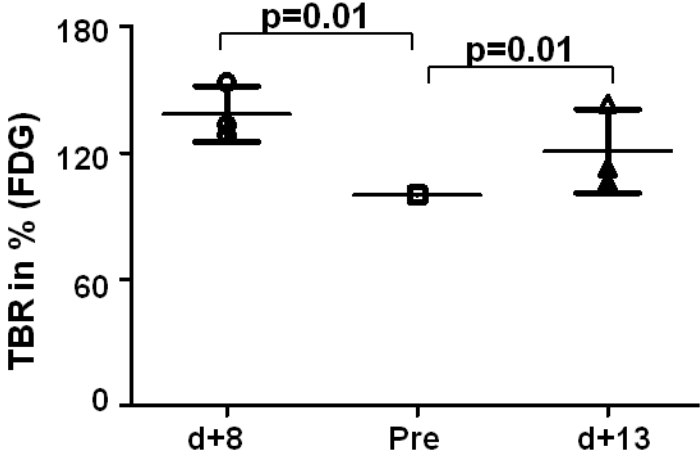


**Fig. 9B:** Determination of FDG-TBR in percentage by comparison with baseline (TBR from pre therapy PET) in control SUDHL-1 lymphoma and TBR on day 0, defined as 100% (“pre”). The bars represent the mean  $\pm$  SD.

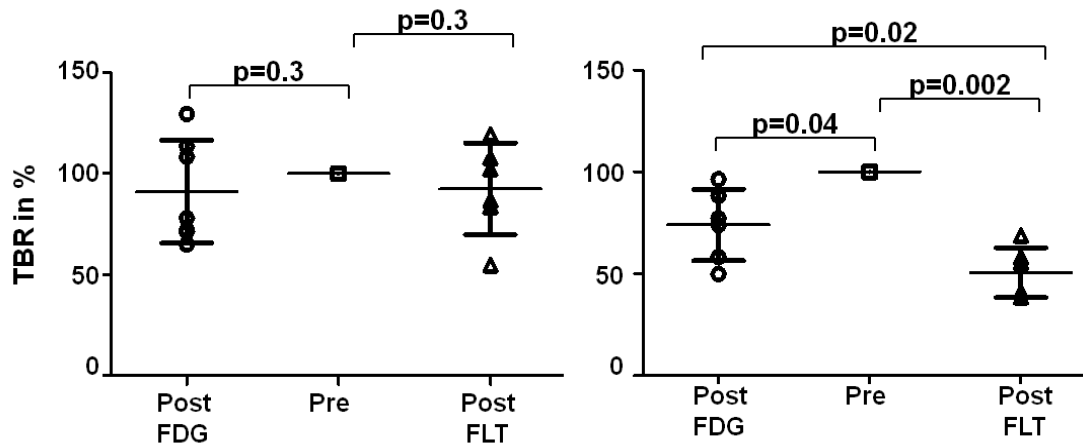


**Fig. 9C:** Determination of TBR in percentage by comparison with baseline (TBR from pre therapy PET) under BGT226 treatment in SUDHL-1 lymphoma and TBR on day 0, defined as 100% (“pre”), and change of TBR compared to pre-treatment values are shown for treated (“post”) (left: after one week; right: after two weeks). The bars represent the mean  $\pm$  SD.

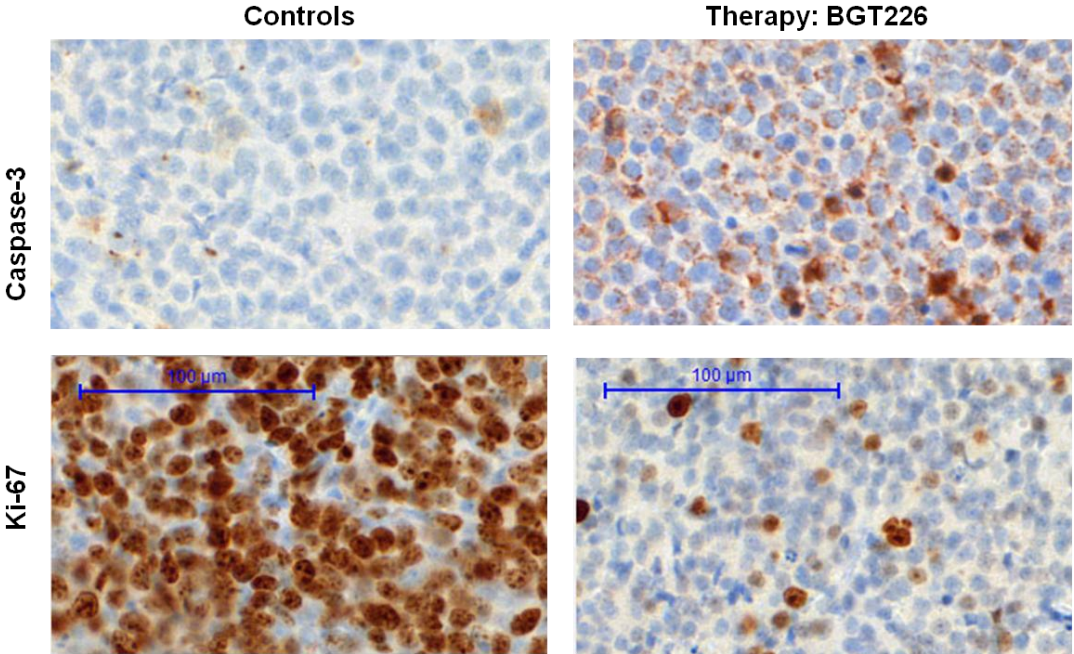
#### 4.2.4 Histological analysis shows decreased proliferation and increased apoptosis induced by the treatment with PI3K/mTOR inhibitor in NPM-ALK lymphoma

To correlate the PET findings with treatment effects of inhibitors on SUDHL-1 xenograft lymphomas, we stained fixed tumor sections with the proliferation marker Ki-67 and the cleaved caspase-3 to analyse the apoptosis. BGT226 treatment led to a significant increase in apoptosis quantified using cleaved caspase-3 positive cells (Fig. 10A,  $n=4$ , mean 6.8%,  $SD=5.3\%$ ) compared to untreated mice ( $n=4$ , mean 1.7%,  $SD=1.3\%$ ). Moreover, the percentage of proliferating cells was substantially decreased by BGT226 as measured using Ki67 staining with a mean of 14.2% ( $SD=7.5\%$ ) in the treated and 63.6% ( $SD=20.3\%$ ) in the control tumors.

The PET findings of Karpas299 lymphomas were confirmed by immunohistochemistry as showed in Fig. 9B. No remarkable increase of the apoptosis was detected after BGT226 treatment compared to the control tumors (controls:  $n=3$ , mean=1.4%,  $SD=1.3\%$ ; therapeutic group:  $n=5$ , mean=1.1%,  $SD=0.8\%$ ). BGT226 only led to a slight reduction of proliferation in

karpas299 lymphomas using Ki67 staining (therapeutic group: mean=43.5%, SD=18.2%; controls: mean=54%, SD=23.9%).

A



B

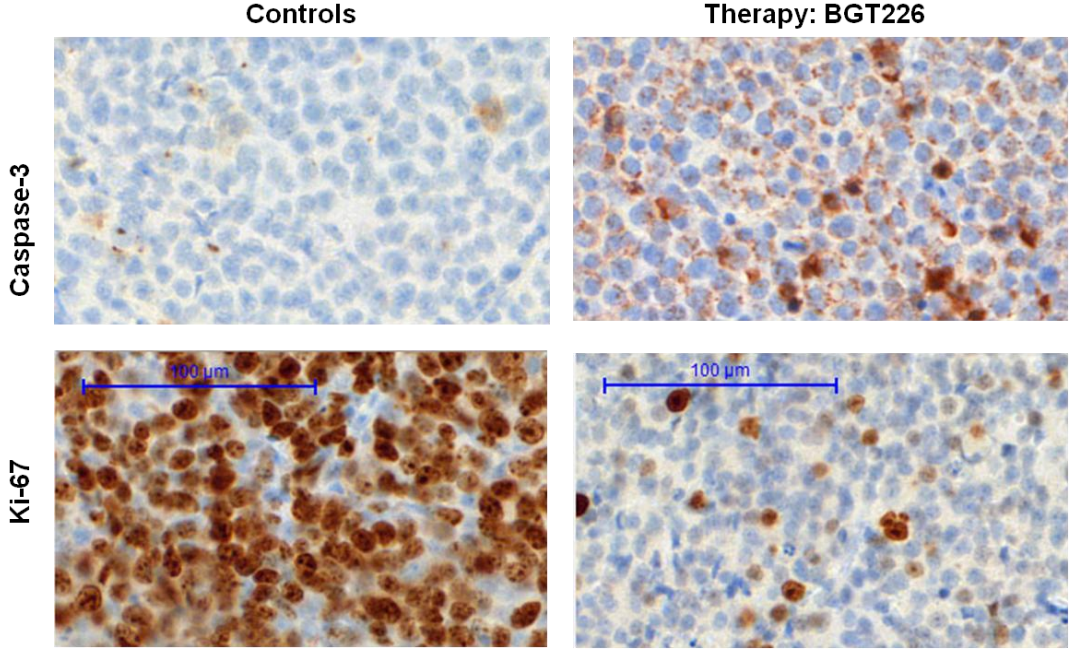


**Fig. 10:** BGT226 treatment triggers a cell death (marker: caspase-3) and a reduction of proliferation (marker: Ki-67) in SUDHL-1 but not in karpas299 lymphoma *in vivo* (A: SUDHL-1

lymphoma, B: karpas299 lymphoma). The lymphoma bearing mice were treated oral with 7.5 mg/kg BGT226 (Therapy) or only placebo (Controls) three times pro week.

To correlate the PET findings with the treatment effects of BGT226 on SUDHL-1 xenograft lymphomas, the histological results were analysed using the Graphpad system (Fig. 11). BGT226 treatment led to a significant increase in apoptosis as quantified by cleaved caspase-3 positive cells compared to untreated mice ( $p=0.02$ , Fig. 12). Moreover, the percentage of proliferating cells was substantially decreased by BGT226 as measured by Ki67staining with a mean of 15.3% for the treated and 63.3% for the control tumors ( $p=0.02$ ).

Taken together, both FDG as well as FLT-uptake correlates with response to HSP90 inhibition *in vivo*. However, FLT-PET is as good as FDG-PET for early *in vivo* response assessment that precedes change of tumor volume to PI3K/mTOR-NPM-ALK-targeted treatment.

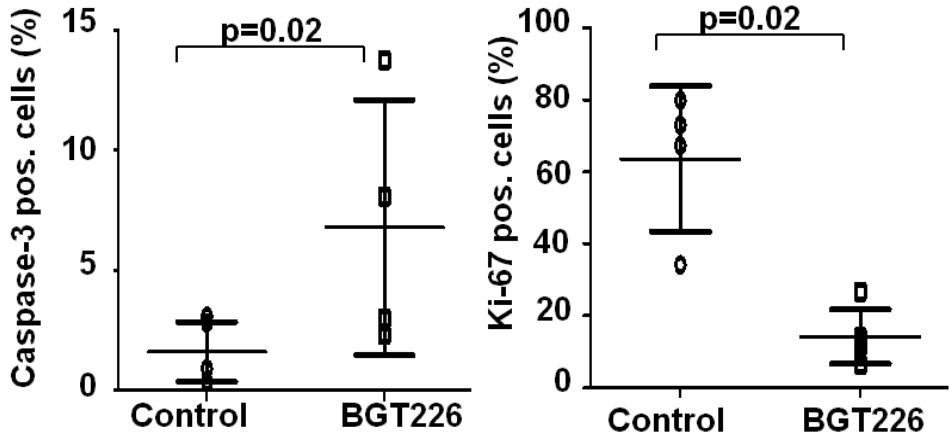


**Fig. 11:** Histological assessment of BGT226 effect on SUDHL-1 lymphoma in using proliferating marker Ki-67 and apoptotic cell death marker caspase-3. The bars represent the mean ± SD.

### **4.3 Inhibition of Hsp90 blocks the proliferation of multiple ALK+ lymphoma cell lines**

#### **4.3.1 The blockage of Hsp90 activity affects the viability of ALK+ lymphoma cells**

Active mitochondria of living cells can cleave MTT to produce a purple-blue formazan, whose intensity indicates the number of living cells. To assess the biological effect of NVP-AUY922 on the survival of lymphoma cells, we performed MTT assays on BaF3-NPMALK, BaF3-parental, JB-6, SUDHL-4, Karpas299 and SUDHL-1 cells which were incubated with increasing concentrations of the drug for 24, 48 and 72 hours (Fig.12). All cell lines showed a dose-dependent decrease in cell viability. Karpas299 cells were less sensitive than the other cell lines to the catatonic activity of NAP-AUY922 after 48 hours of treatment, while the JB-6 was slightly more resistant.

Although lower concentration (1 nM) of NVP-AUY922 had no effect on cell viability within a 24 hours of incubation period, the inhibition rate was 20% at a dose of 10 nM in BaF3-NPMALK and BaF3-parental cells, respectively. It increased to 50% and 20% at the dose of 100 nM (Fig. 12A and 12D). In contrast, there was only a slight reduction of viability in JB-6 and SUDHL-4 cells (Fig. 13A and 13D). At the dose of 10 nM, the viability of SUDHL-1, as well as of Karpas299, was reduced to 70% (Fig. 14A and 14D). After a 48 hours incubation, a dose of 10 nM caused a 40% reduction of the viability in BaF3-NPMALK cells and the reduction was increased to 70% under treatment with 100 nM (Fig. 12B). Interestingly, there were almost no survival BaF3-NPMALK cells after a 72 hours treatment with AUY922 (Fig. 12C). Compared to other cell lines, 10 nM AUY922 reduced BaF3-Parental and SUDHL-4 survival rate to 70% (Fig. 12E and 13E) and the viability of SUDHL-1 cells was reduced to 20% under treatment with 50 nM AUY922 after a 48 hours incubation (Fig. 14E). After 72 hours almost all SUDHL-1 ceased proliferation (Fig. 14F). However, the JB-6 cells showed limited reduction of the cellular proliferation up 72 hours (Fig. 13C). In contrast,  $IC_{50}$  of Karpas299 cells was also found after a 72 hours of an incubation period with a drug dose of 100 nM (Fig. 14C). These findings were also confirmed by the observed cell cycle and apoptosis assay.

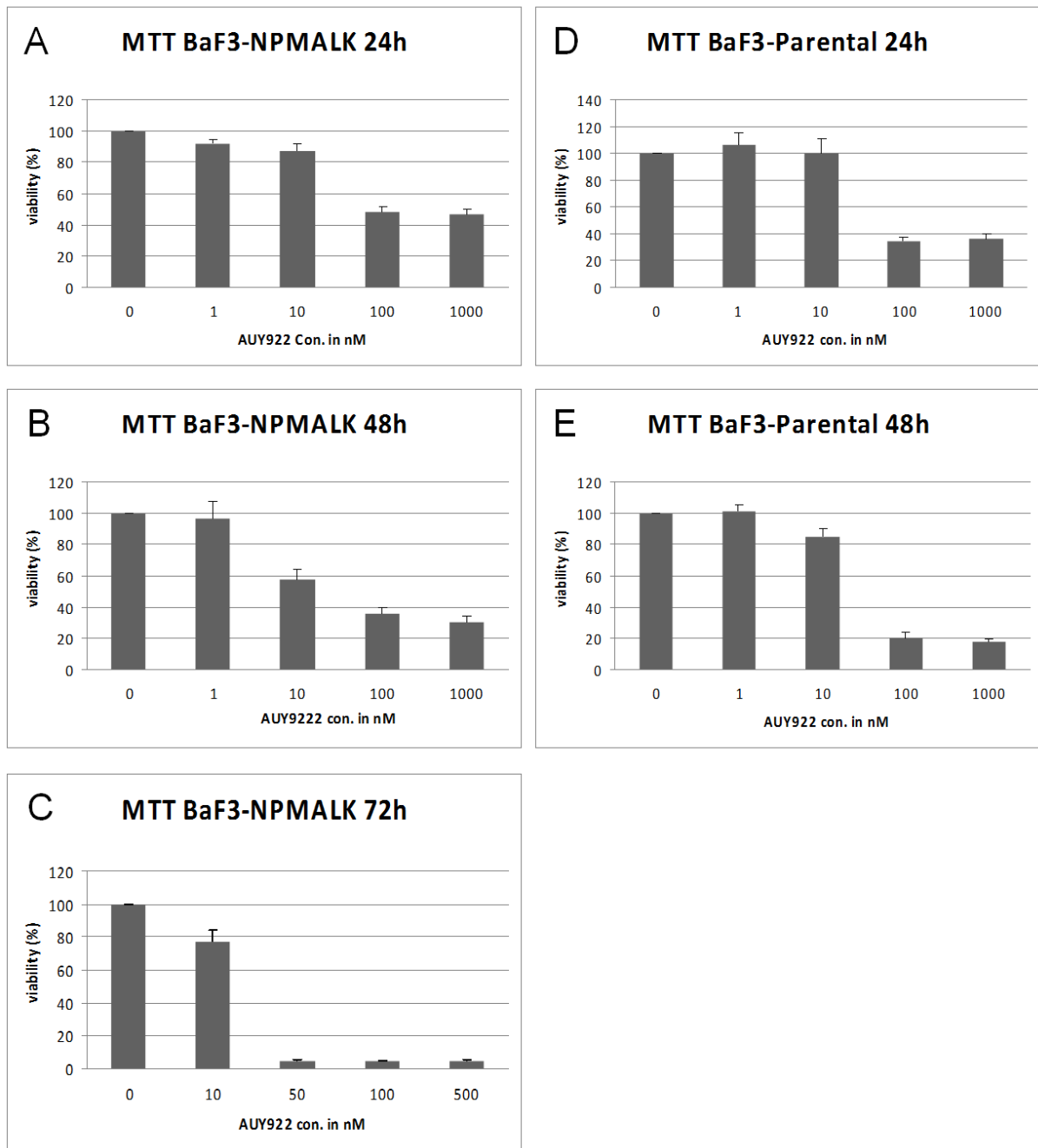


**Fig. 12:** Hsp90 inhibitor NVP-AUY922 inhibits the cell viability in the time and dose dependent Manner in BaF3-NPMALK and BaF3-parental cells. Cells were treated with the indicated concentration of AUY922 for 24 hours, 48 hours and 72 hours. The bars represent the mean  $\pm$  SD of the mean from n=3 experiments.

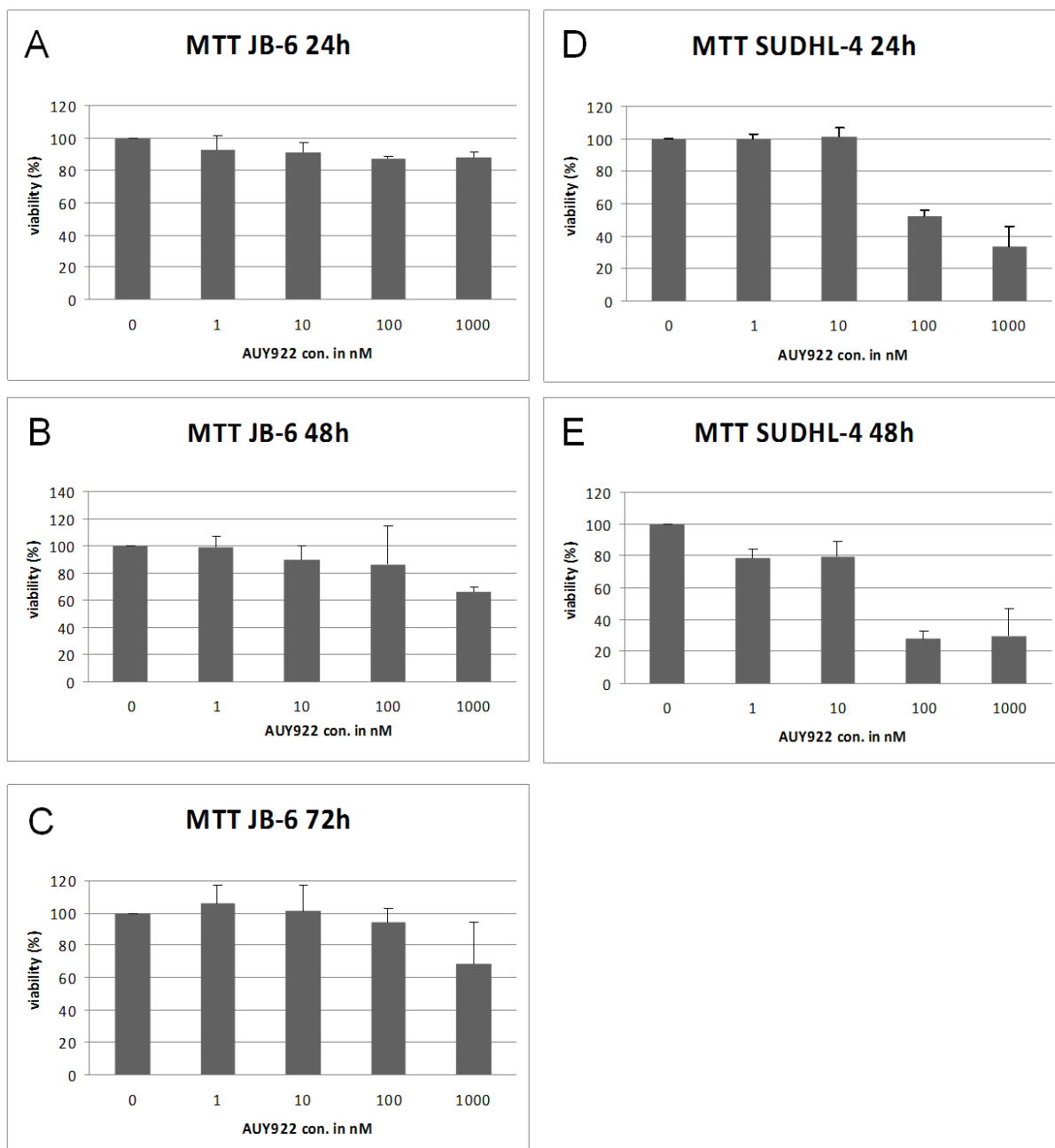


**Fig. 13:** Hsp90 inhibitor NVP-AUY922 inhibits the cell viability in the time and dose dependent Manner in SUDHL-4 cells, but JB-6 cells shown partially resistant to AUY922 treatment. Cells were treated with the indicated concentration of AUY922 for 24 hours, 48 hours and 72 hours. The bars represent the mean  $\pm$  SD of the mean from n=3 experiments.

Fig. 3

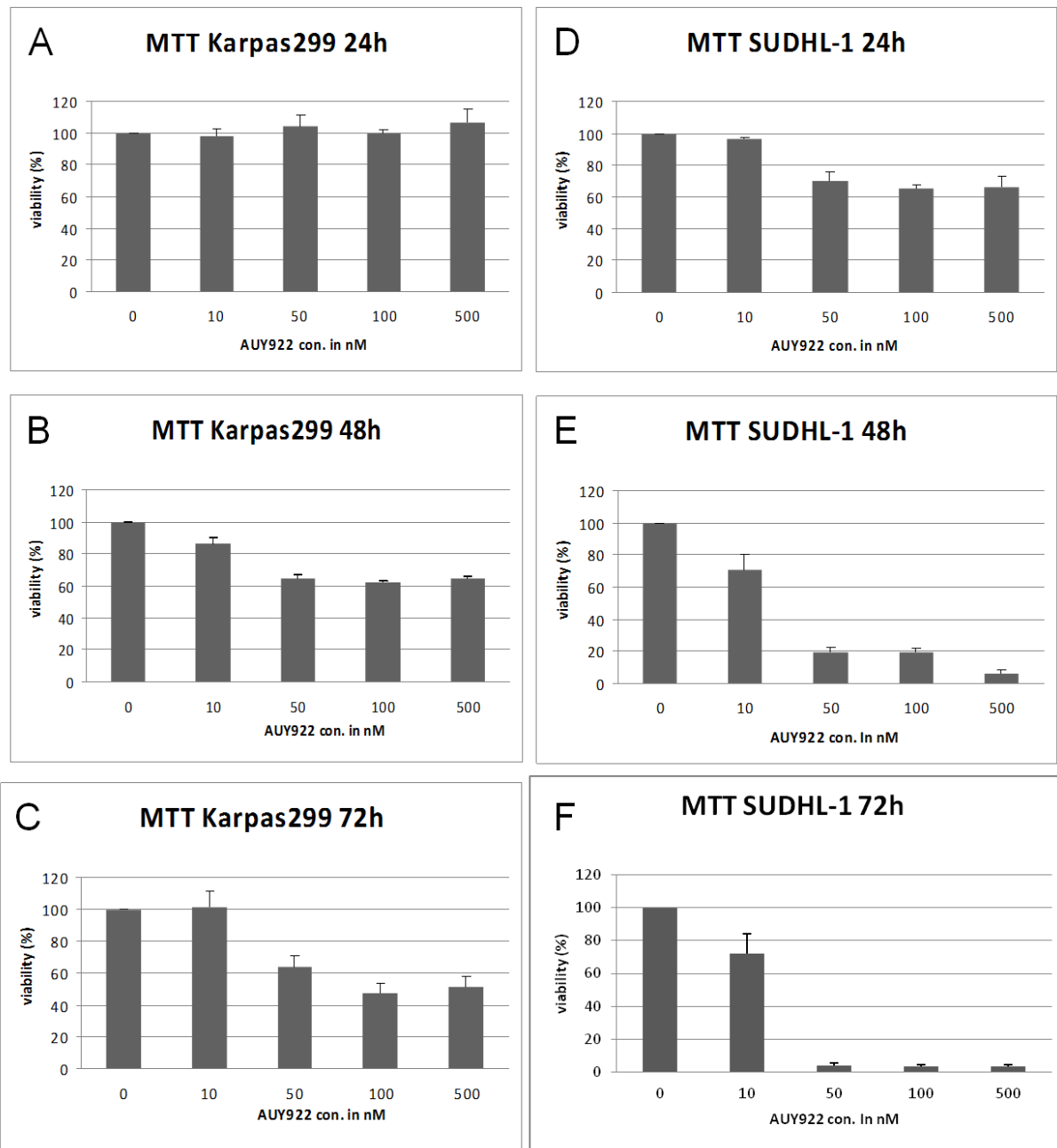


**Fig. 14:** Hsp90 inhibitor NVP-AUY922 inhibits the cell viability in the time and dose dependent Manner in SUDHL-1 cells, but karpas299 cells shown partially resistant to AUY922 treatment. Cells were treated with the indicated concentration of AUY922 for 24 hours, 48 hours and 72 hours. The bars represent the mean  $\pm$  SD of the mean from n=3 experiments.

### **4.3.2 Inhibition of Hsp90 activity triggers the cell cycle arrest and apoptosis of ALK+ lymphoma cells**

At nanomolar concentrations, NVP-AUY922 inhibits in vitro proliferation of human tumor cells selected for their different tissue origins and molecular features. We have studied the effect of NVP-AUY922 treatment for 24 hours, 48 hours and 72 hours on cell cycle of BaF3-NPMALK, BaF3- parental, JB-6, SUDHL-1 and Karpas299 lymphoma cells. The cell cycle was detected using the PI-staining FACS assay. NVP-AUY922 induced accumulation in either the G1 or the G1 plus G2/M phase in most of the investigated cell lines. The results showed that NVP-AUY922 arrested SUDHL-1 lymphoma cells in the original G1 (from 43.4% in control to 58.7% at 50 nM), while the S phase reduction was observed (from 29% in control to 4.5% at 50 nM) as early as 24 hours (Fig.16D). After a 48 hours of the treatment period, cells in the S phase (from 27.1% in control to 10.2% at 50 nM) traversed to the G1 phase (from 50.2% in control to 64% at 50 nM) remained blocked over 72 hours (Fig. 16E and F). The Cells traversed to the subG1 phase (from 5.2% in control to 43.8% at 50 nM) from the G1 phase (from 57.5% in control to 42.2% at 50 nM) and the S phase (from 29.6% in control to 4.6% at 50 nM) indicated apoptosis (Fig. 16E). Upon treatment with NVP-AUY922, BaF3-NPMALK demonstrated an increase in the percentage of cells accumulating in the G1 phase (from 14.6% in control reaching a peak value of 44.2% at 50 nM dosage) and the G2 phase (from 19.7% in control reaching a peak value of 28.2% at 50 nM dosage). The cells of the S phase decreased (from 58.8% in control reaching a value of 18.4% at 50 nM dosage) from 24 hours until 48 hours (Fig. 15A and B). After a 72 hours treatment with the drug, the cells traversed to the sub G1 phase (from 8.25% in control reaching a peak value of 60.39% at 50 nM dosage) from the G1 phase (from 24.7% in control to 7.6% at 50 nM dosage), the S phase (from 58.8% in control reaching to 8.2% at 50 nM dosage) and the G2 phase (from 19.7% in control to 6.4% at 50 nM dosage) (Fig. 15C). However, treatment of Karpas299 cells with NVP-AUY922 induced a therapeutic resistance (Fig. 16A-B). Inhibition of the S phase was detected only with 1% of karpas299 cells (from 18.3% to 17.9%) at a 50 nM dosage, compared with 15% in SUDHL-1 cells. After a 24 hours treatment with NVP-AUY922, only a slight change of the G1 and the G2 phases for Karpas299 cells was found during the incubation time up to 72 hours (Fig. 16A). The cell cycle of BaF3-Parental and BaF3-NPMALK cells changed in a similar way (Fig. 15A-B).

To determinate the NVP-AUY922 induced apoptosis we have studied the effect of NVP-AUY922 treatment 48 hours BaF3-NPMALK, Karpas299, SUDHL-1, SUP-M2 and SR-786 lymphoma cells. The results showed that NVP-AUY922 caused the remarkable cell death in BaF3-NPMALK, SUDHL-1, SUP-M2 and SR-786 lymphoma cells but not in Karpas299

lymphoma cells (Fig. 17 and 18). BaF3-NPMALK and SUP-M2 cells showed more sensitive to NVP-AUY922 treatment than other cells, with almost 100% cell death after 48 hours incubation at a 50 nM dosage of NVP-AUY922 (Fig. 17A and 18A). The dead cells increased from 5% to 40% after 48 hours treatment period with NVP-AUY922 (dosage: 50 nM) in SUDHL-1. Although are the SR-786 less sensitive to NVP-AUY922 treatment than BaF3-NPMALK or SUP-M2 cells. But the NVP-AUY922 still caused a 60% death in SR-789 cells after 48 hours incubation (Fig. 18B). As showed in Fig. 17B is there no remarkable cell death in Karpas299 cells after NVP-AUY922 treatment, means that Karpas299 cells are resistant to NVP-AUY922 treatment in vitro. PI-FACS was also done on SUP-M2 and SR-789 lymphoma cells to determine the cell cycle arrest. No surprisingly, NVP-AUY922 arrests both SUP-M2 and SR-789 lymphoma cells in SubG1 phase (Fig.18).

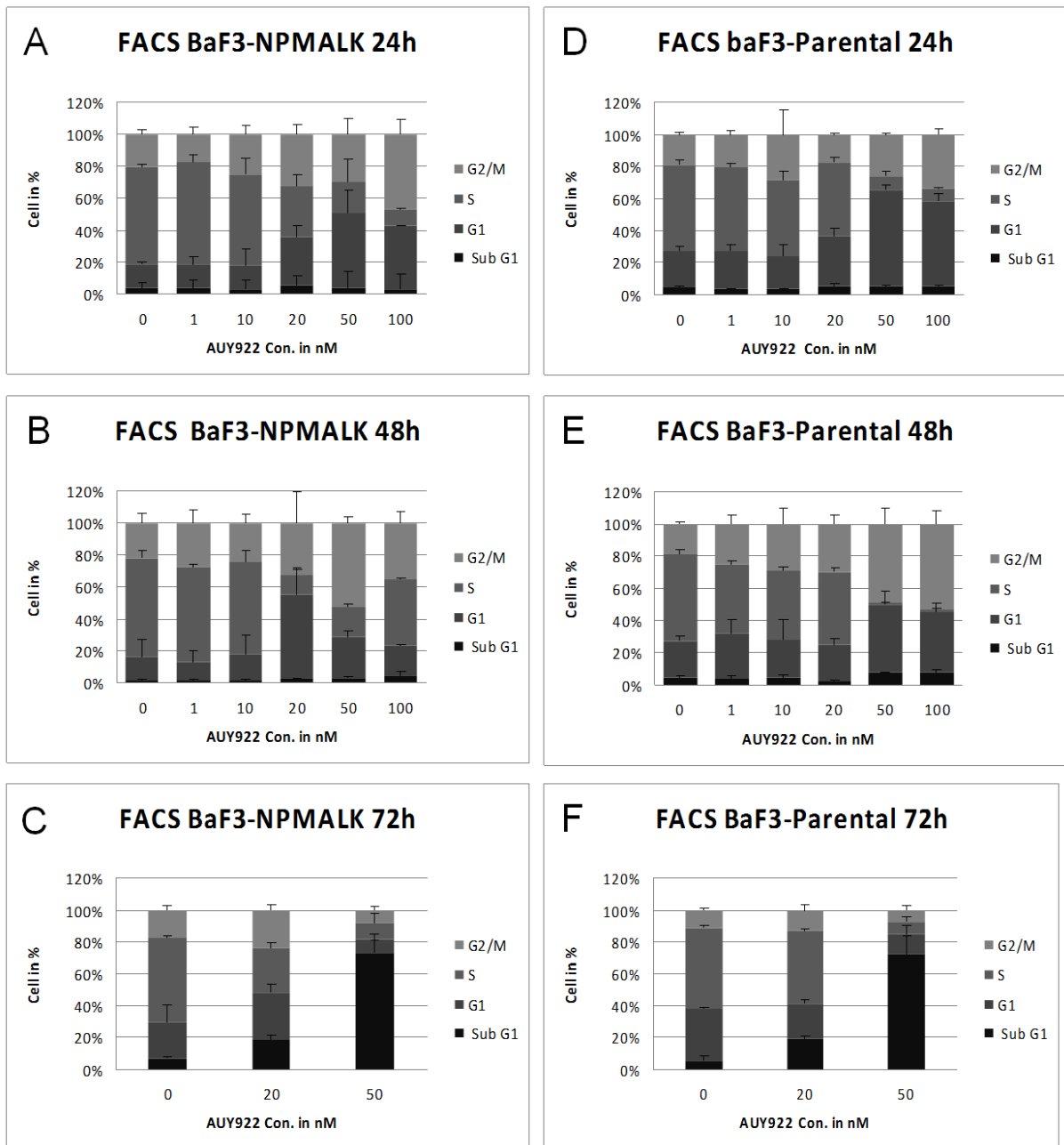


**Fig. 15:** Hsp90 inhibitor NVP-AUY922 induces the cell cycle arrest (G1-phase) and apoptosis in BaF3-NPMALK and BaF3-parental lymphoma cells. Cells were treated with the indicated concentration of AUY922 for 24 hours, 48 hours and 72 hours. The bars represent the mean  $\pm$  SD of the mean from n=3 experiments.

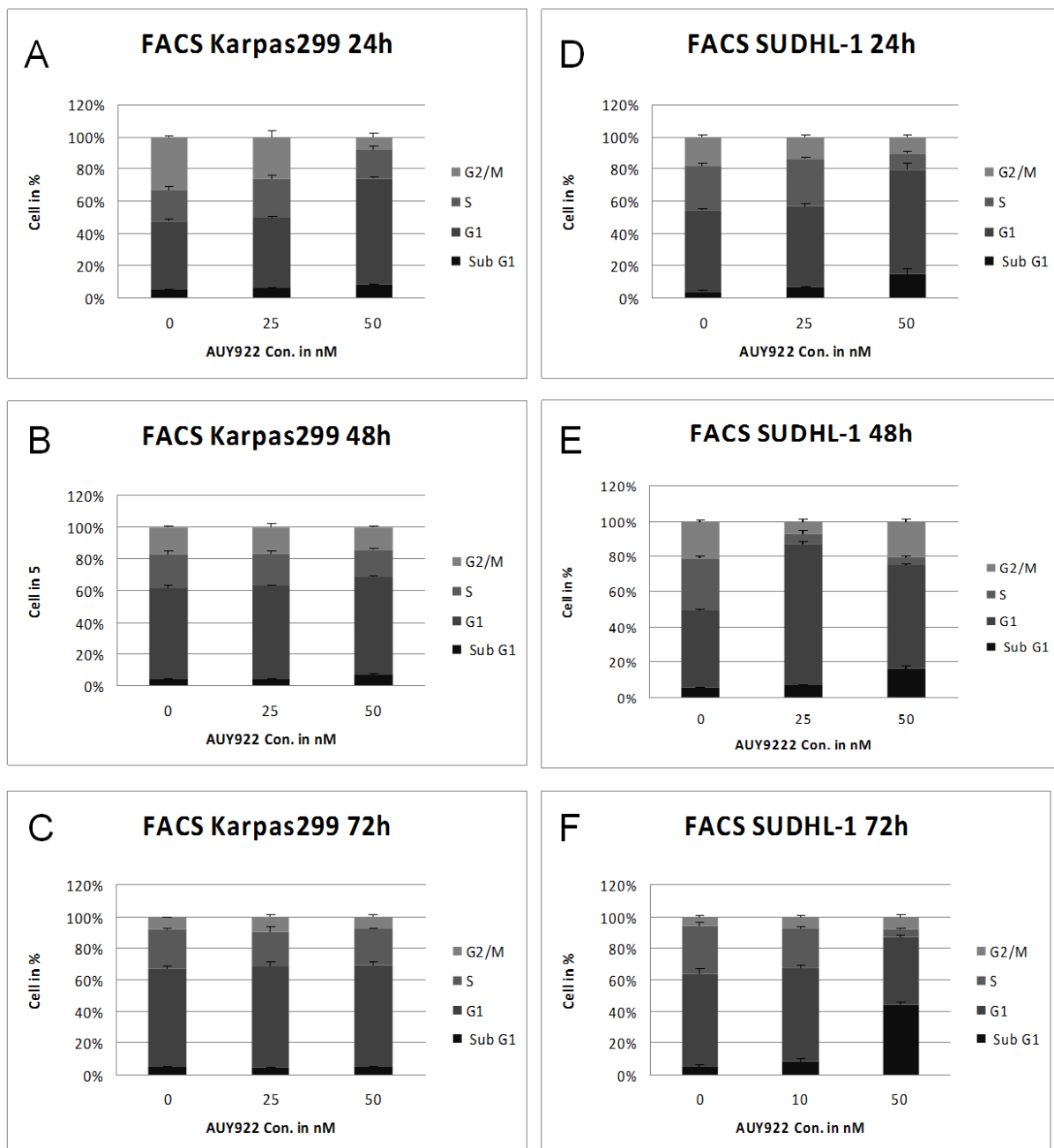


**Fig. 16:** Hsp90 inhibitor NVP-AUY922 induces the cell cycle arrest (G1-phase) and apoptosis in SUDHL-1 lymphoma cells, but karpas299 shown resistance to AUY922 treatment. Cells were treated with the indicated concentration of AUY922 for 24 , 48hours and 72 hours. The bars represent the mean  $\pm$  SD of the mean from n=3 experiments.

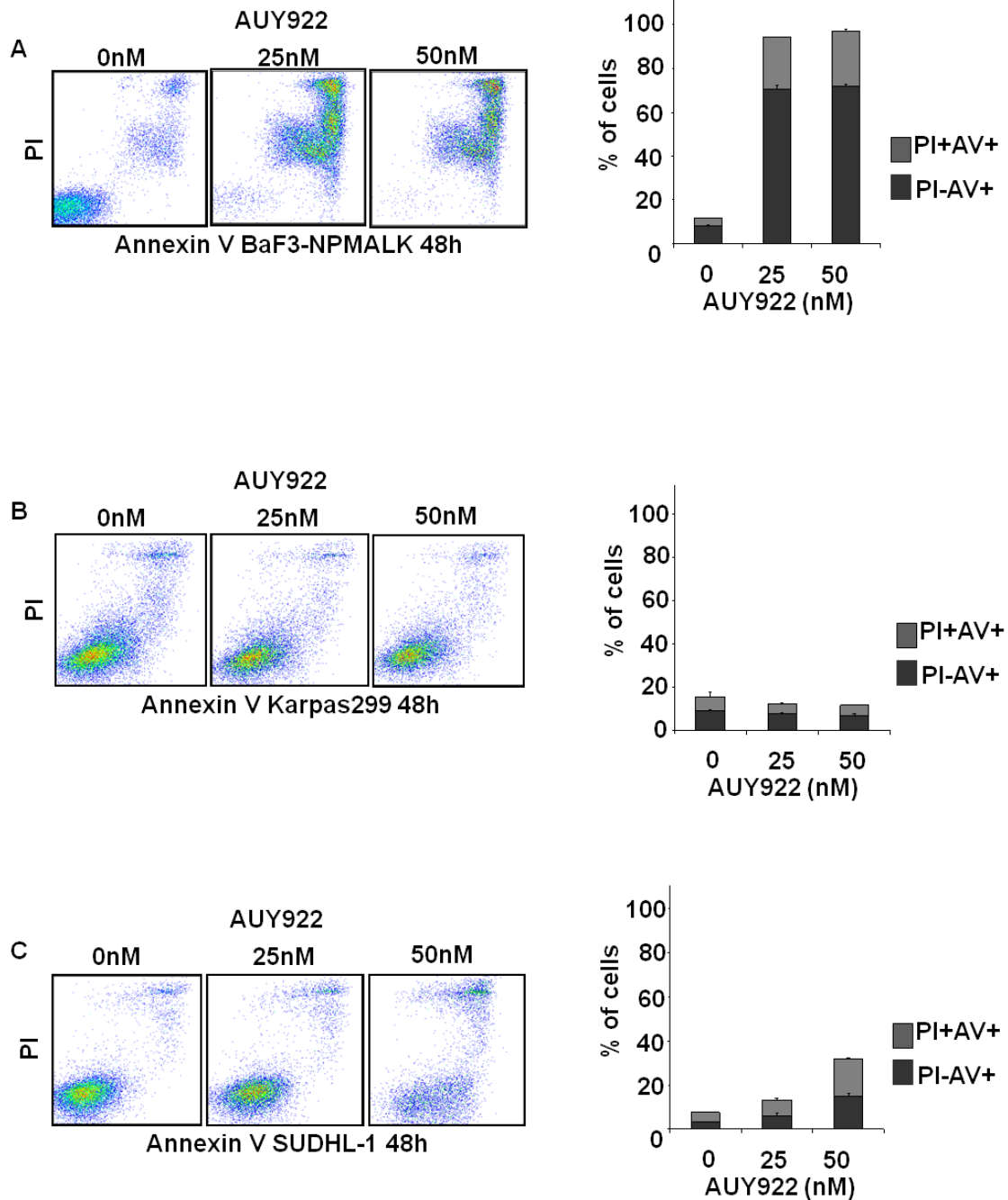


**Fig. 17:** Hsp90 inhibitor NVP-AUY922 induced an apoptosis in ALCL cells (A: BaF3-NPMAL cells, B: Karpas299 cells, C: SUDHL-1 cells) as determined using Annexin V-FACS. Cells were treated with the indicated concentration of AUY922 for 48 hours. The bars represent the mean  $\pm$  SD of the mean from n=3 experiments.

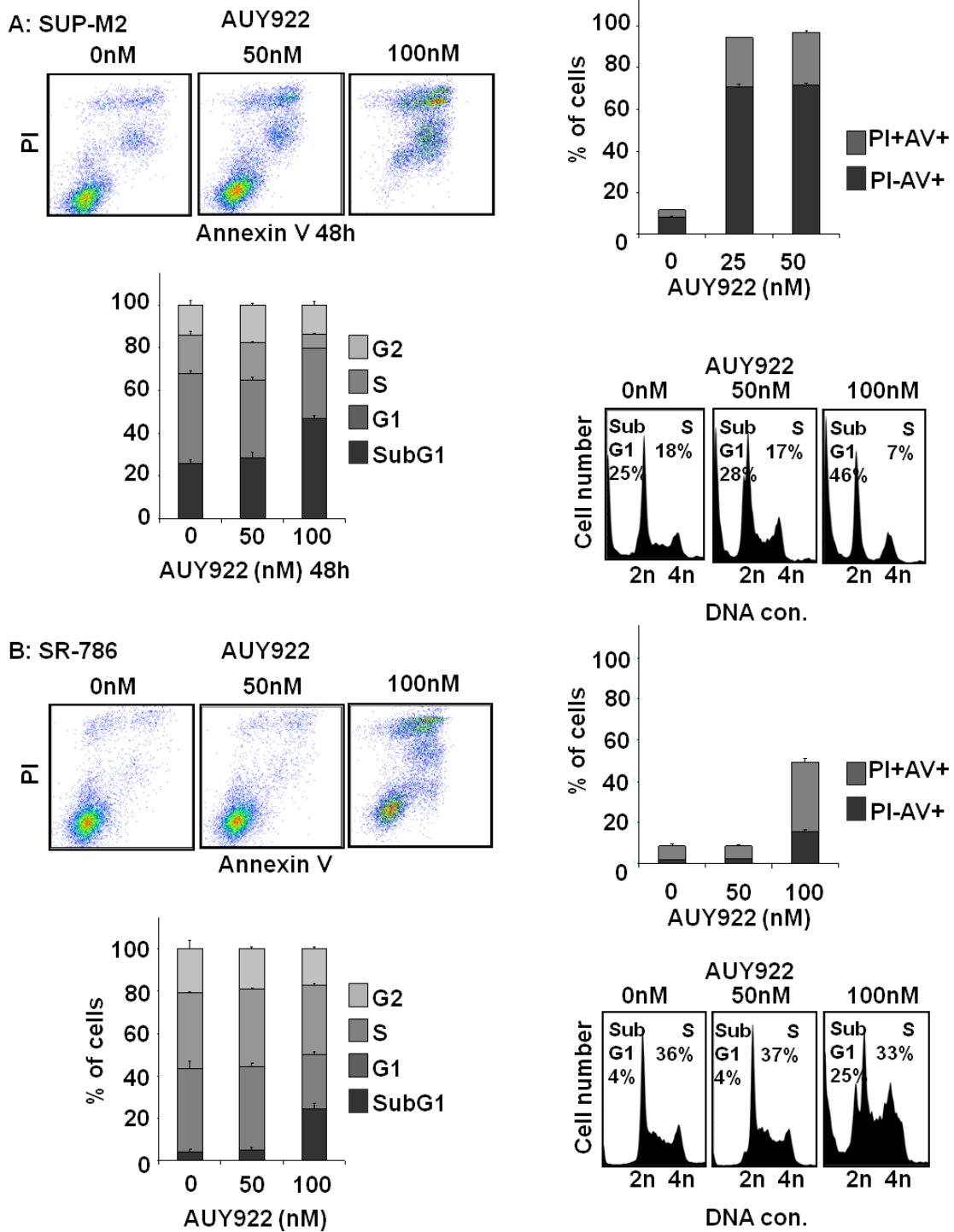


**Fig. 18:** The Hsp90 inhibitor NVP-AUY922 induced apoptosis in ALCL cells (A: SUP-M2 cells, B: SR-786 cells) as determined using Annexin V and PI-FACS. Cells were treated with the indicated concentration of AUY922 for 48 hours. The bars represent the mean  $\pm$  SD of the mean from n=3 experiments.

### 4.3.3 Down-regulation of several oncogenic proteins during exposure of human lymphoma cells to Hsp90 inhibitor

NPM-ALK is a constitutively active fusion tyrosine kinase involved in lymphomagenesis of ALCL cells, whose maturation and activity depend on their association with a Hsp90 protein chaperone. Targeting Hsp90 by NVP-AUY922 promotes degradation of several proteins through ubiquitin-proteasome pathways, including oncogenic AKT, STAT3 and p70S6K.

NPM-ALK expression is down-regulated in lymphoma cells by NVP-AUY922. To study the effect of NVP-AUY922 on expression of NMP-ALK, several cell lines characterized previously by the presence of the t(2;5) translocation were chosen as experimental models, including BaF3-NPMALK, SUDHL-1 and Karpas299, and their proteins were analysed using Western blotting. The lymphoma cells were maintained in log phase growth and treated with different concentrations of NVP-AUY922 for 4 hours, 8 hours, 24 hours or 48 hours (Figs. 19 to 20). Cells were lysed and ALK proteins were detected using an antibody ALK, which is specific for the cytoplasmic region of mature ALK.

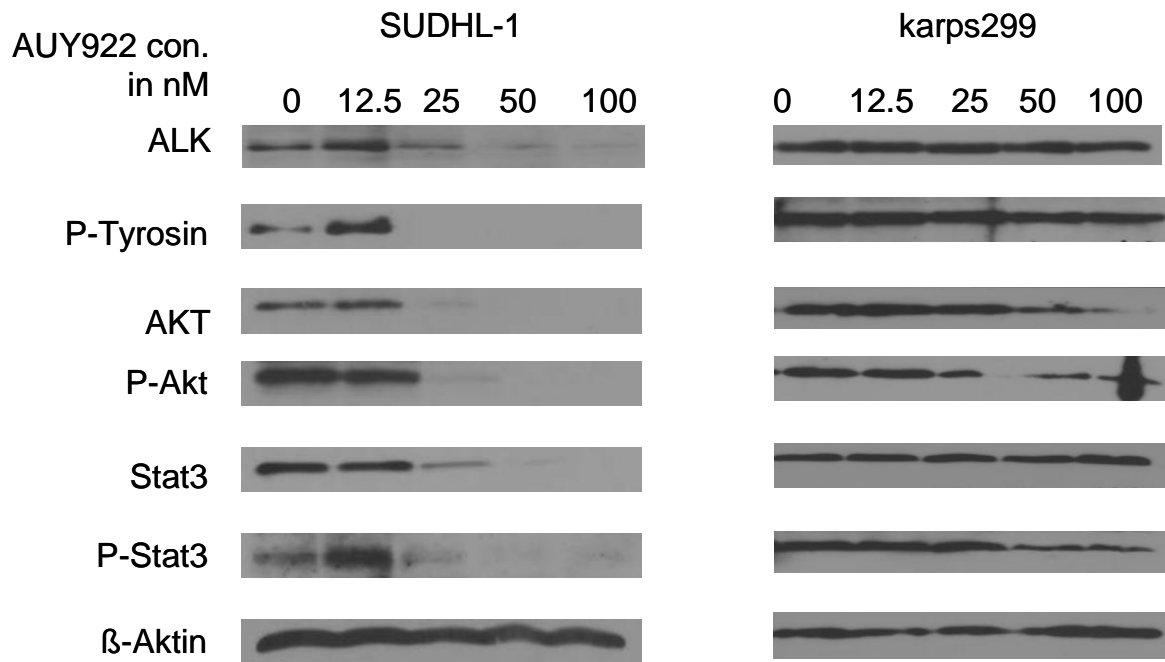
As shown in Fig. 19A, the ALK protein only began to change after a 24 hours treatment in all cell lines. Tyrosine-phosphorylated ALK proteins were detected with p-tyrosine antibody. The cell lines all responded to the NVP-AUY922 treatment. The p-tyrosine decreased proportionally to the increase of the NVP-AUY922 concentrations. In comparison with control cells, the reduction of proteins in SUDHL-1 cells reached 50%, when exposed to 25 nM NVP-AUY922. No phosphorylation of the ALK protein could be detected above a dosage of 50 nM. Remarkably, a decrease in ALK protein was observed after the incubation with AUY922 for 48 hours (Fig. 19B). Moreover, Fig. 19B shows the complete inhibition of ALK above AUY922 concentrations of 50 nM. However, there was still no significant decrease in ALK protein or phosphorylation of ALK protein found in Karpas299 cells. Recruitment and phosphorylation of downstream effected proteins require NPM-ALK dimerization and auto-phosphorylation. Thus, we measured levels of tyrosine-phosphorylated ALK in cells exposed for 24 hours and 48 hours to NVP-AUY922 with different concentrations. Proteins, known not to be Hsp90 client proteins, including  $\beta$ -actin, did not show any decrease in expression. This is consistent with the idea that the responsiveness of these cells to NVP-AUY922 is a result of the degradation of Hsp90 client proteins. Changes in phosphorylation states of signalling protein p-Tyrosine were shown in Figs. 19A and 19B. These decreases in phosphoproteins could result from either a decrease in baseline quantities of the non-phosphorylated versions of ALK proteins, or from the degradation of upstream proteins, which normally phosphorylate ALK and Tyrosine. We also found that reduction of ALK and p-Tyrosine levels in BaF3-NPMALK cells could be observed as early as the 8 hours incubation with AUY922 (Fig. 19B).

Upon exposure to NVP-AUY922, NPM-ALK proteins have shown to be down-regulated in the human lymphoma cells. Additionally, NPM-ALK mediates oncogenesis, at least partially, through phosphorylation and / or activation of phosphatidylinositol 3-kinase (PI3K), the serine/threonine kinase AKT/mammalian target of rapamycin, Janus kinase/signal transducers and activators of transcription pathways, resulting in cell proliferation and anti-apoptotic signals (11). Therefore, AKT kinase is the prominent downstream target of PI3K and one of important protein part in the Hsp90 pathway. AKT is also a critical regulatory compound in many signalling pathways.

Upon administration of NVP-AUY922, AKT has proved to be down-regulated in BaF3-NPMALK and SUDHL-1 cell lines in a dose- and time-dependent manner (Fig. 19A and 19B). NVP-AUY922 reduced AKT proteins in BaF3 cells after only an 8 hours treatment (Fig. 20). Then a 100% inhibition of AKT protein expression was detected in a dosage of 50 nM after 24 hours of treatment period. The resistance of the Karpas299 to NVP-AUY922 was also observed through AKT western blotting. Next, we tested for presence of phosphorylated AKT in the same cells both before and after NVP-AUY922 treatment. In SUDHL-1 and BaF3-NPMALK cell lines, AKT phosphorylation showed a dose-dependent decrease. The reduction resulted in an almost total elimination of the active form of protein with drug concentrations above 50 nM in both cell lines after a 24 hours treatment with NVP-AUY922 and with drug concentrations above 25 nM after 48 hours of treatment period. There was only a slight reduction of phosphorylation AKT protein shown in Karpas299 cells after a 48 hours treatment with AUY922 with drug concentrations above 50 nM.

In addition, we also examined one group of AKT downstream targets tightly associated with cell growth and apoptosis signalling. A member of the STAT protein family – STAT3 acts as a transcription activator, which is crucial to the pathogenesis of ALK+ ALCL. Western blotting was performed to compare Karpas299 cells with SUDHL-1 and BaF3 Cells (Fig. 20) during treatment with NVP-AUY922 in different drug concentrations and incubation times. Decrease in p-STAT3 was more obvious in SUDHL-1 cells than in Karps299 cells after a 24 hours treatment (Fig. 19A), but less than that in AKT and p-AKT proteins. However, after a 48 hours treatment (Fig. 19B) of SUDHL-1 and BaF3-NPMAL cells with NVP-AUY922, the absence of STAT3 and p-STAT3 was detected with the dosage of 50 nM. In contrast, there was no significant change of the STAT3 and p-STAT3 in karpas299 cells.

A



B

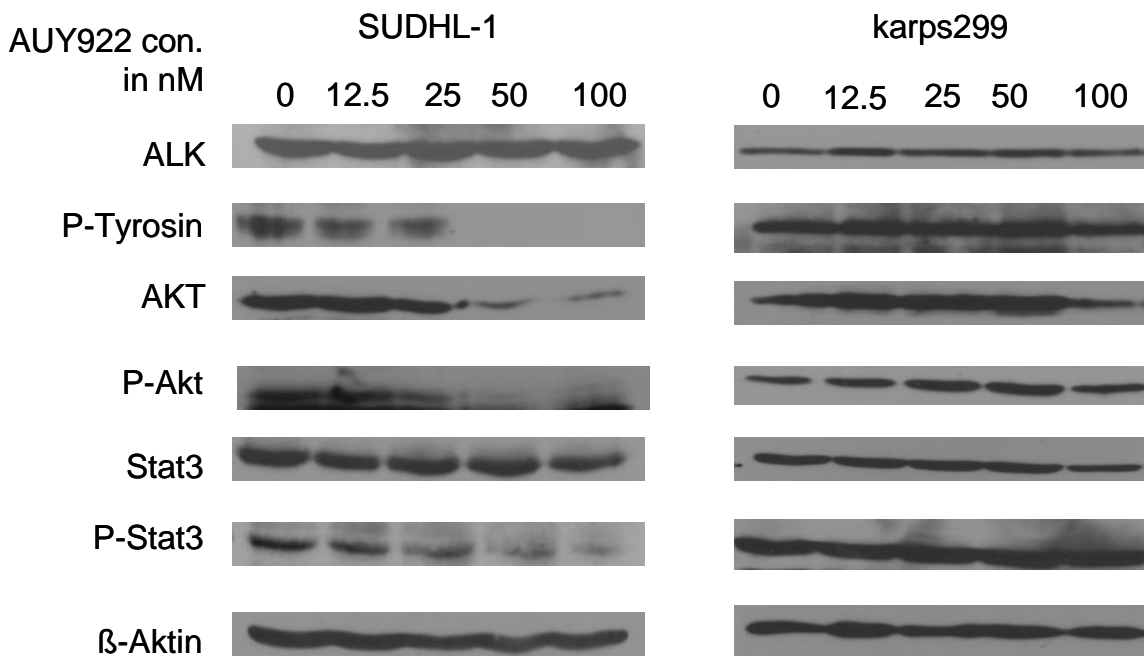


**Fig. 19:** The Hsp90 inhibitor NVP-AUY922 inhibits expression of several oncoproteins or phosphorylation in SUDHL-1 but not in Karpas299 lymphoma cells. Cells were treated with the indicated concentration of AUY922 for 24 hours (A) and 48 hours (B).

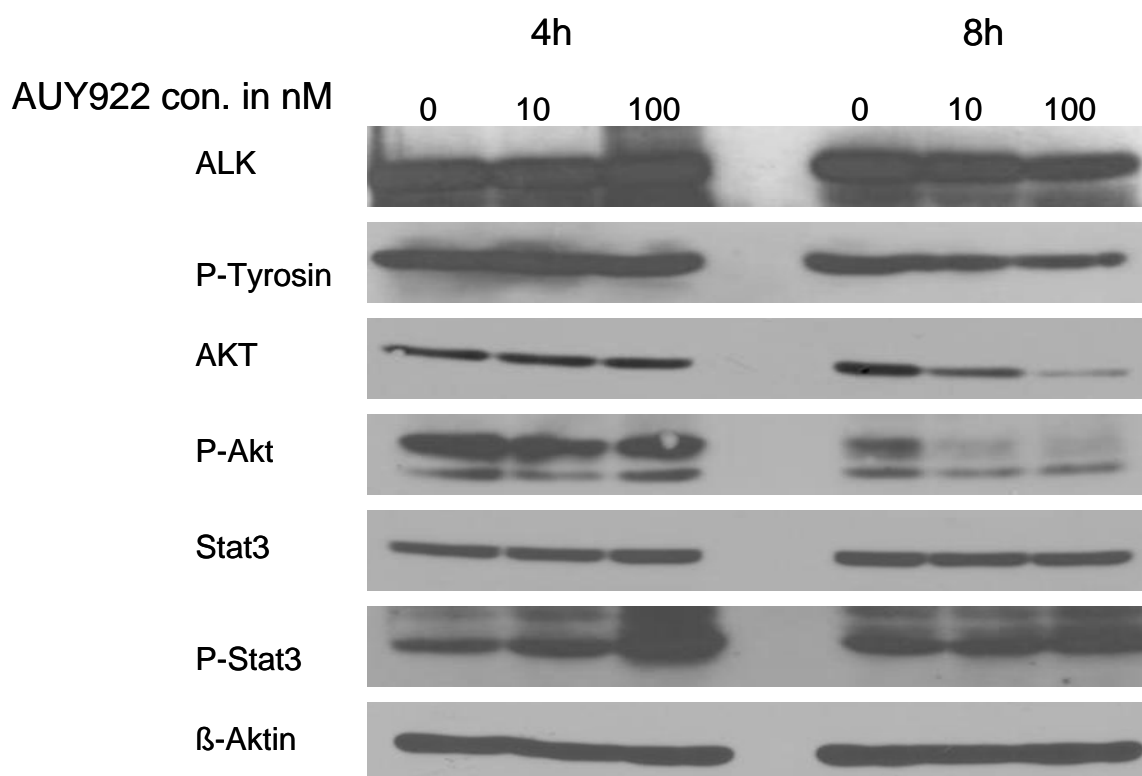


**Fig. 20:** NVP-AUY922 inhibits expression of oncoproteins or phosphorylation in Baf3-NPMALK only after 8 hours incubation. Cells were treated with the indicated concentration of AUY922 for 4 hours and 8 hours.

#### 4.3.4 A sensitive measure for Hsp90 inhibition of NPM-ALK+ ALCL using FLT-uptake in vitro

To determine whether Hsp90-NPM-ALK targeted treatment with AUY922 was assessable by measuring FLT and FDG-uptake, we examined the cellular tracer uptake of FLT and FDG in AUY922 treated BaF3-NPMALK, Karpas299, SUDHL-1 and SR-786 cells (Fig. 20). Cells were incubated with FLT or FDG for 45 min after a 48 hours treatment period and the activity was measured using a gamma-counter. As shown in Fig. 21D, Hsp90 inhibition led to a remarkable reduction of both FLT- and FDG-uptake in SUDHL-1 cells. However, the sensitivity of FLT was significantly higher showing a complete lack of FLT-uptake in the presence of 25 nM AUY922. In contrast, FDG-uptake was only reduced by 40% compared to the vehicle-treated control at the same dose level. These data suggest that FLT-uptake is more sensitive for determining effective NPM-ALK targeted treatment in vitro.

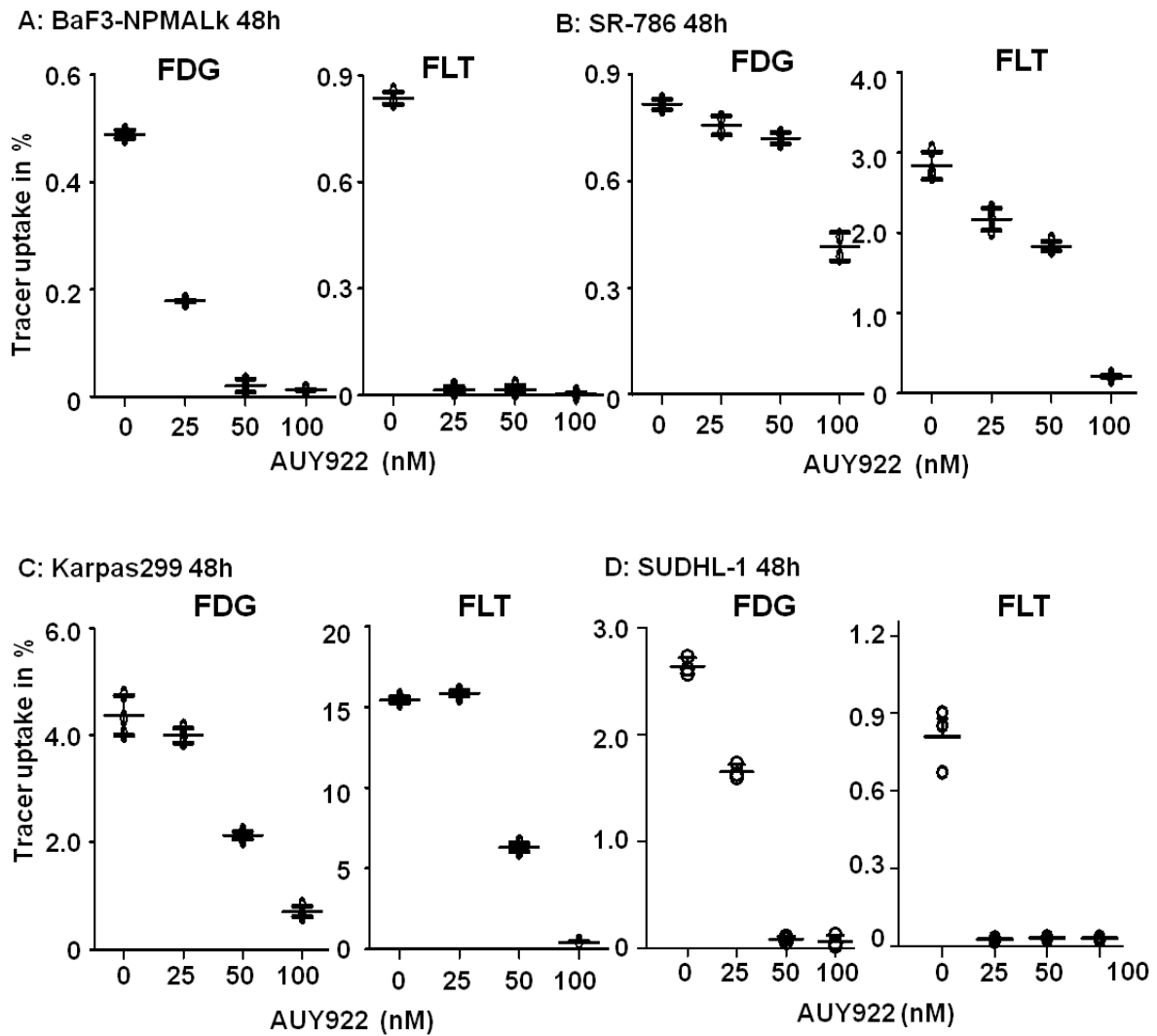


**Fig. 21:** FLT-uptake is more sensitive for determining effective NPM-ALK targeted treatment in vitro (A: BaF3-NPMALK cells, B: SR-786 cells, C: Karpas299 cells and D: SUDHL-1 cells). Cells were treated with the indicated concentration of AUY922 for 48 hours. The bars represent the mean  $\pm$  SD of the mean from n=3 experiments.

## **4.4 Functional *in vivo* imaging of response to Hsp90 inhibition in SUDHL-1 lymphoma by FLT-PET is superior to FDG-PET**

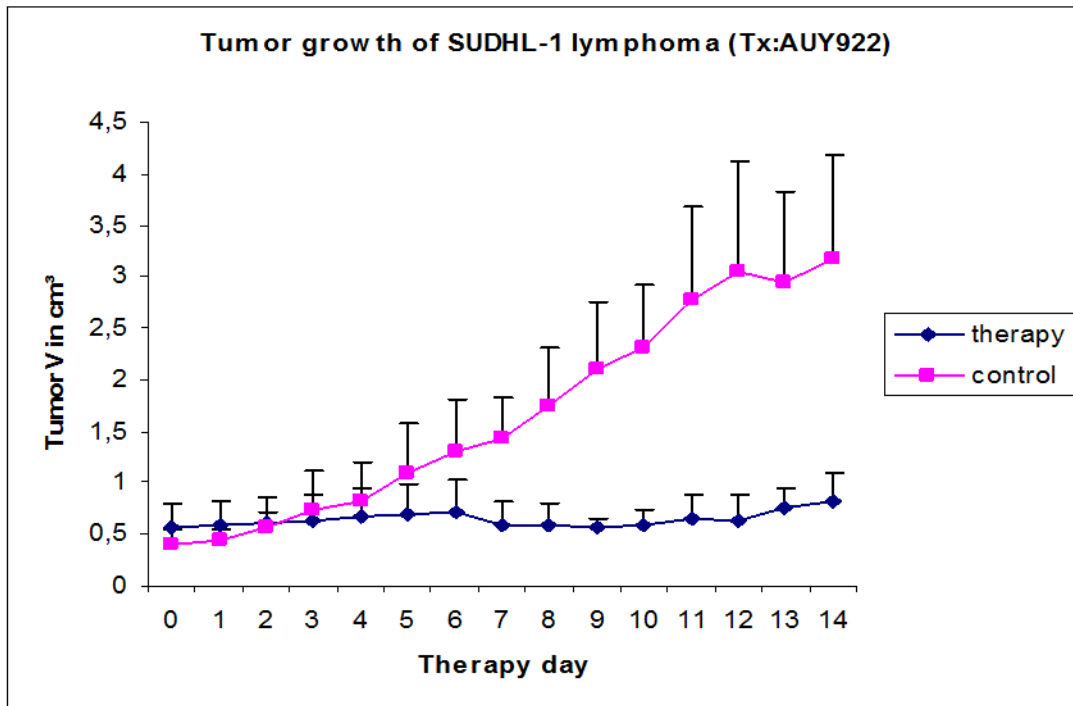
### **4.4.1 *In vivo* Hsp90 inhibition blocks the growth of the NPM-AKL lymphoma**

Once xenotransplants reached a size of approximately 0.3-0.8 cm<sup>3</sup>, mice (n=33) were treated with a single dose of NVP-AUY922 (25 mg/kg, i.p., daily). Tumor size was measured using a shifting calliper and the tumor volume was calculated using the formula:  $L*B*B/2$ .

For SUDHL-1 lymphoma bearing mice, the control group (n=4, d0) received only a glucose solution. Treated mice showed a lower rate of tumor growth at d+7 (n=12, fold=1.3, SD=0.3, range 0.7-1.8-fold) than the control group (fold=2.9, SD=1.5, range 2.2-5.6-fold, Fig. 22A). After two weeks, the tumor volume of the control group increased from 0.4cm<sup>3</sup> (n=4, SD=0.1, range 0.3-0.6) to 3.2cm<sup>3</sup> (n=2, SD=1.0, range 2.46 cm<sup>3</sup>-3.88 cm<sup>3</sup>). In contrast, in the therapeutic group there was only a slight increase from 0.6cm<sup>3</sup> (n=12, SD=0.2, range 0.2 cm<sup>3</sup>-0.9 cm<sup>3</sup>) to 0.8cm<sup>3</sup> (n=3, SD=0.2, range 0.5 cm<sup>3</sup>-1.0 cm<sup>3</sup>, Fig. 22A).

As we showed in the *in vitro* studies, Karpas299 cells were detected with a partial resistance to the AUY922 treatment. Rather than SUDHL-1 cells, Karpas299 cells gave rise to xenograft tumors that were entirely resistant to targeted therapy with AUY922 (n=10, 25 mg/kg i.p. daily, mean 3.2-fold increase, SD=0.4, range 2.9-3.6). The karpas299 xenograft tumors grew at a rate similar to the control tumors (n=7, mean 5.2-fold increase, SD=1.5, range 2.8-7.6) (Fig. 22B).

A



B

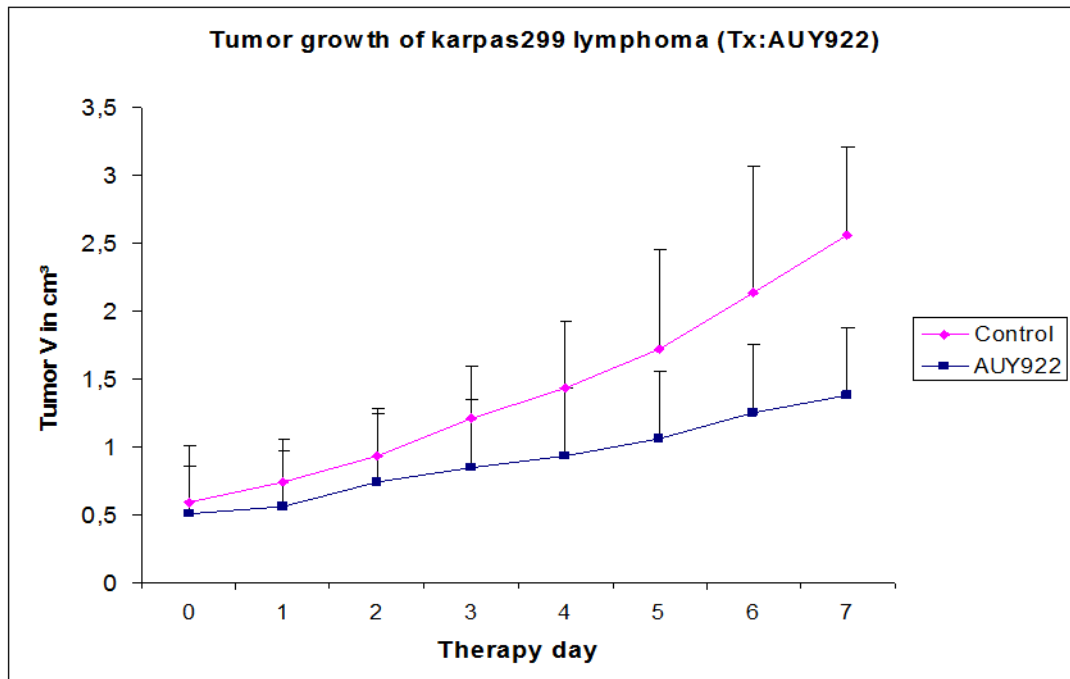


**Fig. 22:** NVP-AUY922 blocks the SUDHL-1 tumor growth. But Karpas299 lymphoma showed partially resistant to NVP-AUY922 treatment (Fig. A: SUDHL-1 lymphoma, Fig.B: Karpas299

lymphoma). The lymphoma bearing mice were treated intraperitoneally with 25 mg/kg AUY922 (Therapy) or only placebo (Control) daily. The bars represent the mean  $\pm$  SD.

#### 4.4.2 FDG-PET imaging analysis shows inhibitory effect of Hsp90 inhibitor on the NPM-ALK lymphoma metabolism

To investigate how SUDHL-1 lymphoma responded to the AUY922 treatment, FDG-PET was performed both before and after therapy at d-1, d+6 and d+14 in this study (Fig. 23A). Mean TBR (tumor to background ratio) of treated mice with a dose of 25 mg/kg reduced from 8.6 (n=12, range 4.6-14.3, SD= 3.5) to 7.5(n=12, range 4.4-10.2, SD= 2.0), while the mean TBR of the untreated mice was increased from 5.7 (n= 4, range 2.3-8.1, SD= 2.5) to 13.2 (n=4, range 4.7-17.6, SD= 5.8) at d+6, but then reduced to 7.3 (n=3, range 5.6-9.0, SD= 1.7) at d+14.

To analyse the therapeutic response of NPM-ALK lymphoma, the TBR of FDG-PET were also analysed statistically (Fig. 23B). FDG-PET analysis of control animals revealed a significant increase in FDG-uptake on day 5 (n=4, mean TBR 205.2%, range 195%-331.2%, SD=65%, p=0.03). In AUY922 treated animals, relative TBR of early FDG-PET did not show a significant reduction compared to the pre-treatment control (n=12, mean TBR 87%, SD=40.3%, range 31-161%; p=0.151, Fig. 23B). Interestingly, the mean TBR of FDG-uptake at later time points (day 15 to 21) decreased to 44% (n=3, SD=33.6%, range 23-85%) (data not shown).

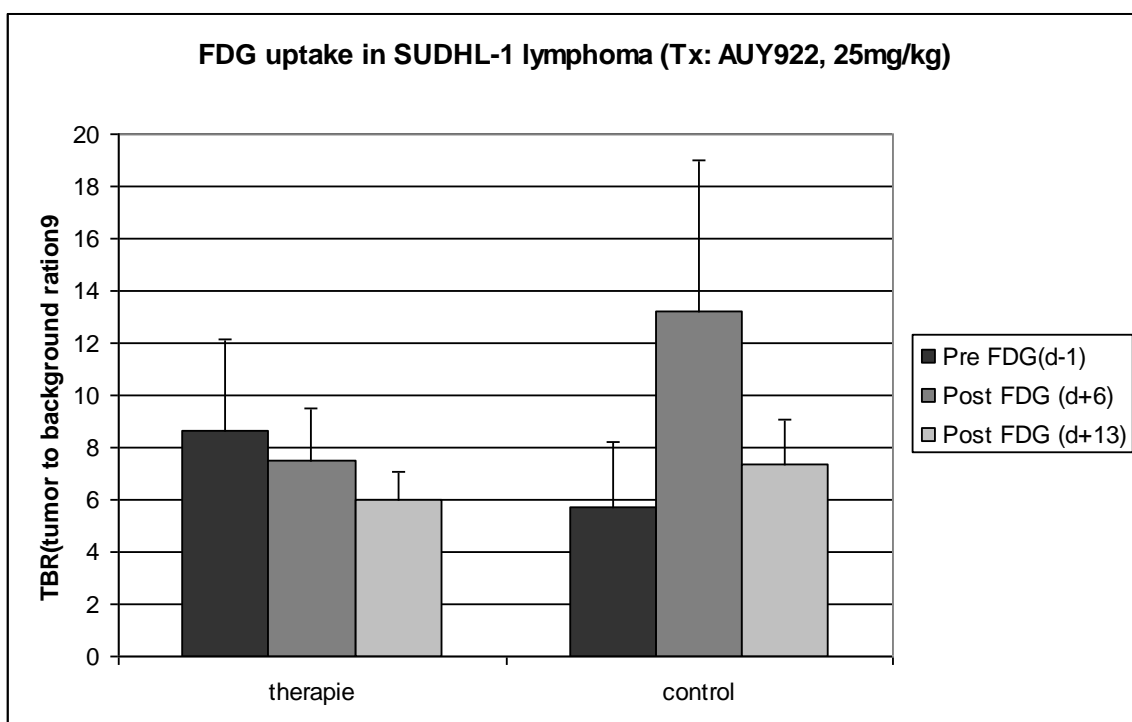


**Fig. 23A:** AUY922 treatment reduces the FDG-tracer-uptake in SUDHL-1 lymphoma. The SUDHL-1 lymphoma bearing mice were treated intraperitoneally with 25 mg/kg AUY922 (Therapy) or only placebo (Control) daily. Pre therapeutic FDG-PET was performed one day before therapy, post therapeutic FDG-PET were performed 6 days and 13 days after therapy. The bars represent the mean  $\pm$  SD.

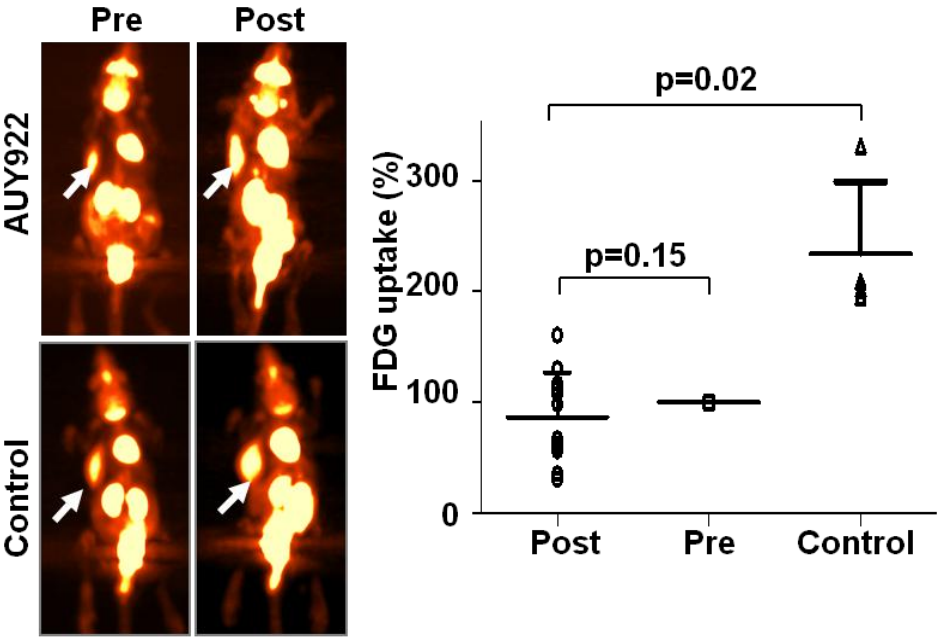
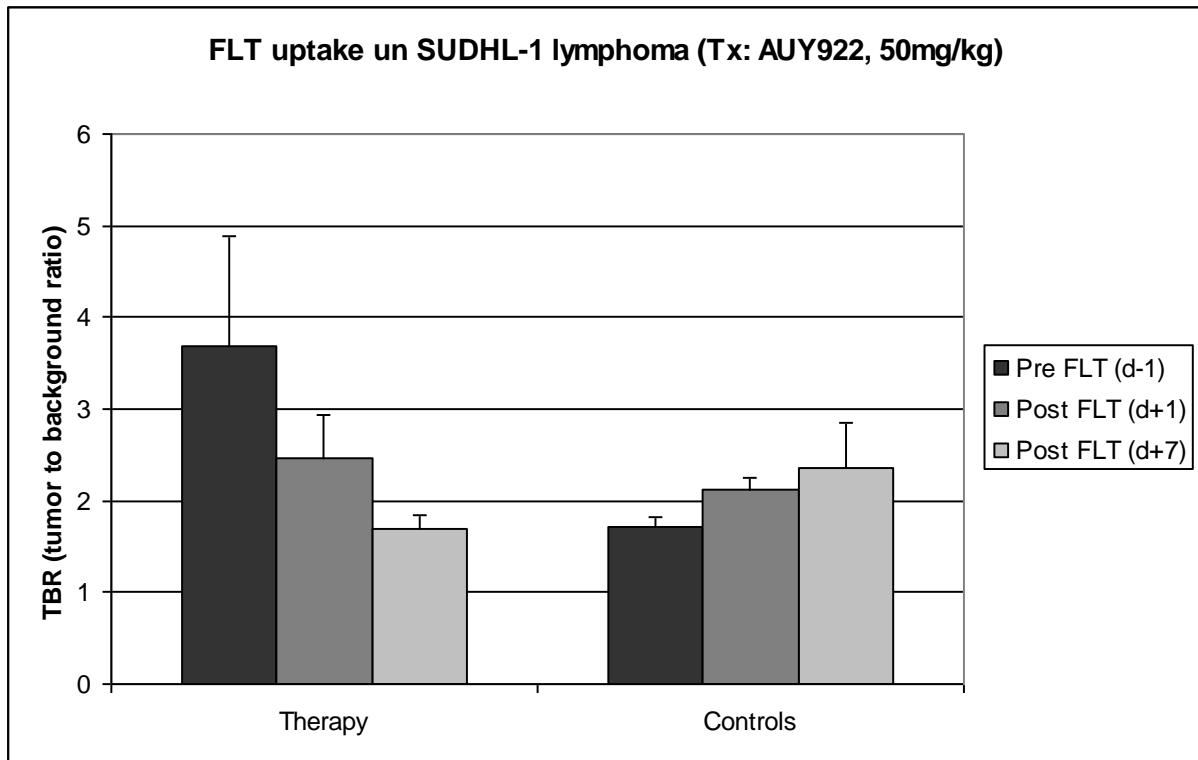
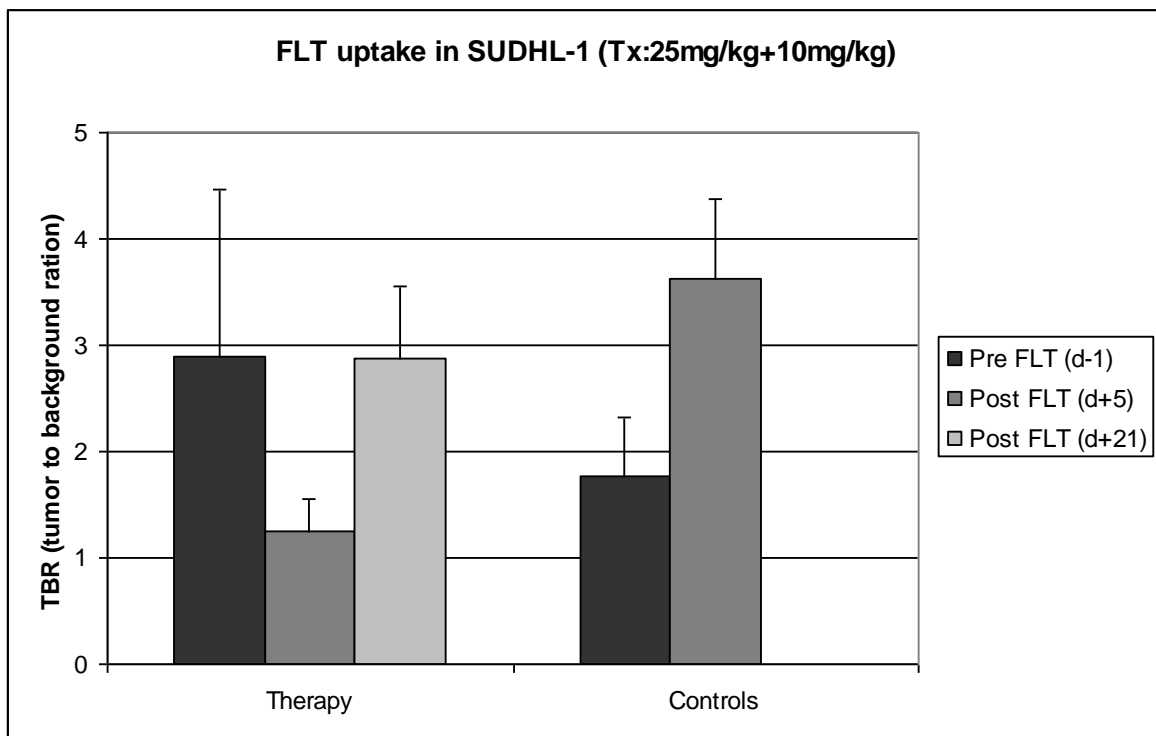


**Fig. 23B:** Functional *in vivo* imaging of response to AUY922 inhibition in SUDHL-1 lymphoma using FDG-PET and TBR on day 0, defined as 100% (“pre”), and change of TBR compared to pre-treatment values are shown for treated (“post”) and control animals.

A



B



C

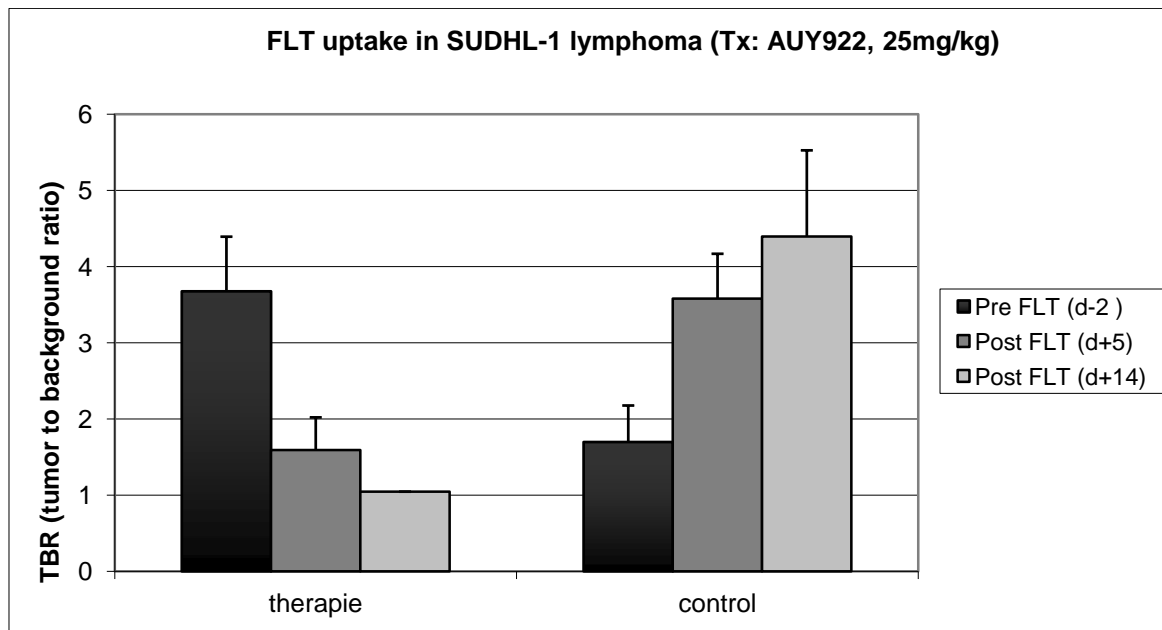


**Fig. 24:** AUY922 treatment reduces the FLT-tracer-uptake in SUDHL-1 lymphoma. The SUDHL-1 lymphoma bearing mice were treated intraperitoneally with 50 mg/kg (Fig. A), 25 mg/kg+10 mg/kg (Fig. B) or 25 mg/kg (Fig. C) AUY922 (Therapy) or only placebo (Control) daily. Pre therapeutic FLT-PET was performed one or two days before therapy, post therapeutic FLT-PET was performed 5 days and 14 days after therapy. The bars represent the mean  $\pm$  SD

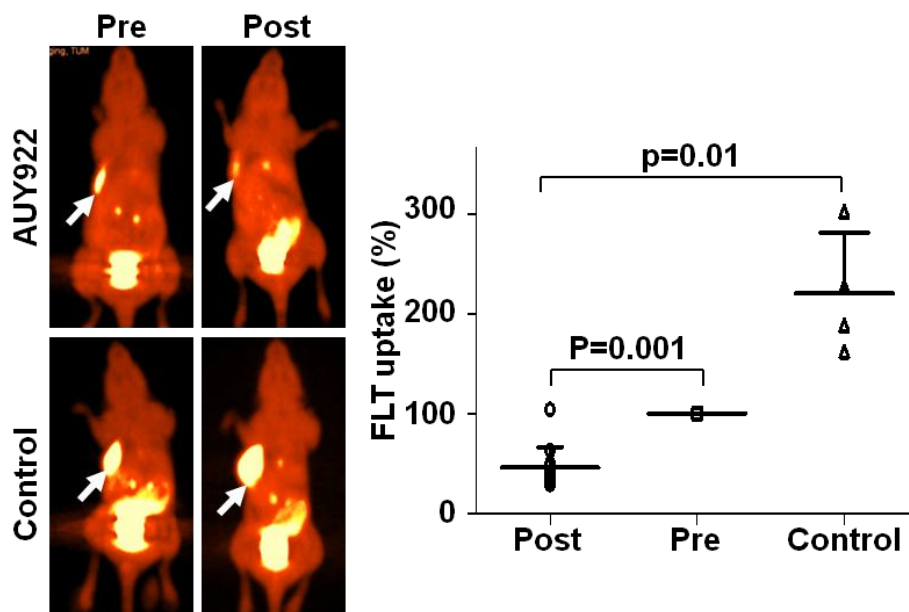


**Fig. 25:** Functional *in vivo* imaging of response to AUY922 inhibition in SUDHL-1 lymphoma using FLT-PET and TBR on day 0, defined as 100% (“pre”), and change of TBR compared to pre-treatment values are shown for treated (“post”) and control animals.

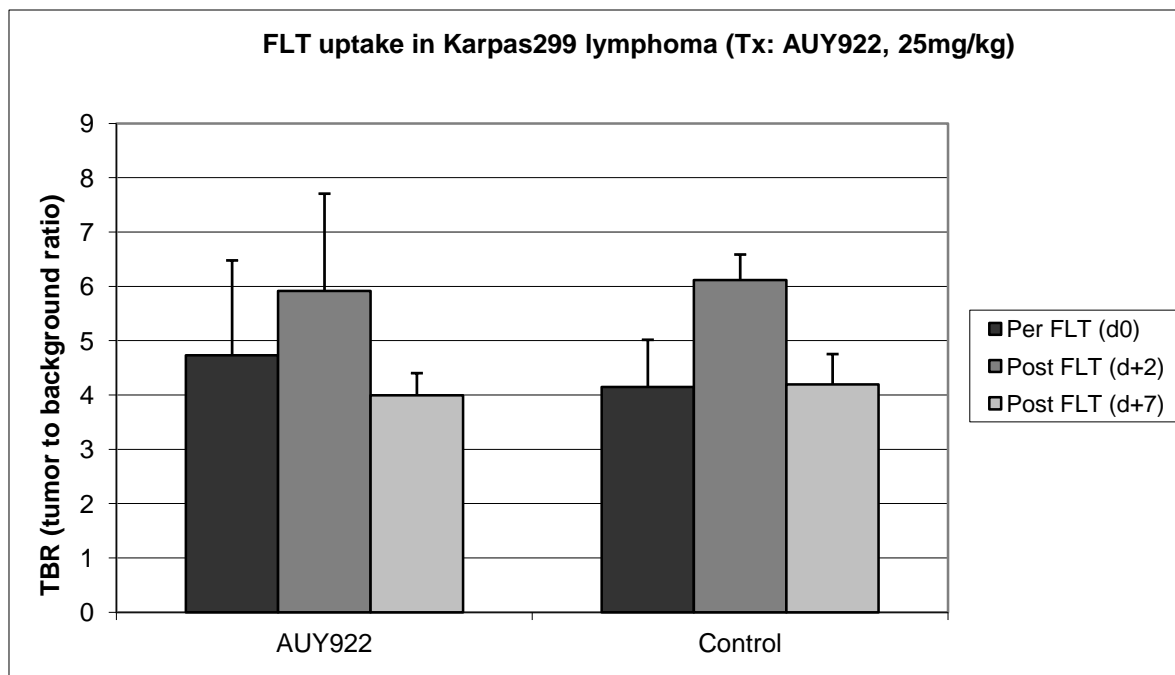


**Fig. 26:** No remarkable difference of FLT-tracer-uptake of karpas299 lymphoma was found in therapeutic group compare to control group. The SUDHL-1 lymphoma bearing mice were treated intraperitoneally with 25 mg/kg AU922 (Therapy) or only placebo (Control) daily. Pre therapeutic FLT-PET was performed before therapy, post therapeutic FLT-PET was performed 2 days and 7 days after therapy. The bars represent the mean  $\pm$  SD.

#### 4.4.3 FLT-PET imaging analysis shows the inhibitory effect of Hsp90 inhibitor on the proliferation of NPM-ALK lymphoma

As a more tumor specific tracer compared to FDG, FLT was also investigated here. SUDHL-1 and Karpas299 bearing mice underwent FLT-PET both before and after therapy at d-1/d-2, d+1/d+5, and d+13, respectively. Figs. 24 to 25 showed representative TBR of different therapeutic groups. A marked decrease of SUDHL-1 FLT-uptake could be observed one day after therapy with 50 mg/kg AU922 (n=5, pre therapeutic uptake: mean TBR= 3.7, range 2.2-5.2, SD=1.2; post therapeutic uptake: mean TBR=2.5, rang 1.7-3.4, SD=0.5). In contrast, FLT-uptake remains high in the control mice (n=2, pre-therapeutic uptake: mean TBR= 1.7, range 1.6-1.8, SD=0.1; post-therapeutic uptake: mean TBR=2.1, rang 2.0-2.2, SD=0.1, Fig. 24A). However, these mice were dead after FLT-PET because of the toxic dose of 50 mg/kg. So we reduced the dose to 10 mg/kg as of d+2. A reduction of TBR of other two mice was

detected at d+1 from 2.1 to 1.7 (n=2, range 1.5-1.8, SD=0.1), while there was an increase of TBR in treated mice to 2.9 (n=2, range 2.7-3.1, SD=0.5) at d+14. There was no clear inhibition of tumor growth detected with 10 mg/kg treatment. The dose was increased to 25 mg/kg in first week and then reduced to 10 mg/kg again to make sure that therapy was not toxic. The mean TBR was decreased from 2.9 (n=4, range 1.6-4.7, SD=1.6) at d-1 to 1.25 (n=4, range 1.0-1.6, SD=0.3) at d+5, and then the dose of AUY922 was reduced to 10 mg/kg from d+5. No toxic effect was noticed until d+21. However, tumor volume began to increase and the mean TBR increased to 2.9 (n=4, range 1.9-3.0, SD=0.7, Fig. 24B) again after 14 days treatment. After that a continuous therapy with 25 mg/kg was decided. The mean TBR was reduced from 3.7 (n=12, range 2.5-4.7, SD=0.7) to 1.6 (n=12, range 1.3-2.6, SD=0.4) at d+5 and further decreases were detected at d+13 ending at 1.0 (n=2, SD=0.01). In contrast, the TBR of all untreated mice increased from 1.7 (n=4, range, SD=0.5) to 3.6 (n=4, range 2.8-4.1, SD=0.6) at d+5 and to 4.4 (n=3, range 3.6-5.7, SD=1.1, Fig. 24C) at d+13. To determine the predictive value of early functional imaging for response assessment, we performed FDG- and FLT-PET scans using a micro PET/CT system five days before or after initiation of AUY922 treatment. To do so, the change of TBR on day 5 was compared to pre-treatment TBR, which was defined as 100%, was calculated (relative TBR). In contrast to FDG assessment, which shown no significant reduction of TBR from day 5, the relative mean TBR of FLT-uptake decreased significantly to 40% compared to baseline (n=12, SD=20.7%, range 32-67%, p=0.001) as early as 5 days after initiation of therapy (Fig. 25). The relative TBR of untreated controls increased to more than 200% during the same time period (n=4, mean TBR 207.8%, range 162.1%-302.4%, SD=61%, p=0.01). Later time points within the treatment group (day 15 to 21) did not show any further reduction in FLT-uptake (data not shown). The therapeutic response was also observed in AUY922 resistant Karpas299 lymphoma bearing mice with a dose of 25 mg/kg (Fig. 26). The mean TBR of the control mice increased from 4.1 (n=7, range 2.9-5.3, SD=0.9) to 6.1(n=7, range 5.5-6.8, SD=0.5) at d+2, and then reduced to 4.2 (n=6, range 3.6-5.0, SD=0.6) at d+7. However, in the therapeutic group, the mean TBR increased from 4.7 (n=10, range 2.8-7.9, SD=1.7) to 5.9 (n=10, range 3.6-9.7, SD=1.8) at d+2, and then went down to 4.0 (n=5, range 3.5-4.5, SD=0.4) at d+7.

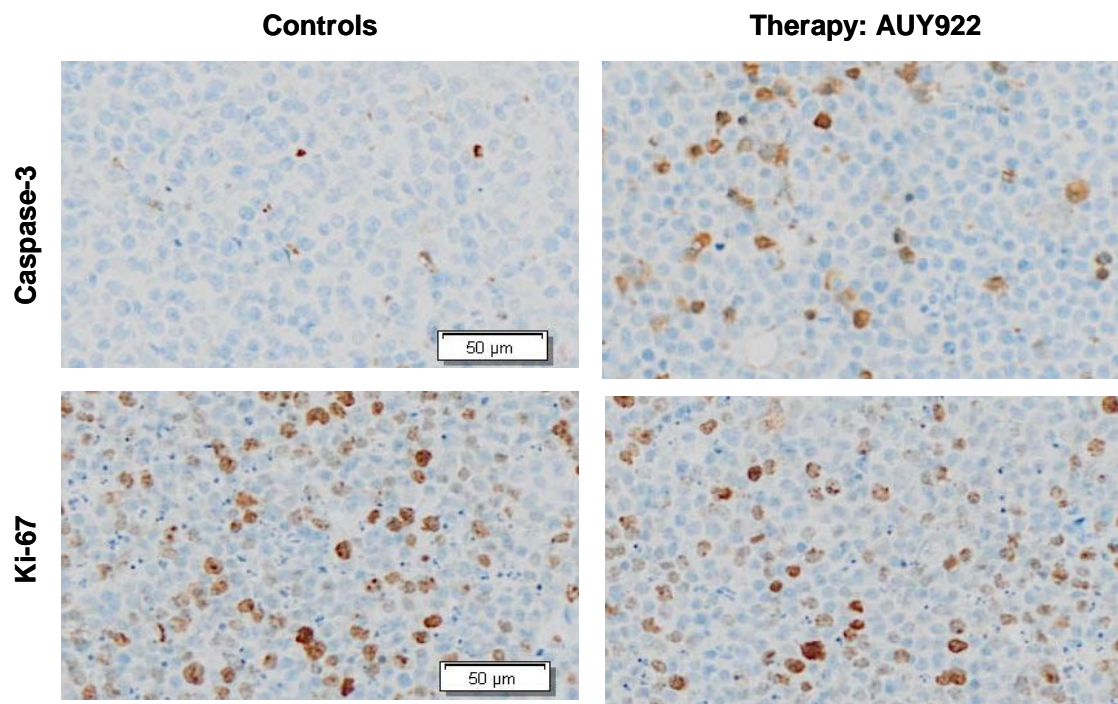
#### **4.4.4 Histological analysis shows decreased proliferation and increased apoptosis induced by treatment with Hsp90 inhibitor in NPM-ALK lymphoma**

To correlate the PET findings with treatment effects of inhibitors on SUDHL-1 xenograft lymphomas, we stained fixed tumor sections using the proliferation marker Ki67 and using

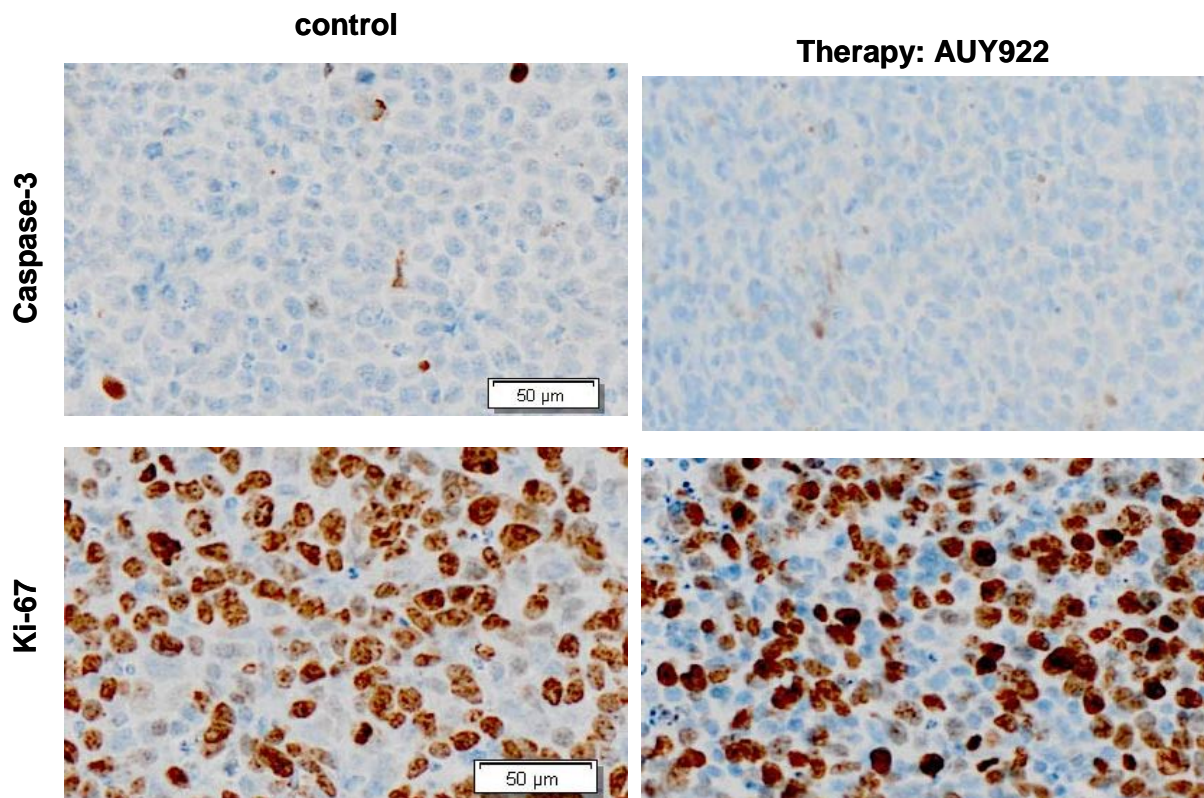
cleaved caspase-3 to analyse apoptosis AUY922 treatment led to a significant increase in apoptosis as quantified by cleaved caspase-3 positive cells (Fig. 27C, n=5, mean 6.1%, SD=3.5%) compared to untreated mice (n=4, mean 1.6%, SD=1.1%; p=0.04). Moreover, the percentage of proliferating cells was substantially decreased by AUY922 as measured by Ki67staining with a mean of 15.3% (SD=0.8%) for the treated and 63.3% (SD=7%) for the control tumors (p=0.03).

The PET findings of Karpas299 lymphomas were confirmed by immunohistochemistry as illustrated in Fig. 27B. No marked increase of apoptosis was detected after AUY922 treatment (mean=0.86%, SD=0.52%) compared to control tumors (n=3, mean=1.0%, SD=0.5%). Moreover, AUY922 only led to a slight reduction of Ki67 staining in Karpas299 tumors (therapeutic group: mean=47.1%, SD=3.1%, control group: mean= 57.7%, SD=5.61%).

A



B



C

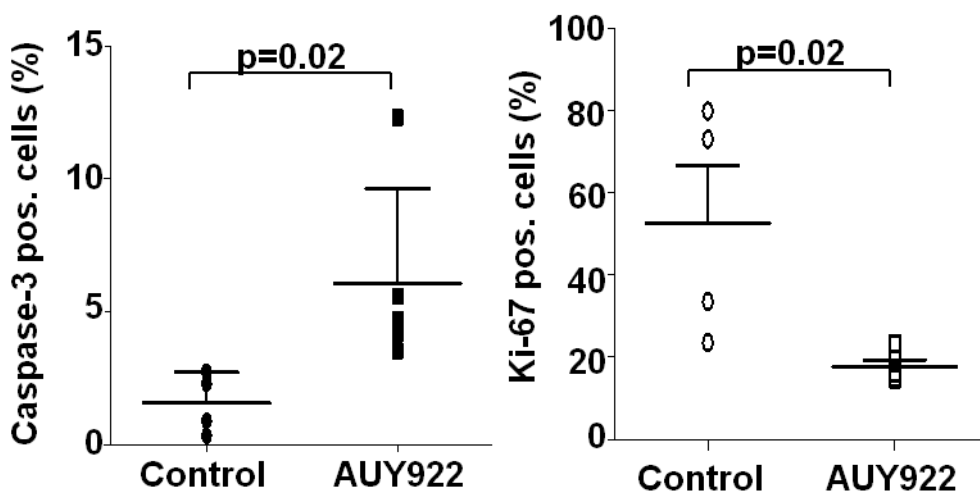


**Fig. 27:** AUY922 treatment triggers a cell death (marker: caspase-3) and a reduction of proliferation (marker: Ki-67) in SUDHL-1 but not in karpas299 lymphoma in vivo (A: SUDHL-1 lymphoma, B: karpas299 lymphoma, C: statistical analysis of SUDHL-1 lymphoma). The

lymphoma bearing mice were treated intraperitoneally with 25 mg/kg AUY922 (Therapy) or only placebo (Control) daily.

## **4.5 Inhibition of mTOR blocks the proliferation of multiple ALK+ lymphoma cell lines**

### **4.5.1 Inhibition of mTOR activity affects the viability of ALK+ lymphoma cells**

To assess the biological effect of RAD001 on lymphoma cell survival, we performed MTT assays on SUDHL-1 and Karpas299 cells, incubated with increasing concentrations of the drug for 24 hours, 48 hours and 72 hours (Fig.28A-F). All the cell lines showed a dose-dependent decrease in cell viability. Both Karpas299 cells and SUDHL-1 cells were sensitive to RAD001. To investigate time dependent effect of RAD001 treatment, SUDHL-1 and Karpas299 cell lines were treated for 24 hours, 48 hours and 72 hours. There was only slight effect on viability after 24 hours of an incubation period in both cell lines (Fig. 28A and 28D). Inhibition rates of SUDHL-1 cells were 59% after the 48 hours incubation and 63% after the 72 hours incubation, respectively (RAD001 concentration: 1 nM) (Fig. 28E and 28F). The IC<sub>50</sub> of SUDHL-1 cells was found after a 48 hours incubation with drug dose of 1 nM. Under treatment with 1 nM RAD001, the viability of Karpas299 cells reduced from 100% of controls to 42% of treated cells (48hours) and to 32% (72hours) (Figs. 28A and 28B). As shown in Figs. 28A-F, although the lower concentrations (0.1 nM) of RAD001 had almost no effect on cell proliferations, RAD001 significantly inhibited proliferation of both cells in a dose-dependent manner. Karpas299 cells viability was from 97% (0.1 nM) to 36% (1000 nM) as early as 24 hours, respectively (Fig. 28A). Additionally, the dramatic inhibition of Karpas299 cells viability was also found after 48 hours and 72 hours incubation with RAD001 (Figs. 28B and 28C). These findings were also confirmed by the observed cell cycle and apoptosis assay.

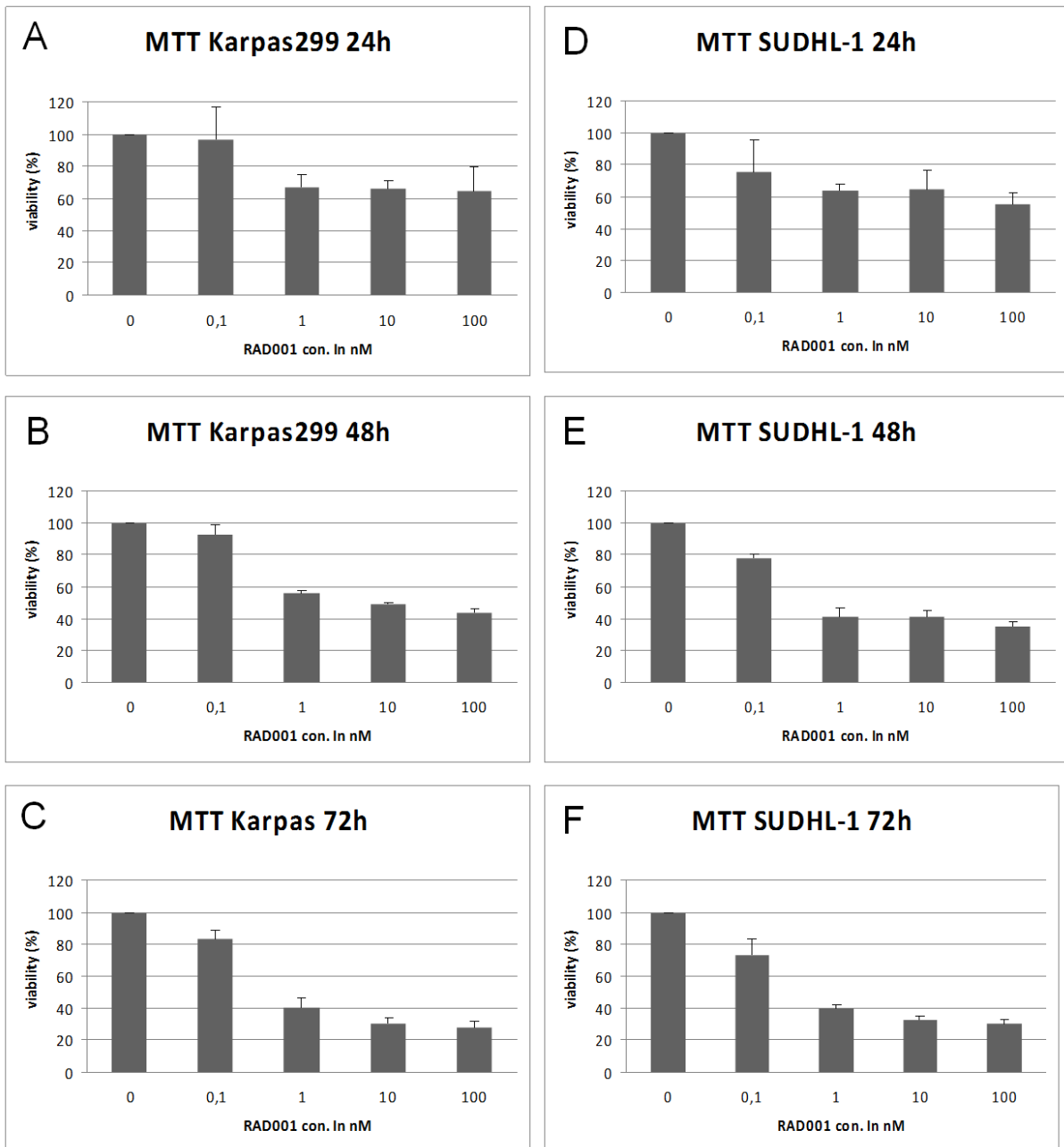


**Fig. 28:** mTOR inhibitor RAD001 (everolimus) inhibits the cell viability in the time and dose dependent Manner in karpas299 and SUDHL-1 cells. Cells were treated with the indicated concentration of RAD001 for 24 hours, 48 hours and 72 hours. The bars represent the mean  $\pm$  SD of the mean from n=3 experiments.

#### 4.5.2 Inhibition of mTOR activity triggers the cell cycle arrest but not apoptosis in ALK+ lymphoma cells *in vitro*

We have studied the effect of RAD001 treatment for 24 hours and 48 hours on the course of cell cycle of SUDHL-1 and Karpas299 lymphoma cells. The cell cycle was detected using PI-staining FACS assay. RAD001 induced marked accumulation in the G1 phase in both cell lines. The results showed that RAD001 arrested SUDHL-1 lymphoma cells in the original the G1 (from 43% in the control to 53% at 1 nM), while a reduction of cells in the S phase was observed (from 22% in control to 14% at 1 nM) as early as 24 hours (Fig.29C). At 48 hours, cells in the S phase (from 19% in control to 10% at 1 nM) had traversed to the G1 phase (from 44% in control to 60% at 1 nM). There was no change in the SubG1 phase, indicating apoptosis (Fig. 29D). Upon treatment with RAD001, Karpas299 cells presented an increase in the percentage of cells accumulating in the G1 phase (from 38% in control reaching a peak value of 55% at 1 nM dosage), while the cells of the S phase decreased (from 27% in control reaching a value of 16% at 1 nM dosage) as early as 24 hours (Fig. 29A). After 48 hours treatment with RAD001, cells traversed to the G1 phase (from 46% in the control reaching a peak value of 54% at the 1 nM dosage) and the S phase (from 23% in control reaching to 17% at 1 nM dosage). There was no significant change in either SubG1 or G2 phase (Fig. 29B).

The Annexin V-FACS was also performed to studied the effect of RAD001 (everolimus) treatment on BaF3-NPMALK, JB-6 Karpas299, SUDHL-1, SUP-M2 and SR-786 lymphoma cells. The results showed that RAD001 (everolimus) caused no remarkable cell death in all these lymphoma cells (Fig. 30 and 31). Furthermore, SUP-M2 and SR-789 lymphoma cells are resistant to RAD001 treatment as detecting with Annexin V and PI-FACS (Fig. 31).

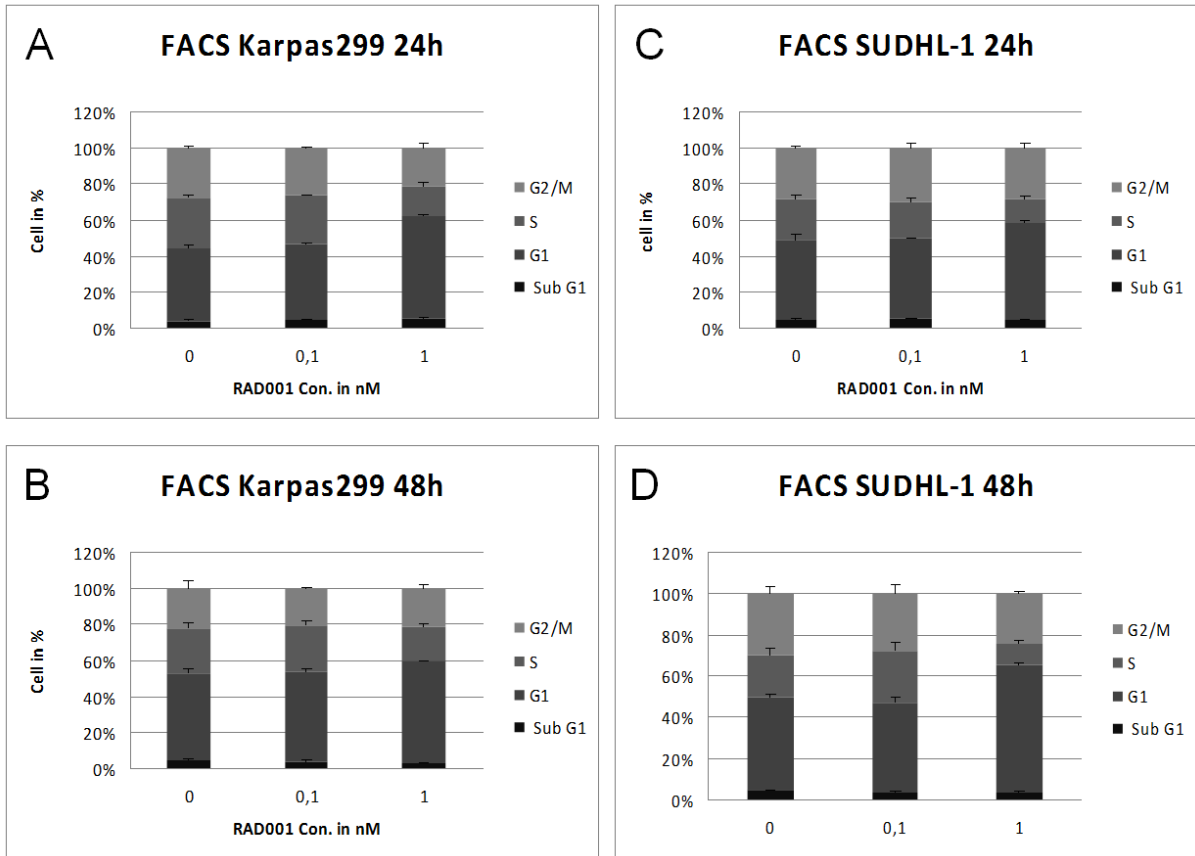


**Fig. 29:** mTOR inhibitor RAD001 (everolimus) induces the cell cycle arrest (G1-phase) but no apoptosis in ALCL lymphoma cells. Cells were treated with the indicated concentration of RAD001 (everolimus) for 24 hours and 48 hours. The bars represent the mean  $\pm$  SD of the mean from n=3 experiments.

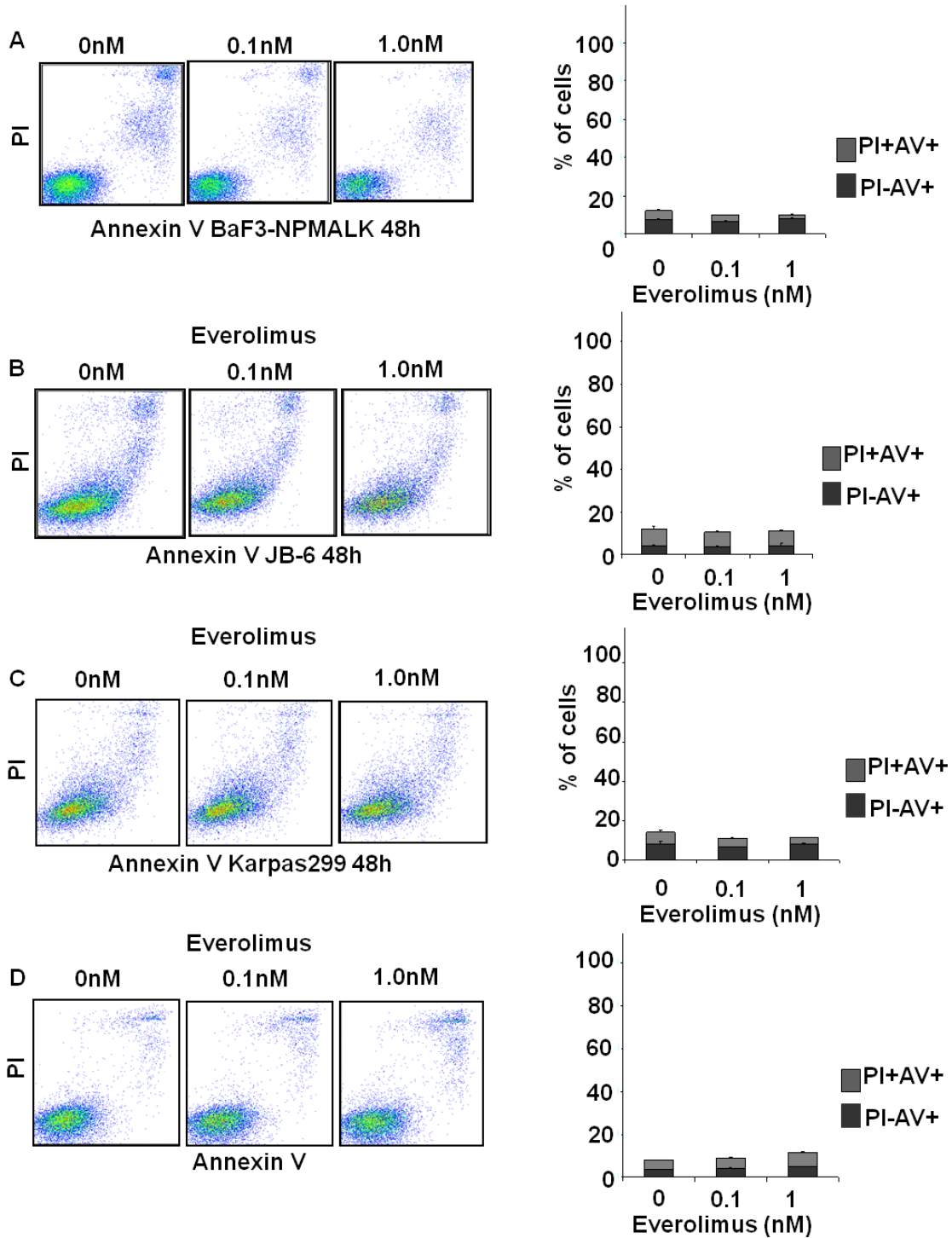


**Fig. 30:** mTOR inhibitor RAD001 (everolimus) treatment did not cause the apoptosis in ALCL cells (A: BaF3-NPMAL cells, B: JB-6 cells, C: Karpas299 cells, D: SUDHL-1 cells) as determined using Annexin V-FACS. Cells were treated with the indicated concentration of RAD001 (everolimus) for 48hours. The bars represent the mean  $\pm$  SD of the mean from n=3 experiments.

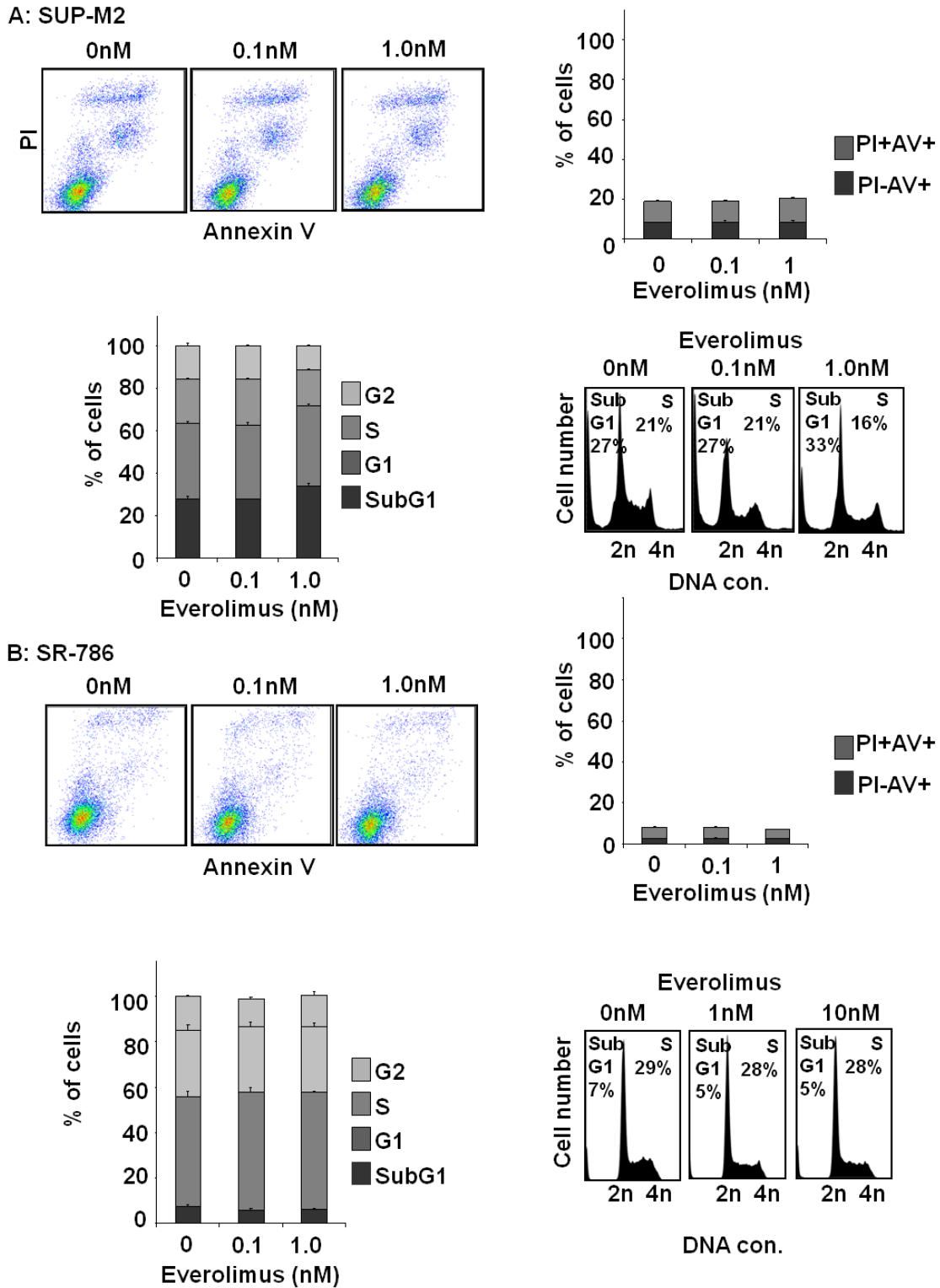
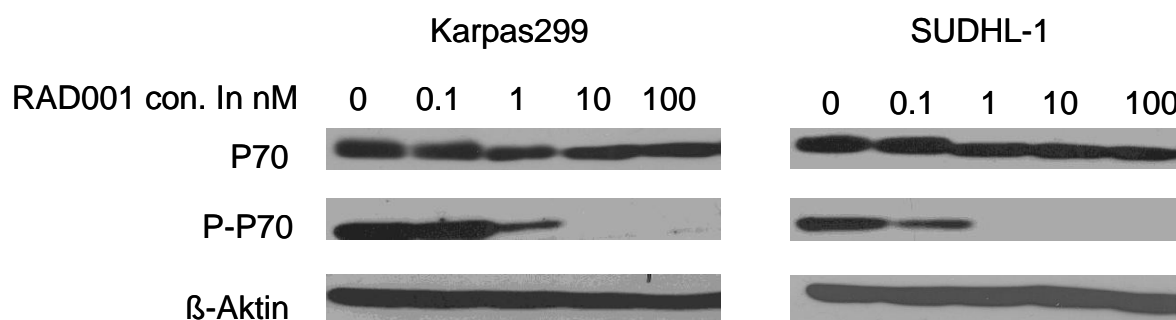


**Fig. 31:** SUP-M2 and SR-789 cells shown resistant to RAD001 (everolimus) treatment as determined using Annexin V and PI-FACS. Cells were treated with the indicated concentration of RAD001 (everolimus) for 48hours. The bars represent the mean  $\pm$  SD of the mean from n=3 experiments.

### 4.5.3 Down-regulation of several oncogenic proteins during exposure of human lymphoma cells to mTOR inhibitor

To investigate effects of RAD001 treatment on mTOR signalling, we used Western blotting to analyse levels of the phosphorylated forms of p70S6K and non-phosphorylated forms of p70S6K after 24 hours and 48 hours exposure of SUDHL-1 and Karpas299 cells to various doses of RAD001. In these two cell lines, levels of the phosphorylated forms of p70S6K were reduced up on increase of concentration of RAD001. However, the effects of RAD001 on non-phosphorylated form of protein levels in these tow cell lines were not found with increasing RAD001 dose (Fig. 32A and Fig. 32B).

A



B

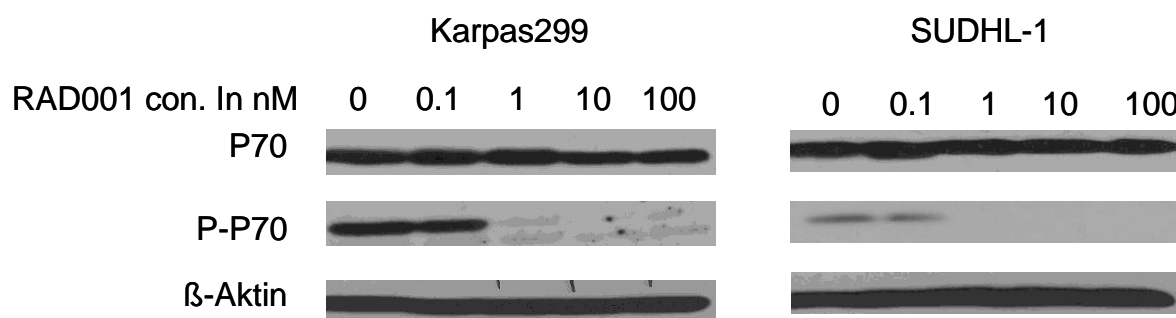


**Fig. 32:** mTOR inhibitor RAD001 (everolimus) inhibits the phosphorylation of p70 S6K in both SUDHL-1 and Karpas299 cells on a dosage dependent manner. Cells were treated with the indicated concentration of RAD001 (everolimus) for 24 hours (A) and 48 hours (B).

#### **4.5.4 A sensitive measure for mTOR inhibition of NPM-ALK+ ALCL using FLT-uptake in vitro**

To determine whether mTOR targeted treatment with RAD001 (Everolimus) was assessable by measuring FLT and FDG-uptake, we examined the cellular tracer uptake of FLT and FDG in RAD001 (Everolimus) treated cells. BaF3-NPMALK, JB-6, Karpas299, SUDHL-1, SUP-M2 and SR-786 cells were incubated with FLT or FDG for 45 min after a 48hours treatment period and the activity was measured using a gamma-counter. As shown in Fig. 35, RAD001 (Everolimus) treatment did not lead to a remarkable reduction of both FLT- and FDG-uptake in most of these cell lines.

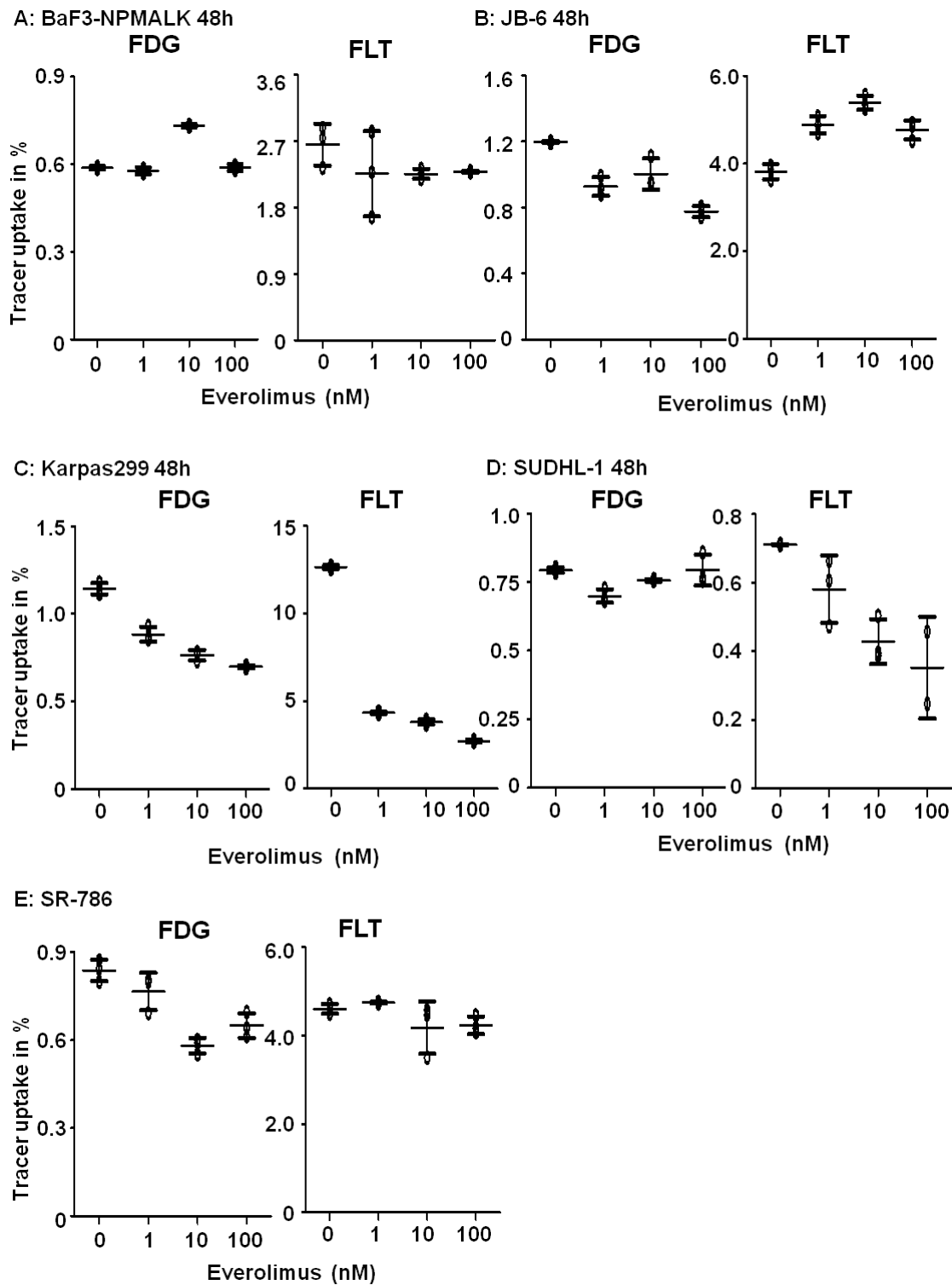


**Fig. 33:** In comparison with NVP-AUY922, RAD001 treatment does not cause the remarkable reduction of tracer-uptake *in vitro*. (A: BaF3-NPMALK cells, B: JB-6 cells, C: Karpas299 cells, D: SUDHL-1 cells and E: SR-786 cells). Cells were treated with the indicated concentration of AUY922 for 48 hours. The bars represent the mean  $\pm$  SD of the mean from n=3 experiments.

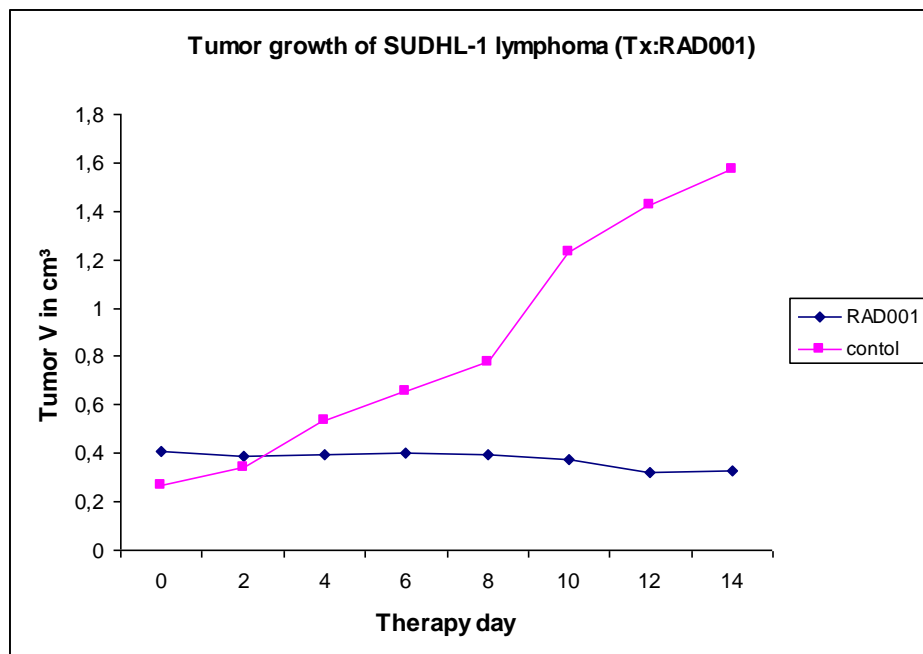
## 4.6 Functional imaging of mTOR inhibition in ALCL xenografts by FLT-PET is superior to FDG-PET

### 4.6.1 *In vivo* mTOR inhibition blocks the growth of the NPM-ALK lymphoma

In SUDHL-1 lymphoma bearing mice, control group received a glucose solution only. The treated mice showed a lower rate of tumor growth at d+7 (n=12, fold=1.0, SD=0.6, range 0.3-2.4-fold) than the control mice (fold=2.6, SD=1.1, range 2.0-4.9-fold, Fig. 34a). After two weeks therapeutic period, the tumor volume of the control group increased from 0.3cm<sup>3</sup> (n=7, SD=0.07, range 0.3-0.4) to 1.2cm<sup>3</sup> (n=4, SD=0.4, range 0.7-2.7 cm<sup>3</sup>). In contrast, the tumor volume of the therapeutic mice reduced from 0.4(n=12, SD=0.2, range 0.3-0.8 cm<sup>3</sup>) to 0.4cm<sup>3</sup> (n=6, SD=0.2, range 0.1-0.5 cm<sup>3</sup>).

As shown in cellular studies, Karpas299 cells are also sensitive to RAD001 treatment *in vitro*. The tumor volume of therapeutic group increased only slightly from 0.5 cm<sup>3</sup> (n=7, range 0.5-0.7 cm<sup>3</sup>, SD=0.1) to 0.8 cm<sup>3</sup> (n=7, range 0.5-1.6 cm<sup>3</sup>, SD=0.4) at d+7. In contrast, the tumor volume of control mice was increased from 0.6 cm<sup>3</sup> (n=7, range 0.3-0.9 cm<sup>3</sup>, SD=0.2) to 2.6 cm<sup>3</sup> (n=7, range 1.3-3.6 cm<sup>3</sup>, SD=0.9) at d+7 (Fig. 34B)

A



B

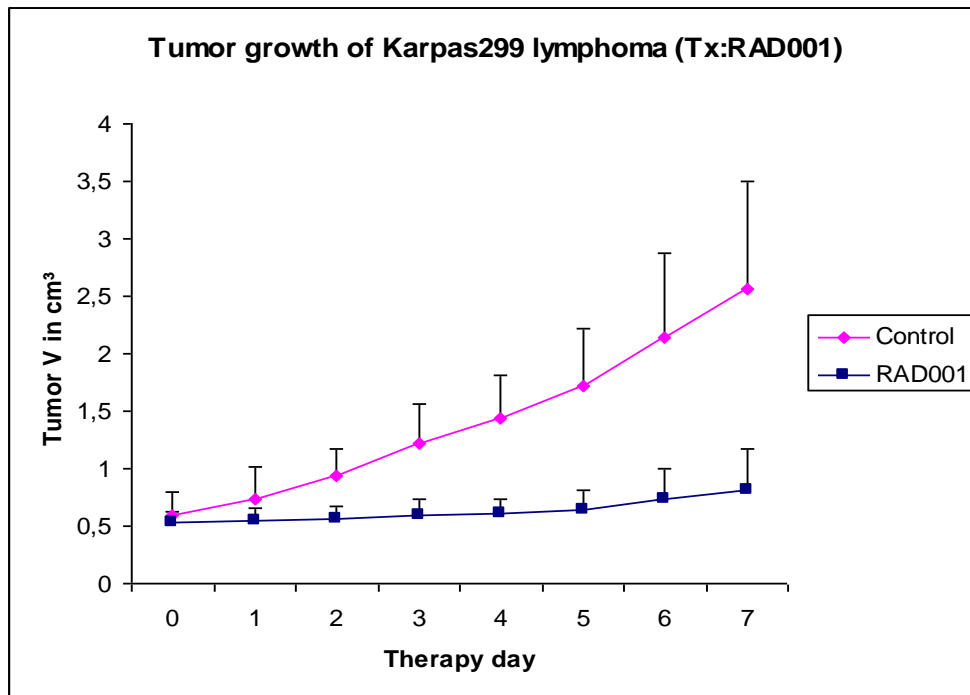


**Fig. 34:** RAD001 (everolimus) blocks the SUDHL-1 and Karpas299 tumor growth (A: SUDHL-1 lymphoma, B: Karpas299 lymphoma). The lymphoma bearing mice were treated oral with 5 mg/kg RAD001 (everolimus) (RAD001) or only placebo (Control) daily. The bars represent the mean  $\pm$  SD.

#### 4.6.2 FDG-PET imaging analysis shows inhibitory effect of mTOR inhibitor on the NPM-ALK lymphoma metabolism

To confirm the predictive value of FLT-PET imaging for early response evaluation using targeted agents, we treated mice bearing SUDHL-1 xenograft tumors with another compound, the mTOR inhibitor RAD001, and evaluated the efficacy of FDG- and FLT-PET monitoring. NPM-ALK-positive cells have previously been shown to undergo cell cycle arrest and apoptosis upon mTOR inhibition (106). Again, treatment was started when mice had measurable xenograft tumors. To investigate SUDHL-1 lymphoma in response to RAD001 treatment, FDG-PET was performed both before and after therapy at d-1 and d+7 (Fig. 35). The mean TBR of the treated mice with a dose of 5 mg/kg was reduced from 8.9 (at d-1: n=9, range 3.4-11.8, SD= 3.6) to 7.1 (at d+7: n=9, range 3.7-8.2, SD= 1.7). The mean TBR of the untreated mice had almost no change (at d-1: n= 7, mean=9.3, range 2.6-15.9, SD= 4.2; at

d+7: n=4, mean=8.9, range 4.2-12.5, SD= 3.3). Furthermore, the statistical analysis using the Graphpad system was also done here. As depicted in Fig. 36, tumor growth was completely inhibited by RAD001 (n=12), whereas the size of control tumors steadily increased over time (n=7, mean 5.6-fold, SD=1.6). By using FDG-PET only a marginal, non-significant reduction of tracer uptake could be observed 5 days after therapy initiation compared to pre-treatment values (p=0.6, Fig. 36). Although RAD001 treated tumors revealed less FDG-uptake compared to control tumors, this difference did not reach statistical significance.

#### **4.6.3 FLT-PET imaging analysis shows inhibitory effect of mTOR inhibitor on the proliferation of NPM-ALK lymphoma**

As a more tumor specific tracer, FLT-uptake in xenograft tumors was investigated during RAD001 treatment. SUDHL-1 and Karpas299 bearing mice were scanned with FLT-PET both before and after therapy at d-2 and d+7, respectively. Figs. 37a and 37b show representative TBRs of different therapeutic groups. A remarkable decrease of SUDHL-1 FLT-uptake could be detected two weeks after therapy with 5 mg/kg RAD001 (n=6, pre-therapeutic uptake: mean TBR= 2.9, range 2.3-4.7, SD=0.7; post-therapeutic uptake: mean TBR=1.3, range 1.0-1.7, SD=0.2). In contrast, the FLT-uptake remained change in the control mice (n=3, pre-therapeutic uptake: mean TBR= 2.6, range 1.9-2.7, SD=0.5; post-therapeutic uptake: mean TBR=2.6, range 2.7-3.6, SD=0.7) until d+14. Only a slight decrease of FLT-uptake of control mice was detected at d+7. The mean TBR of the therapeutic mice was 2.4 (at d+7: n=6, range 1.9-2.8, SD=0.6) and the TBR increased slightly to 2.9 (at d+7: n=3, range 2.1-3.4 SD=0.1) in controls (Fig. 37a). The therapeutic response was observed in RAD001 sensitive Karpas299 lymphoma bearing mice under dose of 5 mg/kg. Fig. 37b showed that the mean TBR of therapeutic group reduced from 3.5 (n=8, range 2.6-4.1, SD=0.6) to 5.8 (n=4, range 4.2-6.8, SD=1.1) at d+2, and then increase slightly to 5.0 (n=4, range 3.6-6.0, SD=1.0) at d+7. In controls, the mean TBR was increased from 4.3 (n=7, range 2.3-6.3, SD=1.4) to 5.4 (n=3, range 4.9-6.1, SD=0.6) at d+2, but then reduced at d+7 (n=3, mean=5.2, range 4.8-5.8, SD=0.5). The statistical analysis of TBR of FLT-PET show that . In contrast of the non-significant reduction of FDG-PET, FLT-PET was able to significantly discriminate between control and treatment group (Fig.38). In addition, we found a modest, but statistically significant reduction of FLT-uptake before and after initiation of RAD001 application (p=0.01).

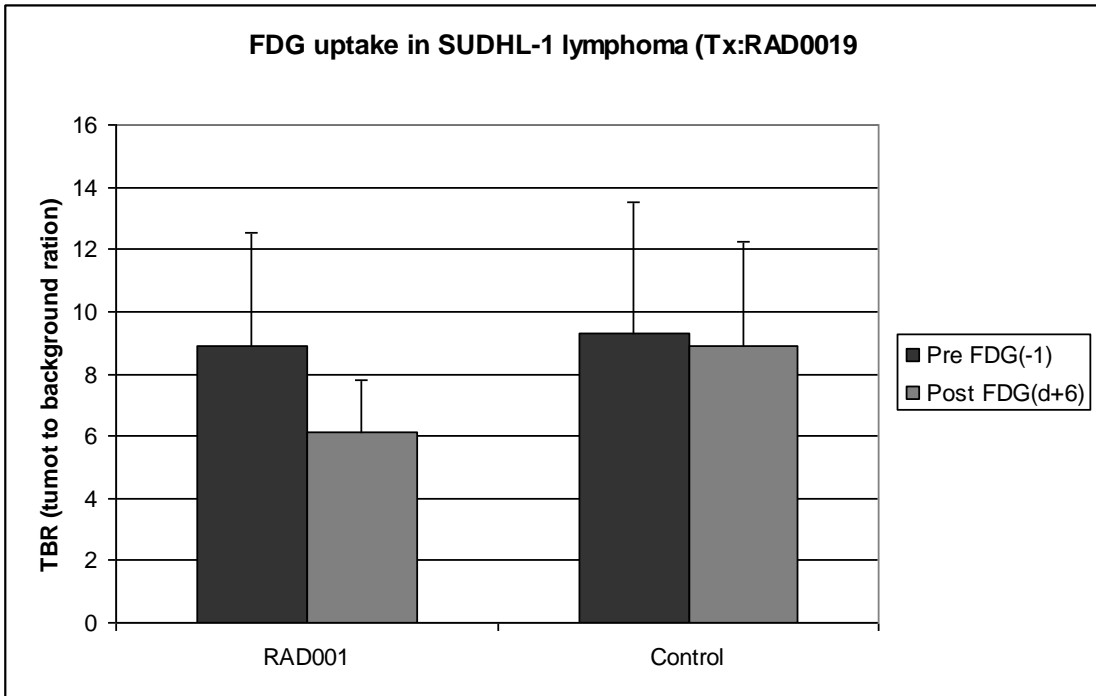


**Fig. 35:** RAD001 (everolimus) treatment reduces the FDG-tracer-uptake in SUDHL-1 lymphoma. The SUDHL-1 lymphoma bearing mice were treated oral with 5 mg/kg RAD001 (everolimus) (RAD001) or only placebo (Control) daily. Pre therapeutic FDG-PET was performed one day before therapy, post therapeutic FDG-PET were performed 6 days after therapy. The bars represent the mean  $\pm$  SD.

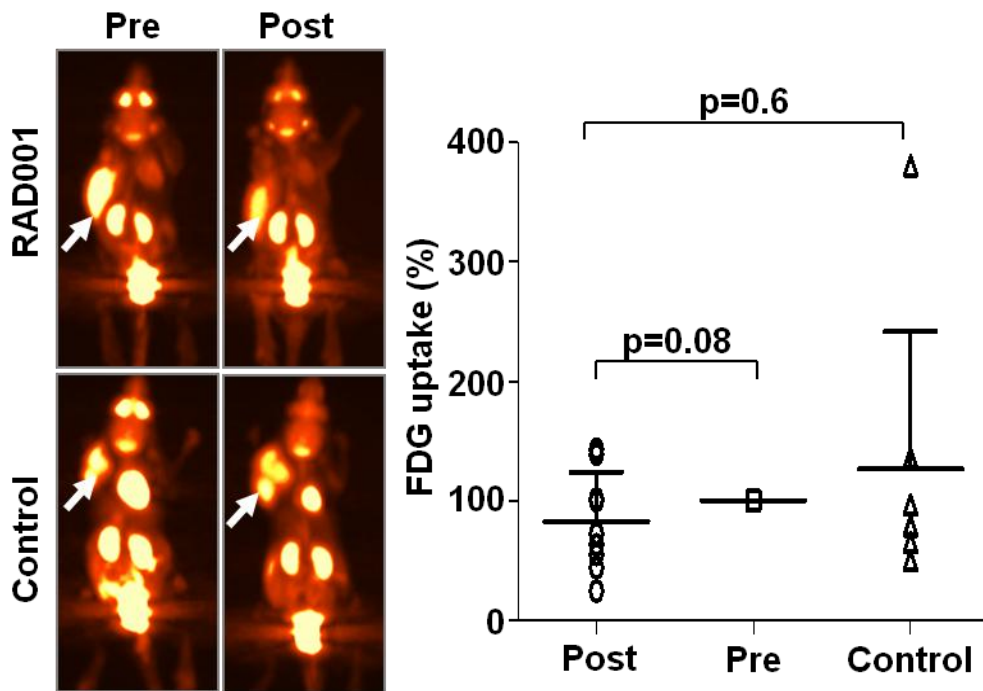
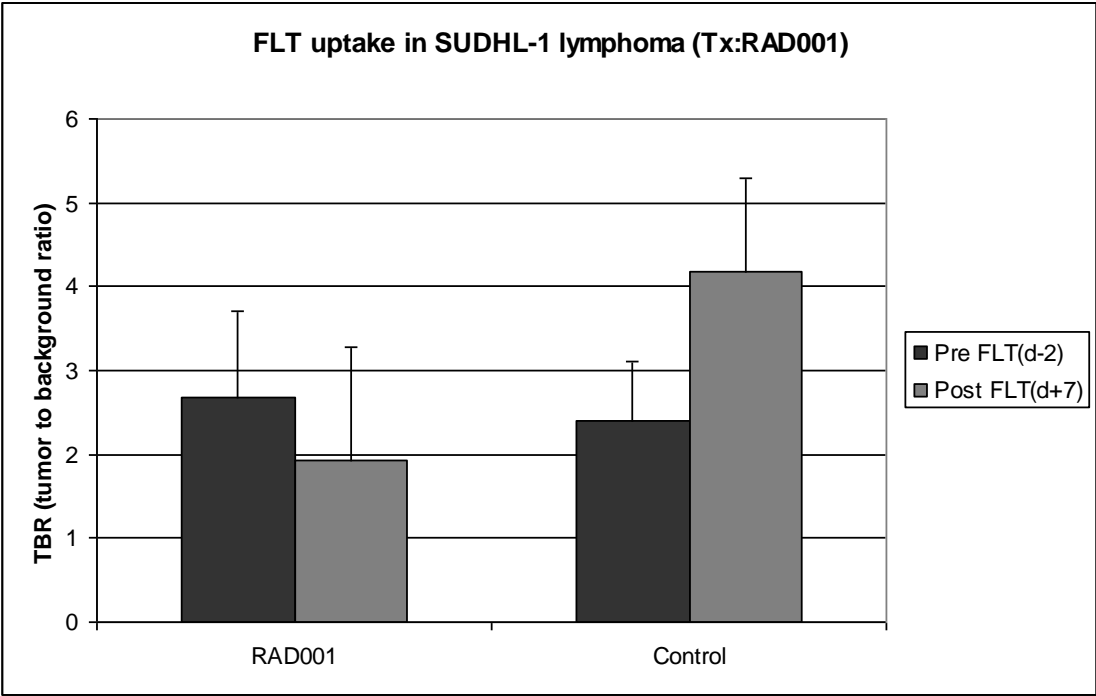


**Fig. 36:** Functional *in vivo* imaging of response to RAD001 inhibition in SUDHL-1 lymphoma using FDG-PET and TBR on day 0, defined as 100% (“pre”), and change of TBR compared to pre-treatment values are shown for treated (“post”) and control animals.

A



B

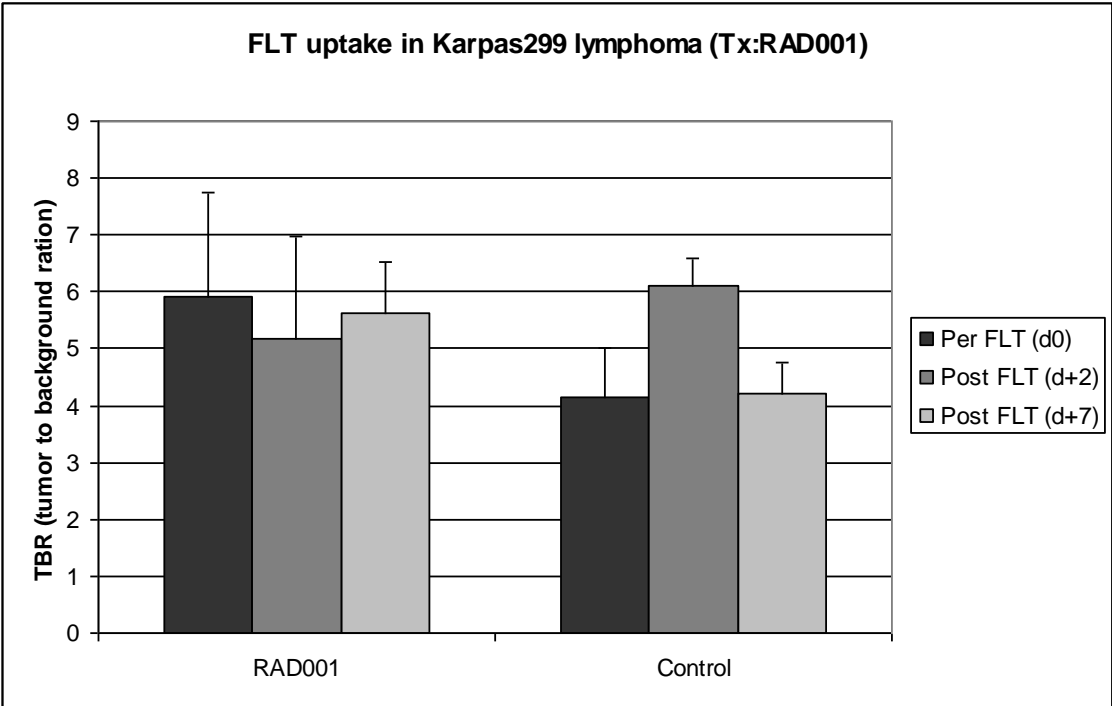


**Fig. 37:** RAD001 (everolimus) treatment reduces the FLT-tracer-uptake in both SUDHL-1 (A) and Karpas299 (B) lymphoma. The lymphoma bearing mice were treated orally with 5 mg/kg RAD001 (everolimus) (RAD001) or only placebo (Control) daily. Pre therapeutic FDG-PET was performed two days before therapy, post therapeutic FLT-PET were performed 2 and 6 or 7 days after therapy. The bars represent the mean  $\pm$  SD.

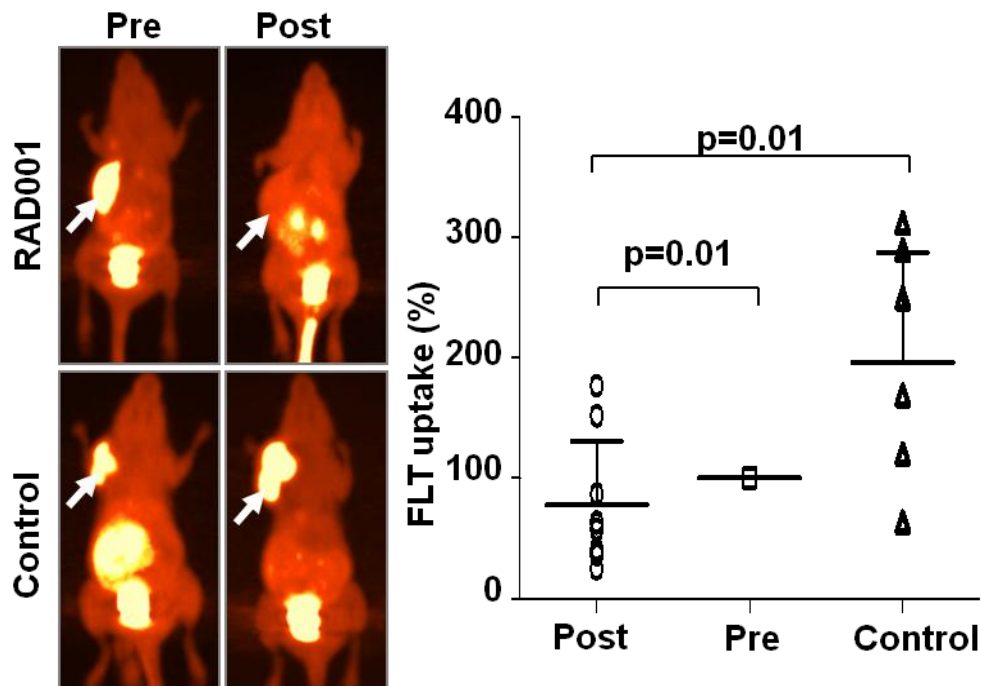


**Fig. 38:** Functional *in vivo* imaging of response to RAD001 inhibition in SUDHL-1 lymphoma using FLT-PET and TBR on day 0, defined as 100% ("pre"), and change of TBR compared to pre-treatment values are shown for treated ("post") and control animals.

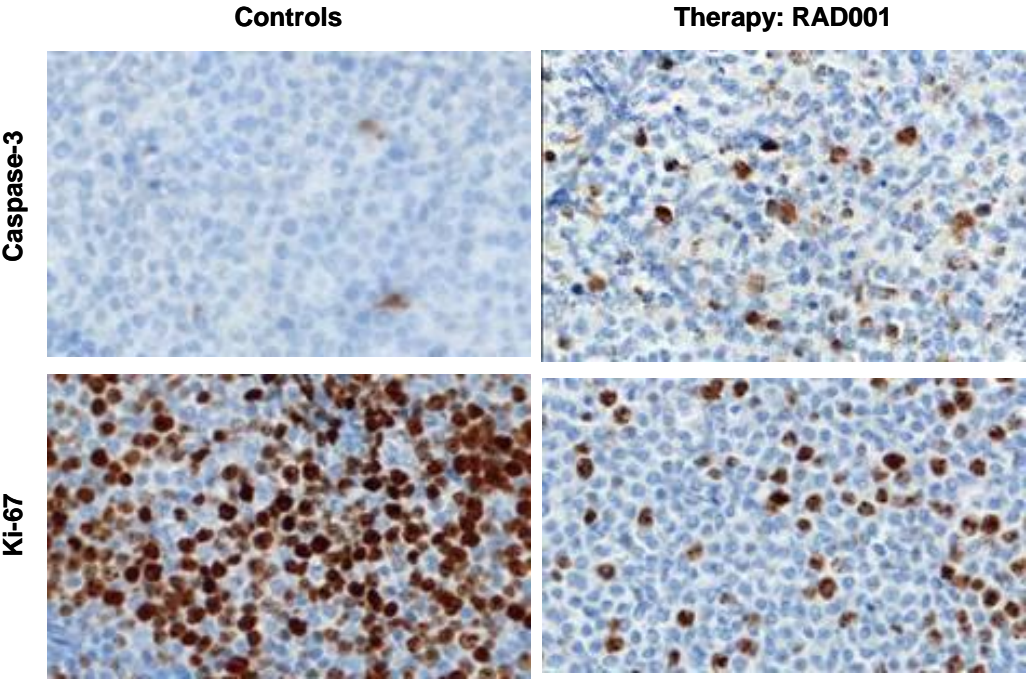
#### 4.6.4 Histological analysis shows decreased proliferation and increased apoptosis induced by treatment with mTOR inhibitor in NMP-ALK lymphoma

To confirm these data on the histological level, we analyzed the tumor tissue for cleaved caspase-3 and Ki67 expression (Fig. 39). Treated tumors harboured more cleaved caspase-3-positive cells compared to control tumors (6.2% vs. 2.2%,  $p=0.04$ ). Notably, exposure to RAD001 dramatically decreased the percentage of Ki67-positive cells from 57.1% to 20.3% ( $p<0.0001$ ). These results were substantiated by further *in vitro* studies. Using MTT assays, we observed a reduction of cell growth to approximately 20% after incubation with 1 nM RAD001 for 48 hours compared to untreated cells (Fig. 28). At the same dose level, PI

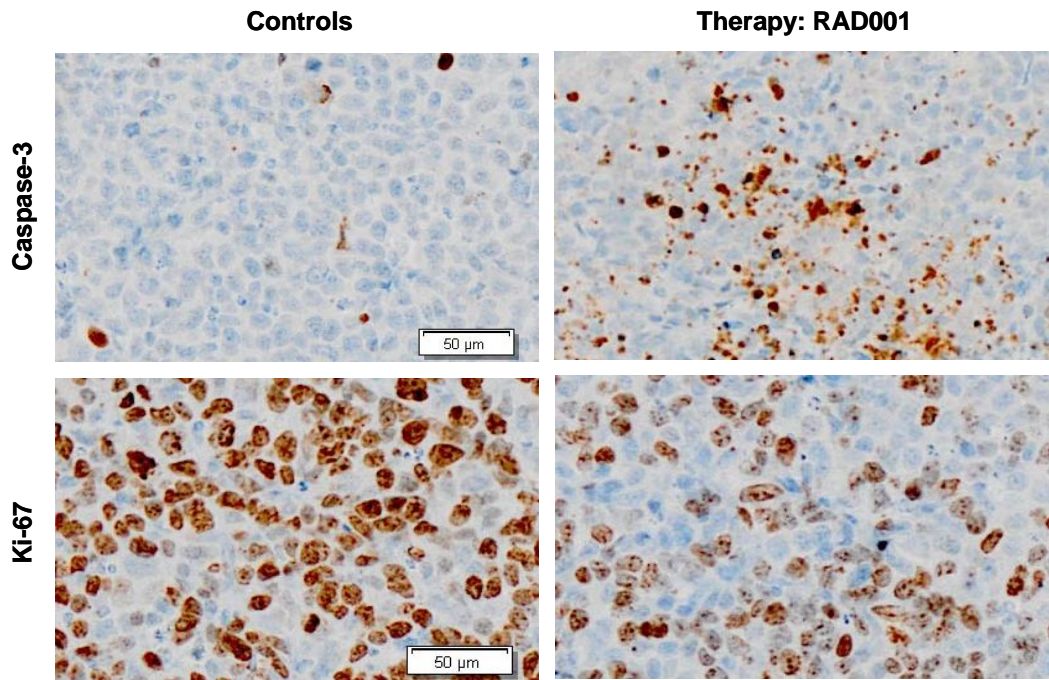
staining revealed a 50% decrease of cells in S phase and a marked increase of cells in G0/G1 phase, whereas the sub-G1 fraction was low and unaffected by mTOR inhibition (Fig. 29).

*In vitro* efficacy could also be demonstrated by immunoblot analysis showing an abrogation of p70S6 kinase phosphorylation at a dose as low as 1 nM (Fig. 32). Thus, functional imaging with FLT-PET rather than FDG-PET has a predictive value for response to mTOR inhibition

A



B



C

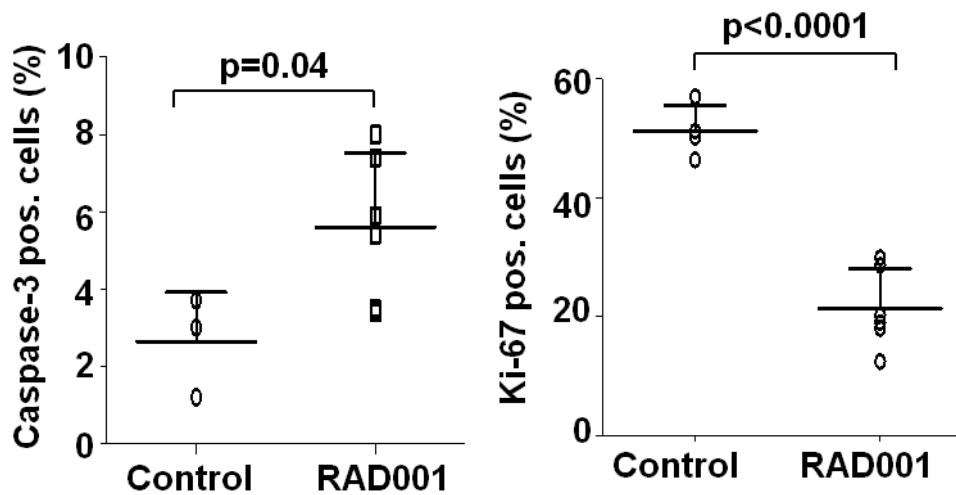


**Fig. 39:** RAD001 (everolimus) treatment triggers a cell death (marker: caspase-3) and a reduction of proliferation (marker: Ki-67) in both SUDHL-1 and in karpas299 lymphoma in vivo (A: SUDHL-1 lymphoma, B: karpas299 lymphoma, C: statistical analysis). The lymphoma bearing mice were treated oral with 5 mg/kg AUY922 (Therapy) or only placebo (Control) daily.

## 4.7 Validating the predictive value of FLT-PET imaging for therapy monitoring *in vivo* and *in vitro*

Depending on our *in vitro* study, Karpas299 ALCL cells were not responsive to HSP90 inhibition by AUY922 treatment but sensitive to mTOR. After a treatment period of 48 hours cell cycle distribution was analyzed by PI staining. *In vitro* study shows that AUY922 had virtually no effect on cell cycle distribution. However, Karpas299 were sensitive to RAD001 treatment resulting in an approximately 50% reduction of cells in S phase compared to control cells (Fig. 29A and B). In order to support the distinct biological effects of HSP90 and mTOR inhibition, we analyzed the biochemical effects of both inhibitors on oncogenic signal transduction by immunoblotting (Fig. 20 and Fig. 32). Consistent with the PI staining results and in sharp contrast to SUHDL-1 cells, HSP90 inhibition did not downregulate ALK or phospho-ALK protein levels. Moreover, the downstream targets phospho-Akt and Akt levels as well as phospho-STAT3 and STAT3 levels were virtually unchanged upon AUY922 treatment up to concentrations of 50 nM and 100 nM, respectively (Fig. 20). Importantly, incubation of Karpas299 cells with RAD001 abrogated the phosphorylation of the mTOR downstream target p70S6 kinase at the same dose level (1 nM) compared to SUDHL-1 cells (Fig. 32).

Then, to evaluate the selectivity of FLT-PET to predict response to pathway targeted therapy, we used a different NPM-ALK expressing lymphoma cell line, Karpas299. Differently from SUDHL-1 ALCL cells, Karpas299 ALCL cells gave rise to xenograft tumors that were entirely resistant to targeted therapy with AUY922 (mean 3.2-fold increase, SD=0.4, range 2.9-3.6), resulting in a similar growth rate as control tumors (n=7, mean 5.2-fold increase, SD=1.5, range 2.8-7.6) (Fig. 40). In contrast, RAD001 treatment (mean 1.0-fold increase, SD=0.2, range 0.9-1.2) abrogated further Karpas299 tumor growth. FLT-PET scans were performed before and two days after initiation of therapy and relative TBRs of each treatment group were calculated. As expected, relative TBR of FLT-uptake of both control and AUY922 treated animals did not differ from each other (p=0.42, Fig. 41) and increased to a mean of 154% (range 107-202%; SD=35.5%) and 149% (range 46% to 175%, SD=47.2%), respectively. Most importantly, FLT-PET imaging showed a significant decrease of the relative TBR of RAD001 treated Karpas299 tumors compared to the respective control (mean 92%, SD=37%, range 44-163%, p=0.001), again correctly predicting tumor growth kinetics of this treatment. Thus, FLT-PET seems to be suitable to discriminate between

response and resistance to targeted therapy at a very early time point. The PET findings were confirmed by immunohistochemistry. Compared to vehicle, RAD001 induced a significant increase of apoptosis as detected by caspase-3 staining (Fig. 42A,  $p=0.02$ ). In contrast, no significant induction of apoptosis was detected after AUY922 treatment compared to control tumors ( $p=0.5$ ). In addition, the percentage of Ki67 positive cells was significantly reduced after treatment with everolimus (Fig. 42B) in contrast to control tumors ( $p=0.02$ ), indicating a strong induction of cell cycle arrest. AUY922 also led to a slight reduction of Ki67 staining, however not to the level of statistical significance ( $p=0.1$ ). Taken together, these data strongly support superiority of FLT-PET imaging for response prediction in vivo, thus allowing an early distinction between sensitive and refractory disease. Our studies thus provide strong evidence that FLT-PET appears to be highly suitable to predict early response to targeted therapy in vivo.

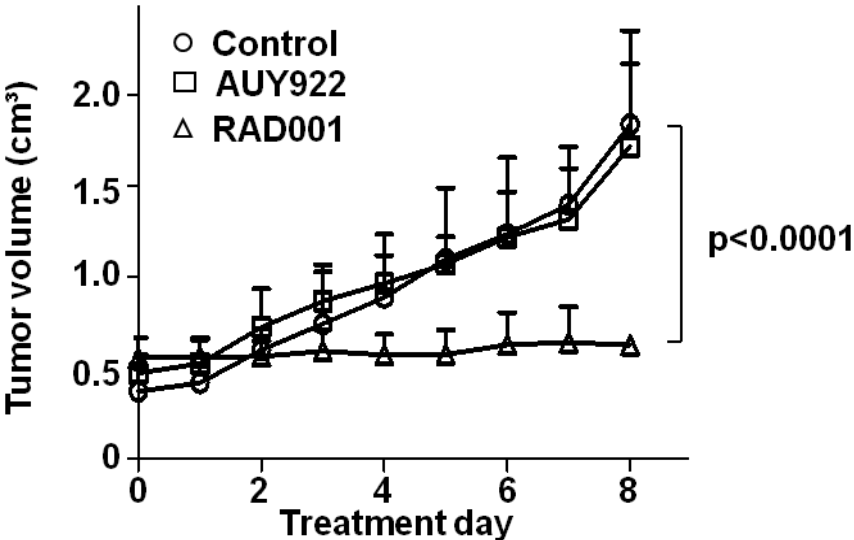


**Fig. 40:** RAD001 but not AUY922 blocks the Karpas299 tumor growth. The karpas299 lymphoma bearing mice were treated intraperitoneally with 25 mg/kg AUY922 or treated oral with 5 mg/kg RAD001 or placebo (Control) daily. The bars represent the mean  $\pm$  SD.

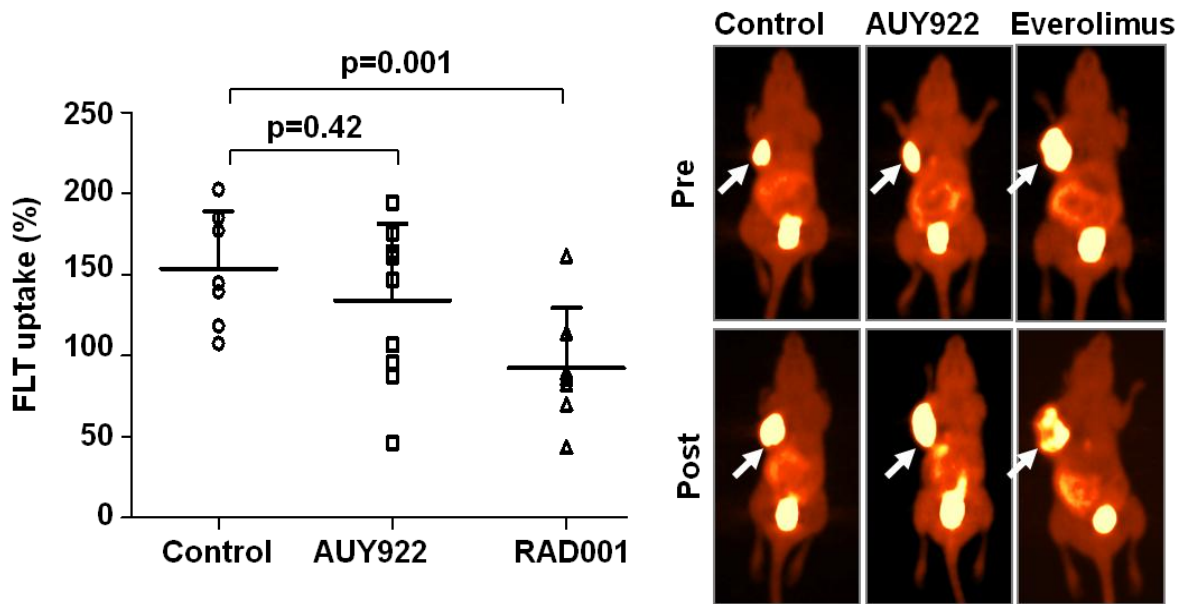
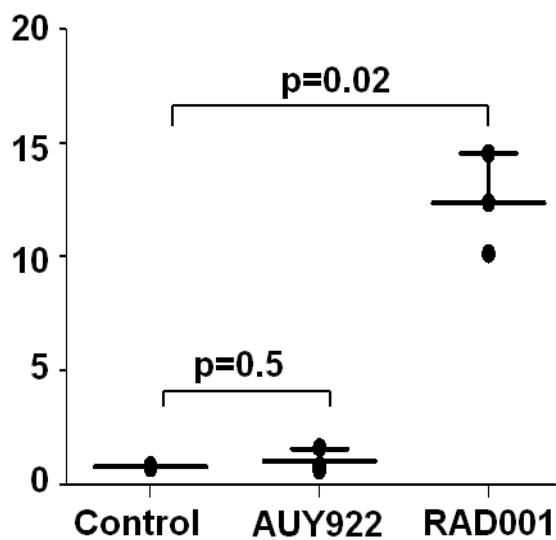


**Fig. 41:** Functional *in vivo* imaging of response to AUY922 or RAD001 inhibition in Karpas299 lymphoma using FLT-PET, was performed before (day 0) and two days after initiation of therapy. Left panel: TBR was calculated and served as an indicator of tracer uptake. TBR on day 0 was defined as 100%. Change of TBR compared to pre-treatment value is shown for each group. Right panel: representative PET scans showing change of tumor tracer uptake (arrows). The bars represent the mean  $\pm$  SD.

A



B

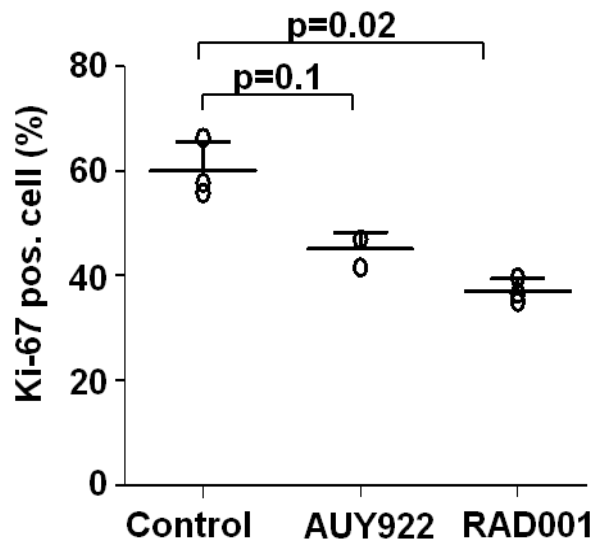


**Fig. 42:** RAD001 but not AUY922 causes the significant cell death (marker: caspase-3, A) and reduction of proliferation (marker: Ki-67, B) of Karpas299 lymphoma *in vivo*. The karpas299 lymphoma bearing mice were treated intraperitoneally with 25 mg/kg AUY922 or treated oral with 5 mg/kg RAD001 or placebo (Control) daily. The bars represent the mean  $\pm$  SD.

## 5 Discussion

Ongoing progress in the understanding of lymphoma pathogenesis has led to the large-scale development of a multitude of pathway targeting drugs (107-109). To optimize design and interpretation of clinical trials using novel compounds it will be crucial to identify biomarkers of sensitivity and response. Once identified, these markers will also accelerate validation of effective drug combinations in the preclinical setting.

Though pharmacodynamic biomarkers assess target inhibition and pathway downregulation, this does not necessarily equate with clinical benefit (110). In addition, many biomarker assays have been neither standardized nor validated (111). Thus, it is unlikely that in the majority of patients with advanced lymphoma the mere presence of a biomarker, a genetic profile, or an activated pathway will suffice to predict response to targeted therapy early in the course of treatment.

For example, the therapy targets PI3K/AKT/mTOR pathway. The PI3Ks are a family of lipid kinases that share the primary biochemical function to phosphorylate the 3-hydroxyl group of phosphoinositides (112). Three classes (I-III) of PI3K are described that vary in structure and substrate preference. The heterodimers that make up class I PI3Ks consist of a regulatory and a catalytic subunit. In the class IA group, these are p85 and p110 ( $\alpha$ ,  $\beta$  and  $\delta$ ), respectively, whereas the class IB PI3K consists of p101 and p110 $\gamma$  (113). Class II PI3Ks are monomeric catalytic isoforms, and the sole class III member is Vps34. Meanwhile, upstream receptor tyrosine kinases (RTKs) that feed into the PI3K pathway include members of the human epidermal growth factor receptor family (EGFR and HER2), platelet derived growth factor receptor, and the insulin and insulin-like growth factor 1 (IGF-1) receptors. Engagement of a growth factor with its RTK is the typical initiating event for activation of class IA PI3Ks, where RTK stimulation leads to an interaction with p85 in the tyrosine kinase domain. Furthermore, AKT, a serine/threonine kinase, is the central mediator of the PI3K pathway with multiple downstream effectors that influence key cellular processes (see figure 1). AKT stimulates protein synthesis and cell growth by activating mTOR (as part of the mTOR-raptor or mTORC1 complex) through effects on the intermediary tuberous sclerosis (TSC) 1/2 complex. It influences cellular proliferation by inactivating cell cycle inhibitors (p27 and p21) and promoting cell cycle proteins (c-Myc and cyclin D1) (114). AKT mediated inhibition of pro-apoptotic genes (BAD and BIM) and degradation of the tumor suppressor protein p53 limits programmed cell death and enhances cell survival (115). PI3K also features in cellular metabolism and insulin signaling through actions on GSK3 (116).

Heretofore, a variety of PI3K/Akt/mTOR pathways has emerged. As part of the mTORC1 complex, mTOR stimulates cell growth and protein synthesis through effects on mRNA translation and ribosome biogenesis (117). Rapamycin is a macrolide antibiotic originally derived from *Streptomyces hygroscopicus* found in the soil on the island of Rapa Nui. Rapamycin (and its analogues, also known as rapalogs) acts by binding to the FKBP12 binding protein, which in turn interacts with the mTORC1 complex, inhibiting downstream signaling (118). The other rapalogs, synthetic derivatives of rapamycin with improved properties, are temsirolimus, everolimus (RAD001) and ridaforolimus (AP23573), formerly known as deforolimus.

At the same time, a series of compounds are currently passing through the early phases of clinical development. 'Pure' PI3K inhibitors target only p110; both pan-p110 inhibitors and isoform-specific inhibitors exist. As the catalytic domains of the p110 subunits and mTOR are structurally similar, dual inhibitors of both PI3K and mTOR are also emerging. SF1126 has shown significant anti-tumor effects in xenograft models of solid tumors including glioblastoma, breast and prostate cancer, and potent anti-angiogenic activity has also been observed, felt partly to be related to a reduction in HIF-1 $\alpha$  levels (48). Two other dual inhibitors are under investigation by Novartis – NVP-BEZ235 and NVP-BGT226 – (there is currently no presented or published data relating to NVP-BGT226, but we have determined the anti-tumor effect of BGT226 in our study). NVP-BEZ235 is an orally available product belonging to the class of imidazoquinolines (119). Preclinical studies demonstrated anti-proliferative activity against a wide range of cancer cell lines, including HER2-overexpressing breast cancer models of trastuzumab and lapatinib resistance (120, 121). NVP-BGT226 as a PI3K/mTOR also shows anti-tumor effect in our ALCL models as described before. The majority of compounds described as pure PI3K inhibitors are pan-p110 inhibitors. However, at least one isoform-specific inhibitor (CAL-101) has had preliminary results presented. NVP-BKM120 is one such agent, and preclinical data showed anti-tumor activity in xenograft models of human cancer both with and without PI3K/PTEN mutations (122).

Direct inhibition of the serine/threonine kinase AKT provides another avenue to pharmacologically regulate activity of the PI3K pathway. The two strategies being explored involve agents that compete for the ATP-binding site (ATP mimetics) and those that act away from this catalytic site (allosteric inhibitors) (123). Perifosine is an allosteric inhibitor that targets the PH domain of AKT, thereby preventing its translocation to the plasma membrane required for activation (124). MK-2206 is another allosteric Akt inhibitor. In preclinical studies, synergism has been demonstrated when MK-2206 has been used in combination with other targeted therapies (erlotinib, lapatinib) or a host of cytotoxic agents (125). Preliminary results of a phase I study in solid tumors have been presented (126). GSK690693 is a potent ATP-

competitive AKT inhibitor that also inhibits the phosphorylation of the downstream target GSK3 in cells. It is currently in clinical development as an intravenous agent for use in patients with solid tumors or hematological malignancies (127).

Biomarker studies are becoming increasingly incorporated into early phase clinical trials. This is largely true for the phase I trials of PI3K pathway inhibitors described above where various predictive and pharmacodynamic (PD) biomarkers have been explored. PD biomarkers are markers of drug effect that assess for target inhibition and pathway downregulation. They necessitate assessment prior to and following an intervention to detect a change from baseline; a correlation with clinical activity is not implied but is desirable (122). At present, an important concern is that many biomarker assays have been neither standardized nor validated. They add to the cost of the trial and may involve invasive procedures that carry a degree of risk to the patient. Markman et al. took the evaluation of PTEN status as a prime example. Because functional PTEN loss can occur through a variety of mechanisms, detection of PTEN protein expression by immunohistochemistry (IHC) on tumor samples is the preferred method. However, the antibodies used to stain samples are not uniform between laboratories, nor has a definitive cut-off been defined below which PTEN is considered to be lost. Further, the adequacy of archival compared to fresh tissue has not been delineated. And given that tumor samples are often small and difficult to obtain, how biomarker studies ought to be prioritized is not clear (122).

Functional *in vivo* imaging could therefore be useful to assess and predict response to a specific treatment very early upon targeted treatment initiation using different Inhibitors, at a time point, when conventional imaging using computed tomography or magnetic resonance techniques cannot be expected to detect either response or resistance.

Our studies used the molecularly defined lymphoma entity ALCL, characterized by ALK-dependent pathway activation, to functionally evaluate the standard PET tracer FDG and the thymidine analogue FLT as early response markers. Constitutive ALK activation is a characteristic of NPM-ALK positive lymphoma and results in the activation of PI3K-AKT-mTOR and JAK-STAT signalling. Both are critical survival and proliferation pathways and have been proposed as pharmacologic targets for malignant diseases including lymphoma (17, 18, 128, 129). Based on the defined oncogene and subsequently deregulated signal transduction, which can be blocked by specific inhibitors, we felt that these lymphoma cells are most suitable for a translational approach comprising both *in vitro* and *in vivo* assays.

BGT226 is a pan PI3K/mTOR inhibitor that is also under investigation by Novartis. We have shown in our work that BGT226 has an anti-tumor activity in the xenograft ALK<sup>+</sup> ALCL models. Moreover, it arrests cell in SubG1-G1 phase and inhibits the Akt phosphorylation as

early as 16 hours after start of incubation. Hsp90 has been identified as an attractive target for anticancer therapy, since its inhibition effectively induced apoptosis in ALK<sup>+</sup> ALCL cell lines through the accelerated degradation of NPM-ALK and other proteins (130, 131). The Hsp90 inhibitor, NVP-AUY922, triggers cell apoptosis and cause cell cycle arrest in G1 phase. Several oncoproteins are down-regulated from AUY922 therapy after 48 hours. Furthermore, AUY922 strongly blocks the ALCL tumor growth *in vivo*. RAD001 is an approved, well-tolerated mTOR inhibitor that has also shown efficacy in numerous tumors including lymphatic malignancies (132). It arrests ALK<sup>+</sup> ALCL cells in G1 phase, but we have not found the cell apoptosis *in vitro* from RAD001 treatment. Phosphorylation of mTOR downstream receptor p70 S6K is totally inhibited from 48 hours RAD001 treatment at 1 nM.

We also show that FLT-uptake by lymphoma cells during inhibition of NPM-ALK or NPM-ALK downstream pathways closely reflected antiproliferative response. Moreover, there is a strong correlation between *in vivo* and *in vitro* results including western blot analyses assessing the activation of NPM-ALK and NPM-ALK-dependent pathways. Most importantly, early changes of TBR of FLT-, but not FDG-PET, preceded change of tumor volume thus allowing distinction between sensitive and resistant cell lines and prediction of therapy response.

FDG-PET after completion of therapy is the non-invasive modality of choice for response classifications of aggressive lymphomas (133). Regarding interim FDG-PET during lymphoma treatment recent clinical studies investigating its predictive value have clearly attenuated the validity in this scenario (134, 135). Moreover, FDG-PET did not predict tumor response during mTOR inhibition both in patients with advanced solid tumors and murine xenograft models (136) emphasizing the need for new surrogate markers reflecting early antiproliferative rather than metabolic response. FLT has been shown to accumulate in a variety of tumor entities due to intracellular trapping upon phosphorylation by the S phase enzyme thymidine kinase 1 (TK1) (93, 96, 99, 100, 137, 138). The correlation between TK1 activity and cellular uptake renders FLT an excellent surrogate marker of proliferation (139, 140).

Since, the lack of FDG to reflect anti-tumor response early after initiation of Hsp90 or mTOR-targeted therapy is in accordance with results from other preclinical models for breast cancer (141, 142), ovarian cancer (143) and pancreatic cancer (136). It is likely that an influx of inflammatory cells which can be observed already 48 hours after mTOR inhibition (144) contributes to higher FDG-uptake *in vivo*. While FDG-uptake of inflammatory cells is similar or may even exceed that of tumor cells, transient increase in stromal reaction may result in overestimation of viable tumor cells (145). The observed dispersion of FDG-uptake might in addition be attributed to a variable degree of inhibition of glycolysis as a consequence of

disruption of the AKT-pathway resulting in altered FDG-uptake (136, 146). On the contrary, FLT-uptake has been proven as a valid imaging biomarker for abrogation of the PI3K-AKT-mTOR pathway in solid tumors (143, 147). Inhibition of the NPM-ALK downstream pathway is known to induce cell cycle arrest in G1 phase due to increase of p27 and decrease of cyclin D1 expression, a state resulting in low TK1 activity (148). Being a substrate of TK1, FLT thus appears as the ideal surrogate marker for inhibition of this pathway. Consistently, we observed a significant reduction of FLT-uptake on day 5 after commencement of both Hsp90 and mTOR inhibition as measured by TBR of FLT-PET. Effective targeting was validated by documentation of tumor growth and immunostaining of explanted lymphomas, which revealed both a significant reduction of the proliferation and, to a lesser extent, increase of the apoptosis.

However, other thymidine analogs such as 2'-[18F]-fluoro-beta-D-arabinofuranosyl-uracil (FMAU) or 1-(2'-deoxy-2'-fluoro-beta-D-arabino-furanosyl)-5-[76Br]-bromouracil (BFU) are incorporated in to DNA up to 97% of total cell activity and are therefore potentially more suitable proliferation markers (149). Yet such radiopyrimidines have not yet been studied in vivo. It remains to be determined which radionucleoside is most appropriate for in vivo-assessment of tumor proliferation. In tumors with low TK1 expression levels or low proliferation fraction (e.g., low-grade lymphomas), [18F]-FLT may be less useful for assessment of therapy response. Recent publications indicate that the metabolism of [18F]-FLT is complex, especially in a post-therapy situation (150). Perumal et al. reported that [18F]-FLT-uptake is related to the expression of equilibrative nucleoside transporters (ENT) (151). Kenny has found a heterogenous pattern of FLT-uptake in primary tumors and metastases from breast cancer (152). Heterogeneity of tumors potentially explains the relatively high variability of [18F]-FLT-uptake found in experimental tumors. A recent study by Muzi et al. indicates that metabolites of [18F]-FLT, especially [18F]-FLT-glucuronide, may count for up to 30% of the blood activity and can therefore contribute to tumoral [18F]-FLT-uptake (153). Furthermore, in a therapy related treatment with inhibitors of thymidine monophosphate de novo synthesis (5-fluorouracil (5-FU), methotrexate), a 7-to10-fold increase of [18F]-FLT-uptake in esophageal carcinoma cells was observed. The authors speculated that this finding was caused by activation of the thymidylate salvage pathway and an increase in TK1 activity (102). In agreement with this *in vivo* study, Barthel et al. have found an increasing in TK1 protein levels 48h after 5-FU treatment of fibrosarcoma bearing mice (97). However, treatment leads to a reduction of proliferation fraction and decreased [18F]-FLT-uptake. This finding may be explained by a decrease in cytoplasmic ATP levels since ATP is an important cofactor of TK1 activity. In the presence of ATP, TK1 forms a tetramer which is 20-fold more effective compared to the dimer regarding phosphorylation of [18F]-FLT. Changes in ATP levels have therefore a major impact on cellular uptake of

[18F]-FLT. In the latter study, a decrease of [18F]-FLT-uptake was also more pronounced compared to [18F]-FDG. However, the detailed uptake mechanism of FLT in various tumors will be determined. These findings further support our hypothesis that antiproliferative effects of drug treatment can be detected early by [18F]-FLT before changes in tumor size become visible. A recent study from Leyton et al. also reported a rapid decrease of tumoral [18F]-FLT-uptake in RIF-1 sarcoma bearing mice as early as 24h after treatment with cisplatin (154). In esophageal carcinoma cells, Dittmann showed a rapid decrease of [18F]-FLT-uptake 24h after therapy with cisplatin (102). A reduction of tumoral [18F]-FLT-uptake related to radiotherapy and androgen ablation therapy was demonstrated recently in animal models of prostate cancer (155). Using an epidermoid carcinoma xenotransplants model, Waldher et al. demonstrated that [18F]-FLT also reflects response to cytostatic therapies such as kinase inhibitors (156).

Up to date, only a few groups studied the potential use of FLT-PET for imaging lymphoma and monitoring response to treatment. Our pilot studies suggest that FLT-PET is sensitive and specific for detection of lymphoma manifestation sites. It has been demonstrated that a linear correlation exists for retention of FLT and proliferation fraction of lymphoma (101, 140).

Of note, we found a significant increase of apoptotic cells in lymphomas treated with RAD001 *in vivo*, but not *in vitro*. This gives rise to the hypothesis that not only targets within the tumor cell, but also within the microenvironment of the tumor seem to contribute to tumor control. Indeed, RAD001 potentially inhibits growth of stromal and endothelial cells *in vitro* and reduces tumor vascularization *in vivo* (157).

Most solid tumors, regardless of their type and origin, cannot grow beyond a certain size ( $\sim 1 \text{ mm}^3$ ) until they establish a blood supply by inducing the formation of new vessels sprouting from existing host capillaries, a process known as angiogenesis (158). Accumulating evidence suggests mTOR to be a critical component of this process (159), because it is part of the phosphatidylinositol 3-kinase/Akt/mTOR signaling pathway, which is also implicated in tumor angiogenesis (160). Although the importance of mTOR signaling in the deregulated cell growth characteristics of human tumor cells is now widely accepted (117, 161), this pathway is also emerging as a key regulator of hypoxia and growth factor-mediated expression of tumor hypoxia-inducible factor-1 $\alpha$  (HIF-1 $\alpha$ ) and HIF-1 $\alpha$ -responsive genes, such as vascular endothelial growth factor (VEGF), as well as endothelial cell function and other stromal cells, thereby regulating tumor vascularization (162-164). Furthermore, mTOR is considered to be very well conserved and ubiquitously expressed including also in endothelial cells (165). RAD001 has been shown previously to have antiangiogenic effects including inhibition of human umbilical vein endothelial cell (HUVEC) growth *in vitro*, reductions in expression of HIF-1 and VEGF in cultured tumor cells (166-168), and

reductions in blood vessel density (BVD) in several different experimental tumor models (167, 168). Similar observations are reported for rapamycin (169, 170) and the rapamycin prodrug temsirolimus (171, 172). Lane et al. expand on this information by comparing the antiangiogenic and antivascular effects caused by mTOR pathway inhibition by RAD001 with those of the pan-VEGF receptor (VEGFR) inhibitor vatalanib (PTK/ZK). They could show that RAD001 has significant antitumor activity in mouse tumor models irrespective of *in vitro* sensitivity of the tumor cell lines used or apparently inadequate drug exposure in tumor tissue for antiproliferative activity in the insensitive models. Moreover, in both scenarios a marked reduction in tumor vascularization and plasma VEGF production is observed. Comparisons of the effects of RAD001 on angiogenic processes both *in vitro* and *in vivo* with those of PTK/ZK indicate overlapping effects on some aspects of endothelial cell biology and angiogenic processes, confirming an integral role of the mTOR pathway in VEGFR-induced proliferative pathways (173).

However, PET monitoring of anti-angiogenic effects of RAD001 failed both with FDG- and FLT-PET in several tumor entities (174, 175). We have shown that the mTOR inhibitor everolimus can rapidly decrease FDG and FLT-uptake in solid tumors that had previously been characterized *in vitro* as sensitive tumors such as SUDHL-1 and Karpas299 tumor. Furthermore, Honer et al. have shown that everolimus did not decrease tracer uptake in tumors characterized as insensitive *in vitro* such as HCT116 and KB31. Similar observations have been reported for rapamycin on human tumor xenografts where decreases in FDG and FLT were linked to changes in hexokinase and thymidine kinase 1 expression (176). However, in that report, rapamycin had no effect on the growth of the insensitive tumors *in vivo* even after 2 weeks of daily treatment. Additionally, tumors characterized as insensitive *in vitro* can have significantly reduced growth *in vivo* in response to everolimus (median T / C = 0.43-0.48), an effect not much weaker than in the two sensitive tumor models (median T / C = 0.25- 0.27). Such antitumor effects are typical of everolimus monotherapy, which tends to reduce tumor growth rather than cause regression (177). These observations on antitumor efficacy, coupled with the demonstration that everolimus potently inhibits growth of endothelial and stromal cells *in vitro*, reduces VEGF release from tumor cells, and reduces tumor vascularization *in vivo* (173). This suggests that inhibition of growth of HCT116 and KB31 tumors probably includes a substantial antiangiogenic/vascular action. Surprisingly, however, the growth inhibitory effect on HCT116 or KB31 *in vivo* could not be detected by changes in uptake of FDG and FLT, suggesting that, for some reason, these PET tracers cannot detect an antiangiogenic MoA. This is an important observation because the clinical effects of everolimus monotherapy are also characterized by stable disease rather than by partial or complete response, that is, tumor growth inhibition rather than regression (178).

The Honer group also compare the effect of other compounds that have antiangiogenic or cytotoxic action mechanisms on FDG-uptake using an orthotopic mammary model: BN472. The BN472 model has been previously characterized as well vascularized, and both cytotoxic and antiangiogenic compounds can inhibit its growth (179, 180). Unfortunately, this model is not derived from a cell line, and thus, the *in vitro* sensitivity of everolimus could not be assessed, although experiments *in vivo* showed weak inhibition after 2 weeks of treatment suggesting an everolimus-insensitive tumor cell (180). In the BN472 model, the microtubule stabilizer patupilone decreased FDG-uptake at both early (day 2) and late time points (day 6) while causing tumor stasis. In contrast, NVP-AAL881, a compound that inhibits both RAF and the VEGF-R2 (KDR), failed to affect FDG-uptake in the BN472 tumors despite causing tumor regression. The pan-VEGF-R inhibitor, PTK/ZK, also failed to reduce FDG-uptake significantly despite inhibiting the growth of these tumors. Although these results are puzzling. The Honer and co-workers consider, that there are several possible explanations that may contribute to this phenomenon. Those include a) increases in TBF (tumor blood flow) and permeability affecting FDG and nutrient delivery, b) a stress response by the tumor cell aiming to avoid apoptosis by increasing transport of various nutrients including glucose and thymidine, b) decreases in plasma glucose causing a relative increase in the levels of FDG, d) induction of hypoxia leading to stimulation of glycolysis through HIF-1, and e) increases in the number of glycolytic macrophages that infiltrate the tumor (101, 181-183). Where the mechanism for FDG-uptake has been studied, investigations demonstrate that the rate-limiting step is at FDG phosphorylation by hexokinase rather than FDG transport by glucose transporters such as Glut-1 (176, 184, 185). This suggests that changes in TBF are unlikely to affect FDG-uptake except perhaps under conditions where TBF is very low, for example, in human tumor xenografts (186). However, everolimus has been shown to decrease TBF (54, 187), and in the B16/BL6 model described there, they could find no effect at all on the parameter BFI (blood flow index), which is equivalent to TBF. Consequently, Honer et al. reason that although they did not measure TBF in the xenograft models, it is unlikely that an everolimus induced increase in TBF in the insensitive models, for example, through normalization (188), can explain the effects observed there. Furthermore, despite a low FDG SUV, the fact that Glut-1 levels were very high in the H596 xenograft (and were unaffected by everolimus treatment) is also suggestive that nutrient supply is not rate-limiting for FDG-uptake. There was no evidence that everolimus caused apoptosis in the mouse models, and thus, a stress response of increased glucose or thymidine-uptake (thus veiling a decrease in FDG- or FLT-uptake) is also unlikely to explain the effects they observed. Furthermore, everolimus tends to slightly increase plasma glucose levels (178), which might cause a decrease in FDG-uptake in tumor. The influence of plasma glucose has been reported to be the order of 10-fold increase in plasma glucose (189, 190). Thus, small changes in plasma

glucose are unlikely to affect their observations on FDG-uptake. Hypoxia can be positively correlated with glycolysis, but this is not always the case (183), and they did not observe it in the BN472 model where there was also no effect of the antiangiogenic PTK/ZK on hypoxia, which might have veiled a decrease in FDG-uptake. Finally, an influx of glycolytic macrophages after cell kill could also veil a decrease in FDG-uptake. But they did not measure macrophages in the xenograft experiments, at least in the rat BN472 model. Moreover, an increase in tumor macrophage content seemed not to be an explanation for NVP-AAL881 because macrophage levels were actually decreased as measured by a contrast-enhanced MRI method, and IHC indicated no change compared with vehicle.

Thus, taken all together, Honer et al. suggest that anti-angiogenic/vascular inhibition of tumor growth does not affect tumor uptake of FDG or FLT as measured by PET in vivo. This may be considered a surprising observation, and further clinical confirmation of this hypothesis is important. A small FDG-PET study of eight patients with NSCLC showed that everolimus induced FDG changes ranging from -72% to +34%, but correlations with patient outcome or investigations of antiangiogenic effects were not made (191). Another report from phase 1/2 studies showed that FDG changes in response to rapamycin were unrelated to tumor response by RECIST (192). Honer et al. were not aware of any clinical FDG/FLT-PET studies with PTK/ZK or NVP-AAL881, and as reported from B. Besse et al. (2006) the data for other agents broadly described as antiangiogenic are minimal. The multikinase inhibitor sunitinib has been shown to significantly reduce FDG-PET in some, but not all, patients with gastrointestinal stromal tumors, and generally, there was a strong correlation between progression-free survival and the early FDG-PET response in this indication (193). However, this drug has a strong potency against cellular c-KIT and PDGF-R equaling that against VEGF-R2 (194, 195), and thus, its activity is not limited to the stromal compartment of the solid tumor. Interestingly, the eponymous antiangiogenic agent bevacizumab when tested for clinical activity against tumor blood volume, flow, permeability, interstitial fluid pressure and FDG-uptake in a six patients, induced rapid changes in all but FDG-uptake, which only changed, if at all, after 3 months of treatment (196).

Our study have shown that the allosteric mTOR inhibitor everolimus can significantly decrease FDG- and FLT-uptake by tumors in mice that are inherently sensitive to the drug. However, in less sensitive models where anti-angiogenic/vascular mechanisms probably predominate, no effect on these tracers could be detected. In a rat model, antiangiogenics also failed to affect FDG-uptake (175). These data suggest that FDG-/FLT-PET may provide false-negatives for anti-angiogenic/vascular inhibition and, consequently, may not be suitable as early response markers for everolimus, other rapalogs, or pure antiangiogenic agents (175).

These observations as well as the fact, that inhibition of cell proliferation can be a transient phenomenon in the setting of intermittent drug administration (143, 144) underline the importance of careful consideration of pharmacodynamics in designing imaging protocols for response assessment.

Here we present a translational study including molecular, cellular, as well as animal *in vivo* analyses to validate the predictive value of PET for early assessment of response to targeted treatment. Our data provide strong evidence that FLT-, but not FDG-uptake represents a reliable, non-invasive surrogate marker to distinguish between sensitive and resistant lymphoma early after treatment initiation. These findings will thus facilitate rapid preclinical and clinical evaluation of novel inhibitors targeting this pathway as well as drug combinations including chemotherapeutic agents.

## 6 Literature

1. Janeway CA, Travers P, Walport M, Shlomchik MJ. Basic concepts in immunology. 2001.
2. Hoppe RT, Mauch PM, Armitage JO, Diehl V, Weiss LM. Hodgkin lymphoma: Lippincott Williams & Wilkins; 2007.
3. Barnes L. Pathology and genetics of head and neck tumours: World Health Organization; 2005.
4. Swerdlow SH. WHO classification of tumours of haematopoietic and lymphoid tissues: World Health Organization; 2008.
5. Watanabe M, Ogawa Y, Itoh K, Koiwa T, Kadin ME, Watanabe T, et al. Hypomethylation of CD30 CpG islands with aberrant JunB expression drives CD30 induction in Hodgkin lymphoma and anaplastic large cell lymphoma. *Laboratory Investigation*. 2007;88:48-57.
6. Shiota M, Fujimoto J, Semba T, Satoh H, Yamamoto T, Mori S. Hyperphosphorylation of a novel 80 kDa protein-tyrosine kinase similar to Ltk in a human Ki-1 lymphoma cell line, AMS3. *Oncogene*. 1994;9:1567-74.
7. Morris SW, Kirstein MN, Valentine MB, Dittmer KG, Shapiro DN, Saltman DL, et al. Fusion of a Kinase Gene, Alk, to a Nucleolar Protein Gene, Npm, in Non-Hodgkins-Lymphoma. *Science*. 1994;263:1281-4.
8. Bai RYY, Tao OY, Miething C, Morris SW, Peschel C, Duyster J. NPM-ALK associated with anaplastic large-cell lymphoma activates the PI3-kinase/AKT antiapoptotic signaling pathway. *Blood*. 2000;96:469a-a.
9. Chiarle R, Simmons WJ, Cai HY, Dhall G, Zamo' A, Raz R, et al. Stat3 is required for ALK-mediated lymphomagenesis and provides a possible therapeutic target. *Nature Medicine*. 2005;11:623-9.
10. Kutok JL, Aster JC. Molecular Biology of Anaplastic Lymphoma Kinase–Positive Anaplastic Large-Cell Lymphoma. *Journal of clinical oncology*. 2002;20:3691.
11. Palmer RH, Vernersson E, Grabbe C, Hallberg B. Anaplastic lymphoma kinase: signalling in development and disease. *Biochemical Journal*. 2009;420:345.
12. Chiarle R, Voena C, Ambrogio C, Piva R, Inghirami G. The anaplastic lymphoma kinase in the pathogenesis of cancer. *Nature Reviews Cancer*. 2008;8:11-23.
13. Iwahara T, Fujimoto J, Wen D, Cupples R, Bucay N, Arakawa T, et al. Molecular characterization of ALK, a receptor tyrosine kinase expressed specifically in the nervous system. *Oncogene*. 1997;14:439.
14. Morris SW, Naeve C, Mathew P, James PL, Kirstein MN, Cui X, et al. ALK, the chromosome 2 gene locus altered by the t (2; 5) in non-Hodgkin's lymphoma, encodes a novel neural receptor tyrosine kinase that is highly related to leukocyte tyrosine kinase (LTK). *Oncogene*. 1997;14:2175.
15. Stoica GE, Kuo A, Aigner A, Sunitha I, Souttou B, Malerczyk C, et al. Identification of anaplastic lymphoma kinase as a receptor for the growth factor pleiotrophin. *Journal of Biological Chemistry*. 2001;276:16772.
16. Stoica GE, Kuo A, Powers C, Bowden ET, Sale EB, Riegel AT, et al. Midkine binds to anaplastic lymphoma kinase (ALK) and acts as a growth factor for different cell types. *Journal of Biological Chemistry*. 2002;277:35990.
17. Zamo A, Chiarle R, Piva R, Howes J, Fan Y, Chilosi M, et al. Anaplastic lymphoma kinase (ALK) activates Stat3 and protects hematopoietic cells from cell death. *Oncogene*. 2002;21:1038-47.
18. Zhang Q, Raghunath PN, Xue L, Majewski M, Carpentieri DF, Odum N, et al. Multilevel dysregulation of STAT3 activation in anaplastic lymphoma kinase-positive T/null-cell lymphoma. *The Journal of Immunology*. 2002;168:466.

19. Amin HM, McDonnell TJ, Ma Y, Lin Q, Fujio Y, Kunisada K, et al. Selective inhibition of STAT3 induces apoptosis and G1 cell cycle arrest in ALK-positive anaplastic large cell lymphoma. *Oncogene*. 2004;23:5426-34.
20. Bromberg JF, Wrzeszczynska MH, Devgan G, Zhao Y, Pestell RG, Albanese C, et al. Stat3 as an oncogene. *Cell*. 1999;98:295-303.
21. Gouilleux-Gruart V, Gouilleux F, Desaint C, Claisse J, Capiod JC, Delobel J, et al. STAT-related transcription factors are constitutively activated in peripheral blood cells from acute leukemia patients. *Blood*. 1996;87:1692.
22. Garcia R, Yu CL, Hudnall A, Catlett R, Nelson KL, Smithgall T, et al. Constitutive activation of Stat3 in fibroblasts transformed by diverse oncoproteins and in breast carcinoma cells. *Cell growth & differentiation: the molecular biology journal of the American Association for Cancer Research*. 1997;8:1267.
23. Grandis JR, Drenning SD, Chakraborty A, Zhou MY, Zeng Q, Pitt AS, et al. Requirement of Stat3 but not Stat1 activation for epidermal growth factor receptor-mediated cell growth *In vitro*. *Journal of Clinical Investigation*. 1998;102:1385.
24. Khoury JD, Medeiros LJ, Rassidakis GZ, Yared MA, Tsioli P, Leventaki V, et al. Differential expression and clinical significance of tyrosine-phosphorylated STAT3 in ALK+ and ALK- anaplastic large cell lymphoma. *Clinical Cancer Research*. 2003;9:3692.
25. Chiarle R, Simmons WJ, Cai H, Dhall G, Zamo A, Raz R, et al. Stat3 is required for ALK-mediated lymphomagenesis and provides a possible therapeutic target. *Nature medicine*. 2005;11:623-9.
26. Chen Y, Takita J, Choi YL, Kato M, Ohira M, Sanada M, et al. Oncogenic mutations of ALK kinase in neuroblastoma. *Nature*. 2008;455:971-4.
27. Mossé YP, Laudenslager M, Longo L, Cole KA, Wood A, Attiyeh EF, et al. Identification of ALK as a major familial neuroblastoma predisposition gene. *Nature*. 2008;455:930-5.
28. George RE, Sanda T, Hanna M, Fröhling S, Luther II W, Zhang J, et al. Activating mutations in ALK provide a therapeutic target in neuroblastoma. *Nature*. 2008;455:975-8.
29. Donella-Deana A, Marin O, Cesaro L, Gunby RH, Ferrarese A, Coluccia AML, et al. Unique substrate specificity of anaplastic lymphoma kinase (ALK): development of phosphoacceptor peptides for the assay of ALK activity. *Biochemistry*. 2005;44:8533-42.
30. Pulford K, Lamant L, Morris SW, Butler LH, Wood KM, Stroud D, et al. Detection of anaplastic lymphoma kinase (ALK) and nucleolar protein nucleophosmin (NPM)-ALK proteins in normal and neoplastic cells with the monoclonal antibody ALK1. *Blood*. 1997;89:1394.
31. Falini B, Bigerna B, Fizzotti M, Pulford K, Pileri SA, Delsol G, et al. ALK expression defines a distinct group of T/null lymphomas ("ALK lymphomas") with a wide morphological spectrum. *The American journal of pathology*. 1998;153:875.
32. Deininger M, Buchdunger E, Druker BJ. The development of imatinib as a therapeutic agent for chronic myeloid leukemia. *Blood*. 2005;105:2640.
33. Kamal A, Thao L, Sensintaffar J, Zhang L, Boehm MF, Fritz LC, et al. A high-affinity conformation of Hsp90 confers tumour selectivity on Hsp90 inhibitors. *Nature*. 2003;425:407-10.
34. Workman P, BURROWS F, NECKERS L, ROSEN N. Drugging the Cancer Chaperone HSP90. *Annals of the New York Academy of Sciences*. 2007;1113:202-16.
35. Xu W, Marcu M, Yuan X, Mimnaugh E, Patterson C, Neckers L. Chaperone-dependent E3 ubiquitin ligase CHIP mediates a degradative pathway for c-ErbB2/Neu. *Proceedings of the National Academy of Sciences of the United States of America*. 2002;99:12847.
36. Pérez-Galán P, Dreyling M, Wiestner A. Mantle cell lymphoma: biology, pathogenesis, and the molecular basis of treatment in the genomic era. *Blood*. 2011;117:26-38.
37. Schatz JH. Targeting the PI3K/AKT/mTOR pathway in non-Hodgkin's lymphoma: results, biology, and development strategies. *Current oncology reports*. 2011;13:398-406.
38. Meadows SA, Vega F, Kashishian A, Johnson D, Diehl V, Miller LL, et al. PI3K $\delta$  inhibitor, GS-1101 (CAL-101), attenuates pathway signaling, induces apoptosis, and

overcomes signals from the microenvironment in cellular models of Hodgkin lymphoma. *Blood*. 2012;119:1897-900.

39. Sain N, Krishnan B, Ormerod MG, De Rienzo A, Liu WM, Kaye SB, et al. Potentiation of paclitaxel activity by the HSP90 inhibitor 17-allylamino-17-demethoxygeldanamycin in human ovarian carcinoma cell lines with high levels of activated AKT. *Molecular cancer therapeutics*. 2006;5:1197.

40. Maira SM, Voliva C, Garcia-Echeverria C. Class IA phosphatidylinositol 3-kinase: from their biologic implication in human cancers to drug discovery. 2008.

41. Münster PN, Marchion DC, Basso AD, Rosen N. Degradation of HER2 by ansamycins induces growth arrest and apoptosis in cells with HER2 overexpression via a HER3, phosphatidylinositol 3 -kinase-AKT-dependent pathway. *Cancer research*. 2002;62:3132.

42. Solit DB, Basso AD, Olshen AB, Scher HI, Rosen N. Inhibition of heat shock protein 90 function down-regulates Akt kinase and sensitizes tumors to Taxol. *Cancer research*. 2003;63:2139.

43. Basso AD, Solit DB, Chiosis G, Giri B, Tsihchlis P, Rosen N. Akt forms an intracellular complex with heat shock protein 90 (Hsp90) and Cdc37 and is destabilized by inhibitors of Hsp90 function. *Journal of Biological Chemistry*. 2002;277:39858.

44. Drysdale M, Brough P, Massey A, Jensen MR, Schoepfer J. Targeting Hsp90 for the treatment of cancer. *Current opinion in drug discovery & development*. 2006;9:483.

45. Pearl L, Prodromou C, Workman P. The Hsp90 molecular chaperone: an open and shut case for treatment. *Biochem J*. 2008;410:439-53.

46. Hollingshead M, Alley M, Burger AM, Borgel S, Pacula-Cox C, Fiebig HH, et al. In vivo antitumor efficacy of 17-DMAG (17-dimethylaminoethylamino-17-demethoxygeldanamycin hydrochloride), a water-soluble geldanamycin derivative. *Cancer chemotherapy and pharmacology*. 2005;56:115-25.

47. Goetz MP, Toft D, Reid J, Ames M, Stensgard B, Safgren S, et al. Phase I trial of 17-allylamino-17-demethoxygeldanamycin in patients with advanced cancer. *Journal of clinical oncology*. 2005;23:1078.

48. Ge J, Normant E, Porter JR, Ali JA, Dembski MS, Gao Y, et al. Design, synthesis, and biological evaluation of hydroquinone derivatives of 17-amino-17-demethoxygeldanamycin as potent, water-soluble inhibitors of Hsp90. *Journal of medicinal chemistry*. 2006;49:4606-15.

49. Sausville EA, Tomaszewski JE, Ivy P. Clinical development of 17-allylamino, 17-demethoxygeldanamycin. *Current cancer drug targets*. 2003;3:377-83.

50. Brough PA, Aherne W, Barril X, Borgognoni J, Boxall K, Cansfield JE, et al. 4, 5-diarylisoazole Hsp90 chaperone inhibitors: potential therapeutic agents for the treatment of cancer. *Journal of medicinal chemistry*. 2007;51:196-218.

51. Amato RJ, Jac J, Giessinger S, Saxena S, Willis JP. A phase 2 study with a daily regimen of the oral mTOR inhibitor RAD001 (everolimus) in patients with metastatic clear cell renal cell cancer. *Cancer*. 2009;115:2438-46.

52. Haritunians T, Mori A, O'Kelly J, Luong Q, Giles F, Koeffler H. Antiproliferative activity of RAD001 (everolimus) as a single agent and combined with other agents in mantle cell lymphoma. *Leukemia*. 2006;21:333-9.

53. Decker T, Sandherr M, Goetze K, Oelsner M, Ringshausen I, Peschel C. A pilot trial of the mTOR (mammalian target of rapamycin) inhibitor RAD001 in patients with advanced B-CLL. *Annals of hematology*. 2009;88:221-7.

54. Shinohara ET, Cao C, Niermann K, Mu Y, Zeng F, Hallahan DE, et al. Enhanced radiation damage of tumor vasculature by mTOR inhibitors. *Oncogene*. 2005;24:5414-22.

55. Armitage JO. Staging Non - Hodgkin Lymphoma. *CA: a cancer journal for clinicians*. 2009;55:368-76.

56. Connors JM. State-of-the-art therapeutics: Hodgkin's lymphoma. *Journal of clinical oncology*. 2005;23:6400-8.

57. Kwee TC, Kwee RM, Nievelstein RAJ. Imaging in staging of malignant lymphoma: a systematic review. *Blood*. 2008;111:504-16.

58. Lister T, Crowther D, Sutcliffe S, Glatstein E, Canellos G, Young R, et al. Report of a committee convened to discuss the evaluation and staging of patients with Hodgkin's disease: Cotswolds meeting. *Journal of clinical oncology*. 1989;7:1630-6.
59. Kreel L. The EMI whole body scanner in the demonstration of lymph node enlargement. *Clinical radiology*. 1976;27:421-9.
60. Lucey BC, Stuhlfaut JW, Soto JA. Mesenteric lymph nodes: detection and significance on MDCT. *American Journal of Roentgenology*. 2005;184:41-4.
61. Vinnicombe SJ, Reznick RH. Computerised tomography in the staging of Hodgkin's disease and non-Hodgkin's lymphoma. *European Journal of Nuclear Medicine and Molecular Imaging*. 2003;30:42-55.
62. la Fougère C, Hundt W, Bröckel N, Pfluger T, Haug A, Scher B, et al. Value of PET/CT versus PET and CT performed as separate investigations in patients with Hodgkin's disease and non-Hodgkin's lymphoma. *European Journal of Nuclear Medicine and Molecular Imaging*. 2006;33:1417-25.
63. Hernandez-Pampaloni M, Takalkar A, Yu JQ, Zhuang H, Alavi A. F-18 FDG-PET imaging and correlation with CT in staging and follow-up of pediatric lymphomas. *Pediatric radiology*. 2006;36:524-31.
64. Phelps ME, Hoffman EJ, Mullani NA, Ter-Pogossian MM. Application of annihilation coincidence detection to transaxial reconstruction tomography. *Journal of nuclear medicine: official publication, Society of Nuclear Medicine*. 1975;16:210.
65. Rohren EM, Turkington TG, Coleman RE. Clinical Applications of PET in Oncology<sup>1</sup>. *Radiology*. 2004;231:305-32.
66. Paul R. Comparison of fluorine-18-2-fluorodeoxyglucose and gallium-67 citrate imaging for detection of lymphoma. *Journal of nuclear medicine: official publication, Society of Nuclear Medicine*. 1987;28:288.
67. Moog F, Bangerter M, Diederichs CG, Guhlmann A, Kotzerke J, Merkle E, et al. Lymphoma: role of whole-body 2-deoxy-2-[F-18] fluoro-D-glucose (FDG) PET in nodal staging. *Radiology*. 1997;203:795-800.
68. Bangerter M, Moog F, Buchmann I, Kotzerke J, Griesshammer M, Hafner M, et al. Whole-body 2-[18F]-fluoro-2-deoxy-D-glucose positron emission tomography (FDG-PET) for accurate staging of Hodgkin's disease. *Annals of oncology*. 1998;9:1117-22.
69. Bangerter M, Griesshammer M, Binder T, Hafner M, Heimpel H, Reske S, et al. New diagnostic imaging procedures in Hodgkin's disease. *Annals of oncology*. 1996;7:S55-S9.
70. Barrington S, Carr R. Staging of Burkitt's lymphoma and response to treatment monitored by PET scanning. *Clinical Oncology*. 1995;7:334-5.
71. Zhang H, Tian M, Oriuchi N, Higuchi T, Tanada S, Endo K. Oncological diagnosis using positron coincidence gamma camera with fluorodeoxyglucose in comparison with dedicated PET. *British journal of radiology*. 2002;75:409-16.
72. Tatsumi M, Kitayama H, Sugahara H, Tokita N, Nakamura H, Kanakura Y, et al. Whole-body hybrid PET with 18F-FDG in the staging of non-Hodgkin's lymphoma. *Journal of Nuclear Medicine*. 2001;42:601-8.
73. Boren Jr EL, Delbeke D, Patton JA, Sandler MP. Comparison of FDG PET and positron coincidence detection imaging using a dual-head gamma camera with 5/8-inch NaI (TI) crystals in patients with suspected body malignancies. *European Journal of Nuclear Medicine and Molecular Imaging*. 1999;26:379-87.
74. Paes FM, Kalkanis DG, Sideras PA, Serafini AN. FDG PET/CT of Extranodal Involvement in Non-Hodgkin Lymphoma and Hodgkin Disease<sup>1</sup>. *Radiographics*. 2010;30:269-91.
75. Mikhaeel N, Timothy A, Hain S, O'Doherty M. 18-FDG-PET for the assessment of residual masses on CT following treatment of lymphomas. *Annals of oncology*. 2000;11:S147-S50.
76. YARARBAŞ U, ARGON AM, ERİNÇ R. The Comparison of Tc-99m MIBI and Ga-67 in the Evaluation of Hodgkin and Non-Hodgkin Lymphomas.
77. Elstrom R, Guan L, Baker G, Nakhoda K, Vergilio JA, Zhuang H, et al. Utility of FDG-PET scanning in lymphoma by WHO classification. *Blood*. 2003;101:3875-6.

78. Tsukamoto N, Kojima M, Hasegawa M, Oriuchi N, Matsushima T, Yokohama A, et al. The usefulness of (18)F-fluorodeoxyglucose positron emission tomography ((18)F-FDG-PET) and a comparison of (18)F-FDG-pet with (67)gallium scintigraphy in the evaluation of lymphoma: relation to histologic subtypes based on the World Health Organization classification. *Cancer*. 2007;110:652-9.
79. Hoffmann M, Wöhrer S, Becherer A, Chott A, Streubel B, Kletter K, et al. 18F-Fluoro-deoxy-glucose positron emission tomography in lymphoma of mucosa-associated lymphoid tissue: histology makes the difference. *Annals of oncology*. 2006;17:1761-5.
80. Alinari L, Castellucci P, Elstrom R, Ambrosini V, Stefoni V, Nanni C, et al. 18F-FDG PET in mucosa-associated lymphoid tissue (MALT) lymphoma. *Leukemia & lymphoma*. 2006;47:2096-101.
81. Karam M, Novak L, Cyriac J, Ali A, Nazeer T, Nugent F. Role of fluorine - 18 fluoro - deoxyglucose positron emission tomography scan in the evaluation and follow - up of patients with low - grade lymphomas. *Cancer*. 2006;107:175-83.
82. Beal K, Yeung H, Yahalom J. FDG-PET scanning for detection and staging of extranodal marginal zone lymphomas of the MALT type: a report of 42 cases. *Annals of oncology*. 2005;16:473-80.
83. Hoffmann M, Kletter K, Becherer A, Jager U, Chott A, Raderer M. 18F-fluorodeoxyglucose positron emission tomography (18F-FDG-PET) for staging and follow-up of marginal zone B-cell lymphoma. *Oncology*. 2003;64:336-40.
84. Hoffmann M, Kletter K, Diemling M, Becherer A, Pfeffel F, Petkov V, et al. Positron emission tomography with fluorine-18-2-fluoro-2-deoxy-D-glucose (F18-FDG) does not visualize extranodal B-cell lymphoma of the mucosa-associated lymphoid tissue (MALT)-type. *Annals of oncology*. 1999;10:1185-9.
85. Najjar F, Hustinx R, Jerusalem G, Fillet G, Rigo P. Positron emission tomography (PET) for staging low-grade non-Hodgkin's lymphomas (NHL). *Cancer Biotherapy and Radiopharmaceuticals*. 2001;16:297-304.
86. Hoffmann M, Chott A, Püspök A, Jäger U, Kletter K, Raderer M. 18F-fluorodeoxyglucose positron emission tomography (18F-FDG-PET) does not visualize follicular lymphoma of the duodenum. *Annals of hematology*. 2004;83:276-8.
87. Valencak J, Becherer A, Der-Petrossian M, Trautinger F, Raderer M, Hoffmann M. Positron emission tomography with [18F] 2-fluoro-D-2-deoxyglucose in primary cutaneous T-cell lymphomas. *haematologica*. 2004;89:115-6.
88. Buck AC, Schirrmeister HH, Guhlmann CA, Diederichs CG, Shen C, Buchmann I, et al. Ki-67 immunostaining in pancreatic cancer and chronic active pancreatitis: does in vivo FDG uptake correlate with proliferative activity? *Journal of Nuclear Medicine*. 2001;42:721.
89. Boothman DA, Davis TW, Sahijdak WM. Enhanced expression of thymidine kinase in human cells following ionizing radiation. *International Journal of Radiation Oncology\* Biology\* Physics*. 1994;30:391-8.
90. Been LB, Suurmeijer AJH, Cobben DCP, Jager PL, Hoekstra HJ, Elsinga PH. [18 F] FLT-PET in oncology: current status and opportunities. *European Journal of Nuclear Medicine and Molecular Imaging*. 2004;31:1659-72.
91. Kong X, Zhu Q, Vidal P, Watanabe K, Polsky B, Armstrong D, et al. Comparisons of anti-human immunodeficiency virus activities, cellular transport, and plasma and intracellular pharmacokinetics of 3'-fluoro-3'-deoxythymidine and 3'-azido-3'-deoxythymidine. *Antimicrobial agents and chemotherapy*. 1992;36:808.
92. Vesselle H, Grierson J, Muzi M, Pugsley JM, Schmidt RA, Rabinowitz P, et al. In vivo validation of 3'deoxy-3'-[(18) F] fluorothymidine ([18) F] FLT) as a proliferation imaging tracer in humans: correlation of [(18) F] FLT uptake by positron emission tomography with Ki-67 immunohistochemistry and flow cytometry in human lung tumors. *Clinical cancer research: an official journal of the American Association for Cancer Research*. 2002;8:3315.
93. Buck AK, Halter G, Schirrmeister H, Kotzerke J, Wurziger I, Glatting G, et al. Imaging proliferation in lung tumors with PET: 18F-FLT versus 18F-FDG. *Journal of Nuclear Medicine*. 2003;44:1426.

94. Buck AK, Schirrmeister H, Hetzel M, von der Heide M, Halter G, Glatting G, et al. 3-deoxy-3-[18F] fluorothymidine-positron emission tomography for noninvasive assessment of proliferation in pulmonary nodules. *Cancer research*. 2002;62:3331.
95. Mathews MB, Bernstein RM, Franza BR, Garrels JI. Identity of the proliferating cell nuclear antigen and cyclin. 1984.
96. Shields AF, Grierson JR, Dohmen BM, Machulla HJ, Stayanoff JC, Lawhorn-Crews JM, et al. Imaging proliferation in vivo with [F-18] FLT and positron emission tomography. *Nature medicine*. 1998;4:1334-6.
97. Mankoff DA, Shields AF, Krohn KA. PET imaging of cellular proliferation. *Radiologic Clinics of North America*. 2005;43:153-67.
98. Barthel H, Perumal M, Latigo J, He Q, Brady F, Luthra SK, et al. The uptake of 3 -deoxy-3 -[18 F] fluorothymidine into L5178Y tumours in vivo is dependent on thymidine kinase 1 protein levels. *European Journal of Nuclear Medicine and Molecular Imaging*. 2005;32:257-63.
99. Kenny LM, Vigushin DM, Al-Nahhas A, Osman S, Luthra SK, Shousha S, et al. Quantification of cellular proliferation in tumor and normal tissues of patients with breast cancer by [18F] fluorothymidine-positron emission tomography imaging: evaluation of analytical methods. *Cancer research*. 2005;65:10104.
100. Wagner M, Seitz U, Buck A, Neumaier B, Schultheiß S, Bangerter M, et al. 3 -[18F] fluoro-3 -deoxythymidine ([18F]-FLT) as positron emission tomography tracer for imaging proliferation in a murine B-cell lymphoma model and in the human disease. *Cancer research*. 2003;63:2681.
101. Buck AK, Kratochwil C, Glatting G, Juweid M, Bommer M, Tepsic D, et al. Early assessment of therapy response in malignant lymphoma with the thymidine analogue [18 F] FLT. *European Journal of Nuclear Medicine and Molecular Imaging*. 2007;34:1775-82.
102. Dittmann H, Dohmen B, Kehlbach R, Bartusek G, Pritzkow M, Sarbia M, et al. Early changes in [18 F] FLT uptake after chemotherapy: an experimental study. *European Journal of Nuclear Medicine and Molecular Imaging*. 2002;29:1462-9.
103. Graf N, Herrmann K, den Hollander J, Fend F, Schuster T, Wester HJ, et al. Imaging proliferation to monitor early response of lymphoma to cytotoxic treatment. *Molecular Imaging and Biology*. 2008;10:349-55.
104. Herrmann K, Wieder HA, Buck AK, Schoffel M, Krause BJ, Fend F, et al. Early response assessment using 3 '-Deoxy-3 '-[F-18]fluorothymidine-positron emission tomography in high-grade non-Hodgkin's lymphoma. *Clinical Cancer Research*. 2007;13:3552-8.
105. Shields AF, Grierson JR, Dohmen BM, Machulla H-J, Stayanoff JC, Lawhorn-Crews JM, et al. Imaging proliferation in vivo with [F-18] FLT and positron emission tomography. *Nature medicine*. 1998;4:1334-6.
106. Vega F, Medeiros LJ, Leventaki V, Atwell C, Cho-Vega JH, Tian L, et al. Activation of mammalian target of rapamycin signaling pathway contributes to tumor cell survival in anaplastic lymphoma kinase-positive anaplastic large cell lymphoma. *Cancer Res*. 2006;66:6589-97.
107. Schneider C, Pasqualucci L, Dalla-Favera R. Molecular pathogenesis of diffuse large B-cell lymphoma. *Seminars in Diagnostic Pathology*. 2011;28:167-77.
108. Sawas A, Diefenbach C, O'Connor OA. New therapeutic targets and drugs in non-Hodgkin's lymphoma. *Curr Opin Hematol*. 2011;18:280-7.
109. Sweetenham JW. Molecular signatures in the diagnosis and management of diffuse large B-cell lymphoma. *Current Opinion in Hematology*. 2011;18:288-92.
110. Tabernero J, Rojo F, Calvo E, Burris H, Judson I, Hazell K, et al. Dose- and schedule-dependent inhibition of the mammalian target of rapamycin pathway with everolimus: a phase I tumor pharmacodynamic study in patients with advanced solid tumors. *J Clin Oncol*. 2008;26:1603-10.
111. Markman B, Dienstmann R, Tabernero J. Targeting the PI3K/Akt/mTOR pathway--beyond rapalogs. *Oncotarget*. 2010;1:530-43.

112. Cantley LC. The phosphoinositide 3-kinase pathway. *Science Signalling*. 2002;296:1655.
113. Carpenter CL, Cantley LC. Phosphoinositide kinases. *Current opinion in cell biology*. 1996;8:153-8.
114. Brunet A, Bonni A, Zigmond MJ, Lin MZ, Juo P, Hu LS, et al. Akt promotes cell survival by phosphorylating and inhibiting a Forkhead transcription factor. *CELL-CAMBRIDGE MA-*. 1999;96:857-68.
115. Engelman JA, Luo J, Cantley LC. The evolution of phosphatidylinositol 3-kinases as regulators of growth and metabolism. *Nature Reviews Genetics*. 2006;7:606-19.
116. Luo J, Sobkiw CL, Hirshman MF, Logsdon MN, Li TQ, Goodyear LJ, et al. Loss of class I  $\alpha$  PI3K signaling in muscle leads to impaired muscle growth, insulin response, and hyperlipidemia. *Cell metabolism*. 2006;3:355-66.
117. Guertin DA, Sabatini DM. Defining the role of mTOR in cancer. *Cancer cell*. 2007;12:9-22.
118. Blay J-Y. Updating progress in sarcoma therapy with mTOR inhibitors. *Annals of Oncology*. 2011;22:280-7.
119. Maira S-M, Stauffer F, Brueggen J, Furet P, Schnell C, Fritsch C, et al. Identification and characterization of NVP-BEZ235, a new orally available dual phosphatidylinositol 3-kinase/mammalian target of rapamycin inhibitor with potent in vivo antitumor activity. *Molecular cancer therapeutics*. 2008;7:1851-63.
120. Eichhorn PJ, Gili M, Scaltriti M, Serra V, Guzman M, Nijkamp W, et al. Phosphatidylinositol 3-kinase hyperactivation results in lapatinib resistance that is reversed by the mTOR/phosphatidylinositol 3-kinase inhibitor NVP-BEZ235. *Cancer research*. 2008;68:9221-30.
121. Serra V, Markman B, Scaltriti M, Eichhorn PJ, Valero V, Guzman M, et al. NVP-BEZ235, a dual PI3K/mTOR inhibitor, prevents PI3K signaling and inhibits the growth of cancer cells with activating PI3K mutations. *Cancer research*. 2008;68:8022-30.
122. Markman B, Dienstmann R, Tabernero J, Markman B, Dienstmann R, Tabernero J. Targeting the PI3K/Akt/mTOR pathway—beyond rapalogs. *Oncotarget*. 2010;1:530.
123. Vasudevan KM, Barbie DA, Davies MA, Rabinovsky R, McNear CJ, Kim JJ, et al. AKT-Independent Signaling Downstream of Oncogenic PIK3CA Mutations in Human Cancer. *Cancer cell*. 2009;16:21-32.
124. Gills JJ, Dennis PA. Perifosine: update on a novel Akt inhibitor. *Current oncology reports*. 2009;11:102-10.
125. Hirai H, Sootome H, Nakatsuru Y, Miyama K, Taguchi S, Tsuchioka K, et al. MK-2206, an allosteric Akt inhibitor, enhances antitumor efficacy by standard chemotherapeutic agents or molecular targeted drugs in vitro and in vivo. *Molecular cancer therapeutics*. 2010;9:1956-67.
126. Yap T, Patnaik A, Fearen I, Olmos D, Papadopoulos K, Tunariu N, et al. First-in-class phase I trial of a selective Akt inhibitor, MK2206 (MK), evaluating alternate day (QOD) and once weekly (QW) doses in advanced cancer patients (pts) with evidence of target modulation and antitumor activity. *J Clin Oncol (Meeting Abstracts)*; 2010; 2010. p. 3009.
127. Levy DS, Kahana JA, Kumar R. AKT inhibitor, GSK690693, induces growth inhibition and apoptosis in acute lymphoblastic leukemia cell lines. *Blood*. 2009;113:1723-9.
128. Bai RY, Ouyang T, Miething C, Morris SW, Peschel C, Duyster J. Nucleophosmin-anaplastic lymphoma kinase associated with anaplastic large-cell lymphoma activates the phosphatidylinositol 3-kinase/Akt antiapoptotic signaling pathway. *Blood*. 2000;96:4319.
129. Slupianek A, Nieborowska-Skorska M, Hoser G, Morrione A, Majewski M, Xue L, et al. Role of phosphatidylinositol 3-kinase-Akt pathway in nucleophosmin/anaplastic lymphoma kinase-mediated lymphomagenesis. *Cancer research*. 2001;61:2194.
130. Bonvini P, Gastaldi T, Falini B, Rosolen A. Nucleophosmin-anaplastic lymphoma kinase (NPM-ALK), a novel Hsp90-client tyrosine kinase: down-regulation of NPM-ALK expression and tyrosine phosphorylation in ALK+ CD30+ lymphoma cells by the Hsp90 antagonist 17-allylamino, 17-demethoxygeldanamycin. *Cancer research*. 2002;62:1559.

131. Kaiser M, Lamottke B, Mieth M, Jensen MR, Quadt C, Garcia Echeverria C, et al. Synergistic action of the novel HSP90 inhibitor NVP AUY922 with histone deacetylase inhibitors, melphalan, or doxorubicin in multiple myeloma. *European journal of haematology*. 2010;84:337-44.
132. Witzig TE, Reeder CB, LaPlant BR, Gupta M, Johnston PB, Micallef IN, et al. A phase II trial of the oral mTOR inhibitor everolimus in relapsed aggressive lymphoma. *Leukemia*. 2011;25:341-7.
133. Juweid ME, Stroobants S, Hoekstra OS, Mottaghy FM, Dietlein M, Guermazi A, et al. Use of positron emission tomography for response assessment of lymphoma: consensus of the Imaging Subcommittee of International Harmonization Project in Lymphoma. *J Clin Oncol*. 2007;25:571-8.
134. Moskowitz CH, Schoder H, Teruya-Feldstein J, Sima C, Iasonos A, Portlock CS, et al. Risk-Adapted Dose-Dense Immunotherapy Determined by Interim FDG-PET in Advanced-Stage Diffuse Large B-Cell Lymphoma. *J Clin Oncol*. 2010;28:1896-903.
135. Han HS, Escalon MP, Hsiao B, Serafini A, Lossos IS. High incidence of false-positive PET scans in patients with aggressive non-Hodgkin's lymphoma treated with rituximab-containing regimens. *Ann Oncol*. 2009;20:309-18.
136. Ma WW, Jacene H, Song D, Vilardell F, Messersmith WA, Laheru D, et al. [18F]fluorodeoxyglucose positron emission tomography correlates with Akt pathway activity but is not predictive of clinical outcome during mTOR inhibitor therapy. *J Clin Oncol*. 2009;27:2697-704.
137. Cobben DCP, Elsinga PH, Suurmeijer AJH, Vaalburg W, Maas B, Jager PL, et al. Detection and grading of soft tissue sarcomas of the extremities with 18F-3 -fluoro-3 -deoxy-1-thymidine. *Clinical Cancer Research*. 2004;10:1685.
138. Pio BS, Park CK, Pietras R, Hsueh WA, Satyamurthy N, Pegram MD, et al. Usefulness of 3 -[F-18] fluoro-3 -deoxythymidine with positron emission tomography in predicting breast cancer response to therapy. *Molecular Imaging and Biology*. 2006;8:36-42.
139. Rasey JS, Grierson JR, Wiens LW, Kolb PD, Schwartz JL. Validation of FLT uptake as a measure of thymidine kinase-1 activity in A549 carcinoma cells. *Journal of Nuclear Medicine*. 2002;43:1210.
140. Buck AK, Bommer M, Stilgenbauer S, Juweid M, Glatting G, Schirrmeister H, et al. Molecular imaging of proliferation in malignant lymphoma. *Cancer research*. 2006;66:11055.
141. Smith-Jones PM, Solit D, Afroze F, Rosen N, Larson SM. Early tumor response to Hsp90 therapy using HER2 PET: comparison with 18F-FDG PET. *Journal of Nuclear Medicine*. 2006;47:793-6.
142. Bergstrom M, Monazzam A, Razifar P, Ide S, Josephsson R, Langstrom B. Modeling spheroid growth, PET tracer uptake, and treatment effects of the Hsp90 inhibitor NVP-AUY922. *Journal of Nuclear Medicine*. 2008;49:1204-10.
143. Jensen MM, Erichsen KD, Bjorkling F, Madsen J, Jensen PB, Hojgaard L, et al. Early detection of response to experimental chemotherapeutic Top216 with [18F]FLT and [18F]FDG PET in human ovary cancer xenografts in mice. *PLoS One*. 2010;5:e12965.
144. Brepoels L, Stroobants S, Verhoef G, De Groot T, Mortelmans L, De Wolf-Peeters C. (18)F-FDG and (18)F-FLT uptake early after cyclophosphamide and mTOR inhibition in an experimental lymphoma model. *Journal of Nuclear Medicine*. 2009;50:1102-9.
145. Kubota R, Yamada S, Kubota K, Ishiwata K, Tamahashi N, Ido T. Intratumoral distribution of fluorine-18-fluorodeoxyglucose in vivo: high accumulation in macrophages and granulation tissues studied by microautoradiography. *Journal of Nuclear Medicine*. 1992;33:1972-80.
146. Plas DR, Thompson CB. Akt-dependent transformation: there is more to growth than just surviving. *Oncogene*. 2005;24:7435-42.
147. Fueterer T, Wanek T, Pflegerl P, Jaeger-Lansky A, Hoeflmayer D, Strommer S, et al. Gastric cancer growth control by BEZ235 in vivo does not correlate with PI3K/mTOR target inhibition but with [18F]FLT uptake. *Clin Cancer Res*. 2011;17:5322-32.
148. Manning BD, Cantley LC. AKT/PKB signaling: navigating downstream. *Cell*. 2007;129:1261-74.

149. Lu L, Samuelsson L, Bergstrom M, Sato K, Fasth KJ, Langstrom B. Rat studies comparing <sup>11</sup>C-FMAU, <sup>18</sup>F-FLT, and <sup>76</sup>Br-BFU as proliferation markers. *Journal of Nuclear Medicine*. 2002;43:1688.
150. Barthel H, Cleij MC, Collingridge DR, Hutchinson OC, Osman S, He Q, et al. 3'-deoxy-3'-[<sup>18</sup>F] fluorothymidine as a new marker for monitoring tumor response to antiproliferative therapy in vivo with positron emission tomography. *Cancer research*. 2003;63:3791.
151. Perumal M, Pillai RG, Barthel H, Leyton J, Latigo JR, Forster M, et al. Redistribution of nucleoside transporters to the cell membrane provides a novel approach for imaging thymidylate synthase inhibition by positron emission tomography. *Cancer research*. 2006;66:8558.
152. Kenny L, Coombes RC, Vigushin DM, Al-Nahhas A, Shousha S, Aboagye EO. Imaging early changes in proliferation at 1 week post chemotherapy: a pilot study in breast cancer patients with 3'-deoxy-3'-[<sup>18</sup>F] fluorothymidine positron emission tomography. *European Journal of Nuclear Medicine and Molecular Imaging*. 2007;34:1339-47.
153. Muzi M, Vesselle H, Grierson JR, Mankoff DA, Schmidt RA, Peterson L, et al. Kinetic analysis of 3'-deoxy-3'-fluorothymidine PET studies: validation studies in patients with lung cancer. *Journal of Nuclear Medicine*. 2005;46:274.
154. Leyton J, Latigo JR, Perumal M, Dhaliwal H, He Q, Aboagye EO. Early detection of tumor response to chemotherapy by 3'-deoxy-3'-[<sup>18</sup>F] fluorothymidine positron emission tomography: the effect of cisplatin on a fibrosarcoma tumor model in vivo. *Cancer research*. 2005;65:4202.
155. Oyama N, Ponde DE, Dence C, Kim J, Tai YC, Welch MJ. Monitoring of therapy in androgen-dependent prostate tumor model by measuring tumor proliferation. *Journal of Nuclear Medicine*. 2004;45:519.
156. Waldherr C, Mellinghoff IK, Tran C, Halpern BS, Rozengurt N, Safaei A, et al. Monitoring antiproliferative responses to kinase inhibitor therapy in mice with 3'-deoxy-3'-<sup>18</sup>F-fluorothymidine PET. *Journal of Nuclear Medicine*. 2005;46:114.
157. Lane HA, Wood JM, McSheehy PMJ, Allegrini PR, Boulay A, Brueggen J, et al. mTOR Inhibitor RAD001 (Everolimus) Has Antiangiogenic/Vascular Properties Distinct from a VEGFR Tyrosine Kinase Inhibitor. *Clinical Cancer Research*. 2009;15:1612-22.
158. Folkman J. Angiogenesis in cancer, vascular, rheumatoid and other disease. *Nature medicine*. 1995;1:27-30.
159. Lee D-F, Hung M-C. All roads lead to mTOR: integrating inflammation and tumor angiogenesis. *Cell Cycle*. 2007;6:3011-4.
160. Jiang B-H, Liu L-Z. PI3K/PTEN signaling in tumorigenesis and angiogenesis. *Biochimica et Biophysica Acta (BBA)-Proteins & Proteomics*. 2008;1784:150-8.
161. Boulay A, Lane HA. The mammalian target of rapamycin kinase and tumor growth inhibition. *Targeted Interference with Signal Transduction Events*. 2007:99-124.
162. KIEFER FN, BERNIS H, RESINK TJ, BATTEGAY EJ. Hypoxia enhances vascular cell proliferation and angiogenesis in vitro via rapamycin (mTOR)-dependent signaling. *The FASEB journal*. 2002;16:771-80.
163. Viñals F, Chambard JC, Pouyssegur J. p70 S6 kinase-mediated protein synthesis is a critical step for vascular endothelial cell proliferation. *Journal of Biological Chemistry*. 1999;274:26776-82.
164. Yu Y, Sato JD. MAP kinases, phosphatidylinositol 3-kinase, and p70 S6 kinase mediate the mitogenic response of human endothelial cells to vascular endothelial growth factor. *Journal of cellular physiology*. 1999;178:235-46.
165. Dormond O, Madsen JC, Briscoe DM. The effects of mTOR-Akt interactions on anti-apoptotic signaling in vascular endothelial cells. *Journal of Biological Chemistry*. 2007;282:23679-86.
166. Mabuchi S, Altomare DA, Cheung M, Zhang L, Poulidakos PI, Hensley HH, et al. RAD001 inhibits human ovarian cancer cell proliferation, enhances cisplatin-induced apoptosis, and prolongs survival in an ovarian cancer model. *Clinical Cancer Research*. 2007;13:4261-70.

167. Mabuchi S, Altomare DA, Connolly DC, Klein-Szanto A, Litwin S, Hoelzle MK, et al. RAD001 (Everolimus) delays tumor onset and progression in a transgenic mouse model of ovarian cancer. *Cancer research*. 2007;67:2408-13.
168. Manegold PC, Paringer C, Kulka U, Krimmel K, Eichhorn ME, Wilkowski R, et al. Antiangiogenic therapy with mammalian target of rapamycin inhibitor RAD001 (Everolimus) increases radiosensitivity in solid cancer. *Clinical Cancer Research*. 2008;14:892-900.
169. Semela D, Piguet A-C, Kolev M, Schmitter K, Hlushchuk R, Djonov V, et al. Vascular remodeling and antitumoral effects of mTOR inhibition in a rat model of hepatocellular carcinoma. *Journal of hepatology*. 2007;46:840-8.
170. Phung TL, Ziv K, Dabydeen D, Eyiah-Mensah G, Riveros M, Perruzzi C, et al. Pathological angiogenesis is induced by sustained Akt signaling and inhibited by rapamycin. *Cancer cell*. 2006;10:159.
171. Del Bufalo D, Ciuffreda L, Trisciuglio D, Desideri M, Cognetti F, Zupi G, et al. Antiangiogenic potential of the mammalian target of rapamycin inhibitor temsirolimus. *Cancer research*. 2006;66:5549-54.
172. Melillo G. Targeting hypoxia cell signaling for cancer therapy. *Cancer and Metastasis Reviews*. 2007;26:341-52.
173. Lane HA, Wood JM, McSheehy PM, Allegrini PR, Boulay A, Brueggen J, et al. mTOR inhibitor RAD001 (everolimus) has antiangiogenic/vascular properties distinct from a VEGFR tyrosine kinase inhibitor. *Clinical Cancer Research*. 2009;15:1612-22.
174. Honer M, Ebenhan T, Allegrini PR, Ametamey SM, Becquet M, Cannet C, et al. Anti-Angiogenic/Vascular Effects of the mTOR Inhibitor Everolimus Are Not Detectable by FDG/FLT-PET. *Translational Oncology*. 2010;3:264-U172.
175. Honer M, Ebenhan T, Allegrini PR, Ametamey SM, Becquet M, Cannet C, et al. Anti-angiogenic/vascular effects of the mTOR inhibitor everolimus are not detectable by FDG/FLT-PET. *Translational Oncology*. 2010;3:264.
176. Wei LH, Su H, Hildebrandt IJ, Phelps ME, Czernin J, Weber WA. Changes in tumor metabolism as readout for mammalian target of rapamycin kinase inhibition by rapamycin in glioblastoma. *Clinical Cancer Research*. 2008;14:3416-26.
177. O'Reilly T, McSheehy PM. Biomarker development for the clinical activity of the mTOR inhibitor everolimus (RAD001): processes, limitations, and further proposals. *Translational Oncology*. 2010;3:65.
178. Motzer RJ, Escudier B, Oudard S, Hutson TE, Porta C, Bracarda S, et al. Efficacy of everolimus in advanced renal cell carcinoma: a double-blind, randomised, placebo-controlled phase III trial. *The Lancet*. 2008;372:449-56.
179. Ferretti S, Allegrini PR, O'Reilly T, Schnell C, Stumm M, Wartmann M, et al. Patupilone induced vascular disruption in orthotopic rodent tumor models detected by magnetic resonance imaging and interstitial fluid pressure. *Clinical Cancer Research*. 2005;11:7773-84.
180. Schnell CR, Stauffer F, Allegrini PR, O'Reilly T, McSheehy PM, Dartois C, et al. Effects of the dual phosphatidylinositol 3-kinase/mammalian target of rapamycin inhibitor NVP-BEZ235 on the tumor vasculature: implications for clinical imaging. *Cancer research*. 2008;68:6598-607.
181. Haberkorn U, Bellemann ME, Brix G, Kamencic H, Morr I, Traut U, et al. Apoptosis and changes in glucose transport early after treatment of Morris hepatoma with gemcitabine. *European Journal of Nuclear Medicine and Molecular Imaging*. 2001;28:418-25.
182. Mankoff DA, Muzi M, Krohn KA. Quantitative positron emission tomography imaging to measure tumor response to therapy: what is the best method? *Molecular imaging and biology: MIB: the official publication of the Academy of Molecular Imaging*. 2003;5:281.
183. Rajendran JG, Mankoff DA, O'Sullivan F, Peterson LM, Schwartz DL, Conrad EU, et al. Hypoxia and glucose metabolism in malignant tumors evaluation by [18F] fluoromisonidazole and [18F] fluorodeoxyglucose positron emission tomography imaging. *Clinical Cancer Research*. 2004;10:2245-52.

184. Aloj L, Caracó C, Jagoda E, Eckelman WC, Neumann RD. Glut-1 and Hexokinase Expression Relationship with 2-Fluoro-2-deoxy-d-glucose Uptake in A431 and T47D Cells in Culture. *Cancer research*. 1999;59:4709-14.
185. Tseng J, Dunnwald LK, Schubert EK, Link JM, Minoshima S, Muzi M, et al. 18F-FDG kinetics in locally advanced breast cancer: correlation with tumor blood flow and changes in response to neoadjuvant chemotherapy. *Journal of Nuclear Medicine*. 2004;45:1829-37.
186. Ebenhan T, Honer M, Ametamey S, Schubiger P, Becquet M, Ferretti S, et al. Comparison of [18 F]-Tracers in Various Experimental Tumor Models by PET Imaging and Identification of an Early Response Biomarker for the Novel Microtubule Stabilizer Patupilone. *Molecular Imaging and Biology*. 2009;11:308-21.
187. Broillet A, Hantson J, Ruegg C, Messenger T, Schneider M. Assessment of microvascular perfusion changes in a rat breast tumor model using SonoVue to monitor the effects of different anti-angiogenic therapies. *Academic radiology*. 2005;12:S28.
188. Jain RK. Normalizing tumor vasculature with anti-angiogenic therapy: a new paradigm for combination therapy. *Nature medicine*. 2001;7:987-9.
189. Wahl R, Henry C, Ethier S. Serum glucose: effects on tumor and normal tissue accumulation of 2-[F-18]-fluoro-2-deoxy-D-glucose in rodents with mammary carcinoma. *Radiology*. 1992;183:643-7.
190. Lindholm P, Minn H, Leskinen-Kallio S, Bergman J, Ruotsalainen U, Joensuu H. Influence of the blood glucose concentration on FDG uptake in cancer--a PET study. *Journal of nuclear medicine: official publication, Society of Nuclear Medicine*. 1993;34:1.
191. Nogová L, Boellaard R, Kobe C, Hoetjes N, Zander T, Gross SH, et al. Downregulation of 18F-FDG uptake in PET as an early pharmacodynamic effect in treatment of non-small cell lung cancer with the mTOR inhibitor everolimus. *Journal of Nuclear Medicine*. 2009;50:1815-9.
192. Ma WW, Jacene H, Song D, Vilardell F, Messersmith WA, Laheru D, et al. [18F] fluorodeoxyglucose positron emission tomography correlates with Akt pathway activity but is not predictive of clinical outcome during mTOR inhibitor therapy. *Journal of clinical oncology*. 2009;27:2697-704.
193. Prior JO, Montemurro M, Orcurto M-V, Michielin O, Luthi F, Benhattar J, et al. Early prediction of response to sunitinib after imatinib failure by 18F-fluorodeoxyglucose positron emission tomography in patients with gastrointestinal stromal tumor. *Journal of clinical oncology*. 2009;27:439-45.
194. Mendel DB, Laird AD, Xin X, Louie SG, Christensen JG, Li G, et al. In Vivo Antitumor Activity of SU11248, a Novel Tyrosine Kinase Inhibitor Targeting Vascular Endothelial Growth Factor and Platelet-derived Growth Factor Receptors Determination of a Pharmacokinetic/Pharmacodynamic Relationship. *Clinical Cancer Research*. 2003;9:327-37.
195. Hu-Lowe DD, Zou HY, Grazzini ML, Hallin ME, Wickman GR, Amundson K, et al. Nonclinical antiangiogenesis and antitumor activities of axitinib (AG-013736), an oral, potent, and selective inhibitor of vascular endothelial growth factor receptor tyrosine kinases 1, 2, 3. *Clinical Cancer Research*. 2008;14:7272-83.
196. Willett CG, Boucher Y, di Tomaso E, Duda DG, Munn LL, Tong RT, et al. Direct evidence that the VEGF-specific antibody bevacizumab has antivascular effects in human rectal cancer. *Nature medicine*. 2004;10:145-7.

## Acknowledgements

I want to express my gratitude to Prof. Dr. Ulrich Keller, Prof. Dr. Andreas Buck, PD Dr. Tobias Dechow and Prof. Dr. Christine Spitzweg, for the supervision of my project and for the opportunity of working in the group. The experience I made has certainly represented a leap forward for my scientific knowledge, and have given me the chance to live a multicultural experience.

I want to thank PD. Dr. Nicolas Graf, PD. Dr. Ken Herrmann, Dr. Alex Höllein and Dr. Christop Seidl, for their supervision, support and continuous supply of motivation during the project.

Sincere thanks to all the SFB 824 fellows, and in particular to Prof. Dr. Markus Schwaiger, for his efforts in the coordination and organization of the network. I had the chance to meet fantastic people among my colleagues, sharing with them an enriching experience, on a professional and personal level. All my thanks to Johanna, Daniel, Alexandra, Geoffrey, Maro, Gloria, Victoria, Birgit, Christina and other colleague at the TUM and the LMU, with whom I had scientific and non-scientific discussions.

I am thankful to Prof. Dr. Sybille Ziegler and her group, for introducing me to the techniques in the study of molecular imaging.

Thanks are due to Prof. Dr. Walch and his group from the Institute for Pathology at the Helmholtz Zentrum München (German Research Center for Environmental Health) for their support in the histochemical analysis.

My work could have not been completed without the help of my lab colleagues, with their precious suggestions and vivid ideas. Daniela Zwisler, Barbara Numberger, Madlen Oelsner, Michaela Wagner, Stephanie Schöffmann helped me in the beginning and throughout my Ph.D., providing constant and valuable techniques and advice. A special thank to Jolanta Slawska, Sabine Pirsig, Annette Frank for their support and for all the time spent together in and out the lab.

I want to thank Han for being always on my side and all my old friends at home and abroad for their long distance but true friendship. Thanks to my family, for supporting and standing me and being often right on many things.